International Ocean Discovery Program Expedition 398 Scientific Prospectus

Hellenic Arc Volcanic Field

Volcanism and tectonics in an island arc rift environment (VolTecArc): Christiana-Santorini-Kolumbo marine volcanic field, Greece

Timothy Druitt
Co-Chief Scientist
Magmas and Volcanoes Laboratory
University of Clermont Auvergne
France

Steffen Kutterolf
Co-Chief Scientist
Research Division 4: Dynamics of the Ocean Floor
GEOMAR Helmholtz Centre for Ocean Research Kiel
Germany

Tobias W. Höfig
Expedition Project Manager/Staff Scientist
International Ocean Discovery Program
Texas A&M University
USA

Publisher's notes

This publication was prepared by the *JOIDES Resolution* Science Operator (JRSO) at Texas A&M University (TAMU) as an account of work performed under the International Ocean Discovery Program (IODP). This material is based upon work supported by the JRSO, which is a major facility funded by the National Science Foundation Cooperative Agreement Number OCE1326927. Funding for IODP is provided by the following international partners:

National Science Foundation (NSF), United States
Ministry of Education, Culture, Sports, Science and Technology (MEXT), Japan
European Consortium for Ocean Research Drilling (ECORD)
Ministry of Science and Technology (MOST), People's Republic of China
Australia-New Zealand IODP Consortium (ANZIC)
Ministry of Earth Sciences (MoES), India

Portions of this work may have been published in whole or in part in other IODP documents or publications.

This IODP *Scientific Prospectus* is based on precruise *JOIDES Resolution* Facility advisory panel discussions and scientific input from the designated Co-Chief Scientists on behalf of the drilling proponents. During the course of the cruise, actual site operations may indicate to the Co-Chief Scientists, the Expedition Project Manager/Staff Scientist, and the Operations Superintendent that it would be scientifically or operationally advantageous to amend the plan detailed in this prospectus. It should be understood that any substantial changes to the science deliverables outlined in the plan presented here are contingent upon the approval of the IODP JRSO Director and/or *JOIDES Resolution* Facility Board.

Disclaimer

Copyright

Citation

Druitt, T., Kutterolf, S., and Höfig, T.W., 2022. *Expedition 398 Scientific Prospectus: Hellenic Arc Volcanic Field*. International Ocean Discovery Program. https://doi.org/10.14379/iodp.sp.398.2022

ISSN

World Wide Web: 2332-1385

March 2022

Abstract

The understanding of island arc volcanism and associated hazards requires study of the processes that drive such volcanism and how the volcanoes interact with their marine surroundings. What are the links and feedbacks between crustal tectonics, volcanic activity, and magma genesis? What are the dynamics and impacts of submarine explosive volcanism and caldera-forming eruptions? How do calderas collapse during explosive eruptions and then recover to enter new magmatic cycles? What are the reactions of marine ecosystems to volcanic eruptions? The Christiana-Santorini-Kolumbo (CSK) volcanic field on the Hellenic volcanic arc is a unique system for addressing these questions. It consists of three large volcanic centers (Christiana, Santorini, and Kolumbo), and a line of small submarine cones, founded on thinned continental crust in a 100 km long rift zone that cuts across the island arc. The marine rift basins around the CSK field, as well as the Santorini caldera, contain volcano-sedimentary fills up to several hundreds of meters thick, providing rich archives of CSK volcanic products, tectonic evolution, magma genesis and paleoenvironments accessible only by deep drilling backed up by seismic interpretations. We will drill four primary sites in the rift's basins and two additional primary sites inside the Santorini caldera. The expedition science has five main objectives, each with a leading testable hypothesis, and two secondary objectives. Deep ocean drilling will enable us to identify, characterize, and interpret depositional packages visible on seismic images, chemically correlate primary volcaniclastic layers in the rift fills with their source volcanoes, fill in the many gaps in the onshore volcanic records, provide a tight chronostratigraphic framework for rift tectonic and sedimentary histories, and sample deep subsurface microbial life.

Plain language summary

About 800 million people are threatened by volcanic eruptions around the globe: high plumes of ash, ground-hugging flows of hot ash and rock, earthquakes, and associated tsunamis. The Christiana, Santorini, and Kolumbo volcanic group in the Aegean Sea of Greece is particularly hazardous because the volcanoes have produced many eruptions in the past, and some of them were highly explosive. Santorini is an iconic volcano because of its well-known eruption in the Late Bronze Age, and it is a major tourist destination. Much has been learned about the eruption history of the Aegean volcanoes on land, but most of their volcanic products lie on the seafloor, requiring research to move offshore. During International Ocean Discovery Program (IODP) Expedition 398 we will drill the submarine sequences of muds and volcanic products that fill the marine basins around the volcanoes and inside the Santorini caldera. These will provide a rich record of volcanic activity much older than that known on the islands above sea level. The drilling will access sediments and volcanic layers to depths of several hundred meters below the seabed at six sites, enabling us to reconstruct the volcanic history of the region back to 3 million years or more. Postexpedition research will then be able to show the connection of the volcanic history and how the basins formed and whether major events of faulting of the Earth's crust or earthquakes coincided with switching on or shutting down the different volcanic centers and triggering any of their large eruptions in the past. Another aim will be to improve our knowledge and understanding of the Late Bronze Age eruption regarding the amount of magma erupted and possible effects of the eruption on the Minoan civilization on the island of Crete. We will also drill through and sample the products of the submarine volcanoes of Kameni inside the Santorini caldera and Kolumbo outside of it, allowing us to reconstruct their histories and better evaluate the hazards posed by underwater explosions and tsunamis. Moreover, the sediment layers of the marine basins have recorded sea level changes and the subsidence of the Aegean region over the last few million years, enabling us to reconstruct the change from continental to marine environments with time. Finally, drilling deep inside the Santorini caldera will seek evidence for microbial life below the seafloor and how it may have responded to repeated eruptions of the volcano in the past.

1. Schedule for Expedition 398

International Ocean Discovery Program (IODP) Expedition 398 is based on IODP drilling Proposals 932-Full, 932-Add, and 932-Add2 (available at **http://iodp.tamu.edu/scienceops/expeditions/hellenic_arc_volcanic_field.html**). Following evaluation by the IODP Scientific Advisory Structure, the expedition was scheduled for the research vessel (R/V) *JOIDES Resolution*, operating under contract with the *JOIDES Resolution* Science Operator (JRSO). At the time of publication of this Scientific Prospectus, the expedition is scheduled to start in Tarragona, Spain, on 11 December 2022 and to end in Heraklion, Greece, on 10 February 2023. Accounting for 5 days of port call and 6 days of transit, a total of 50 days will be available for drilling, coring, and downhole measurements described in this report (for the current detailed schedule, see **http://iodp.tamu.edu/scienceops**). Further details about the facilities aboard *JOIDES Resolution* can be found at **http://iodp.tamu.edu/labs/index.html**.

2. Introduction

Volcanic hazards and risks lie at the heart of global geoscience, with about 800 million people threatened by eruptions (Loughlin et al., 2015). Volcanoes in island arc settings impact humans and the environment through explosions (both subaerial and submarine), tephra fallout, pyroclastic flows, earthquakes, tsunamis, and ocean acidification (Sigurdsson, 2015). Some large eruptions, such as the Late Bronze Age (LBA; also called "Minoan") eruption of Santorini, may destabilize entire civilizations (Bruins et al., 2008). On the other hand, volcanoes can host rich ecosystems and fertilize the oceans (Duggen et al., 2010; Christakis et al., 2018).

Better understanding of the processes governing arc volcanoes and their hazards is important as the 21st century unfolds (McGuire et al., 2017; National Academies of Sciences, Engineering, and Medicine, 2017). Crustal tectonics is one process that strongly influences volcanism, but it has rarely been studied at high spatial and temporal resolutions (e.g., Cembrano and Lara, 2009). Crustal thickness and thermal structure affect the production of magmas in the mantle and their subsequent evolution through crystal fractionation, crustal contamination, and magma mixing (Farner and Lee, 2017). Extensional crustal motions across many island arcs create space for magma ascent and influence the depths and sizes of magma storage regions (Acocella and Funiciello, 2010; Bachmann and Huber, 2016). Large earthquakes cause changes in crustal stresses sufficient to induce eruptions up to several hundreds of kilometers away (Walter and Amelung, 2007). Changes in sea level driven by tectonics or climate modulate volcanic activity by loading or unloading the magma plumbing system (Kutterolf et al., 2013; Sternai et al., 2017; Satow et al., 2021).

The Christiana-Santorini-Kolumbo (CSK) volcanic field is an excellent site at which to address these fundamental questions. It is one of the most active in Europe, having produced over 100 explosive eruptions in the last 360,000 y (Druitt et al., 1999). Situated in a rift zone that cuts northeast–southwest across the island arc, the field includes the extinct Christiana Volcano, Santorini caldera with its intracaldera Kameni Volcano, Kolumbo Volcano, and the 22 submarine cones of the Kolumbo volcanic chain (Figures **F1**, **F2A**) (Hooft et al., 2017; Nomikou et al., 2013), all of which have discharged their volcanic products into adjacent marine basins, creating a rich archive of past eruptions. Santorini is one of the most explosive arc volcanoes in the world (Figure **F3A**, **F3B**); its onland products have been mapped, dated, and chemically fingerprinted (Figure **F3C**), and its historical eruptions are well documented (Druitt et al., 1999; Pyle and Elliott, 2006). Kolumbo Volcano has had at least five large explosive eruptions; the last one was in 1650 (Hübscher et al., 2015).

We have a record of Santorini volcanism since 650 ka, but it is only detailed since 360 ka (Figure **F3A**). Although the onland record is inevitably discontinuous, the deep marine record promises to be much more complete (e.g., Schindlbeck et al., 2016). Apart from the 1650 eruption, the past volcanism of Kolumbo is poorly documented and that of Christiana is unknown. Offshore drilling will enable us to use the thick volcano-sedimentary records of the rift basins and Santorini caldera as time capsules for reconstructing the volcanic and tectonic histories of the area since rift incep-

tion in the Pliocene. Drilling will allow (1) groundtruthing of marine seismic profiles, (2) characterization and dating of seismic packages, (3) measurement of the physical properties of submarine strata, and (4) sampling of subsurface ecosystems.

Hazards from the CSK rift zone include earthquakes, eruptions, and tsunamis (Vougioukalakis et al., 2016). The level of seismicity is amongst the highest in Europe (Sachpazi et al., 2016), and the largest 20th century shallow earthquake in Europe (M 7.5) took place there in 1956 (Okal et al., 2009). The LBA eruption of Santorini in about 1630 BCE was one of the largest of the Holocene epoch worldwide; it may have influenced the decline of the Minoan civilization on Crete and thus is an iconic event in both volcanology and archaeology (Bruins et al., 2008). The 1650 Kolumbo eruption killed 70 people on Santorini through gas release and tsunami inundation (Cantner et al., 2014). Santorini had an episode of bradyseismic unrest in 2011–2012 (Parks et al., 2015), raising awareness of the eruption threat at these islands visited by two million tourists per year.

Drilling will be carried out in the context of several new research initiatives in the marine environment of the volcanic field. A dense network of subseafloor seismic reflection profiles exists across the rift zones, providing high-resolution images of sedimentary fills and faults (Figure **F2A**) (Hübscher et al., 2015; Nomikou et al., 2016a, 2018). Detailed correlations and interpretations of these profiles from northeast to southwest across the volcanic field has led to a seismic stratigraphic model (Figure **F4**) that will be refined by deep drilling (Preine et al., 2022). In 2015, an active seismic tomography experiment of the CSK system was carried out (Plumbing Reservoirs of the Earth under Santorini [PROTEUS]; Hooft et al., 2017). It identified an enigmatic, low-density anomaly 400–3000 meters below seafloor (mbsf) beneath the Santorini caldera (Hooft et al., 2019), as well as an upper crustal magma reservoir beneath Santorini and extending northeastward toward the Kolumbo Volcano (McVey et al., 2019). Multibeam bathymetric surveys have imaged submarine volcanic edifices and calderas (Nomikou et al., 2012, 2013, 2016a). Seismic reflection profiles

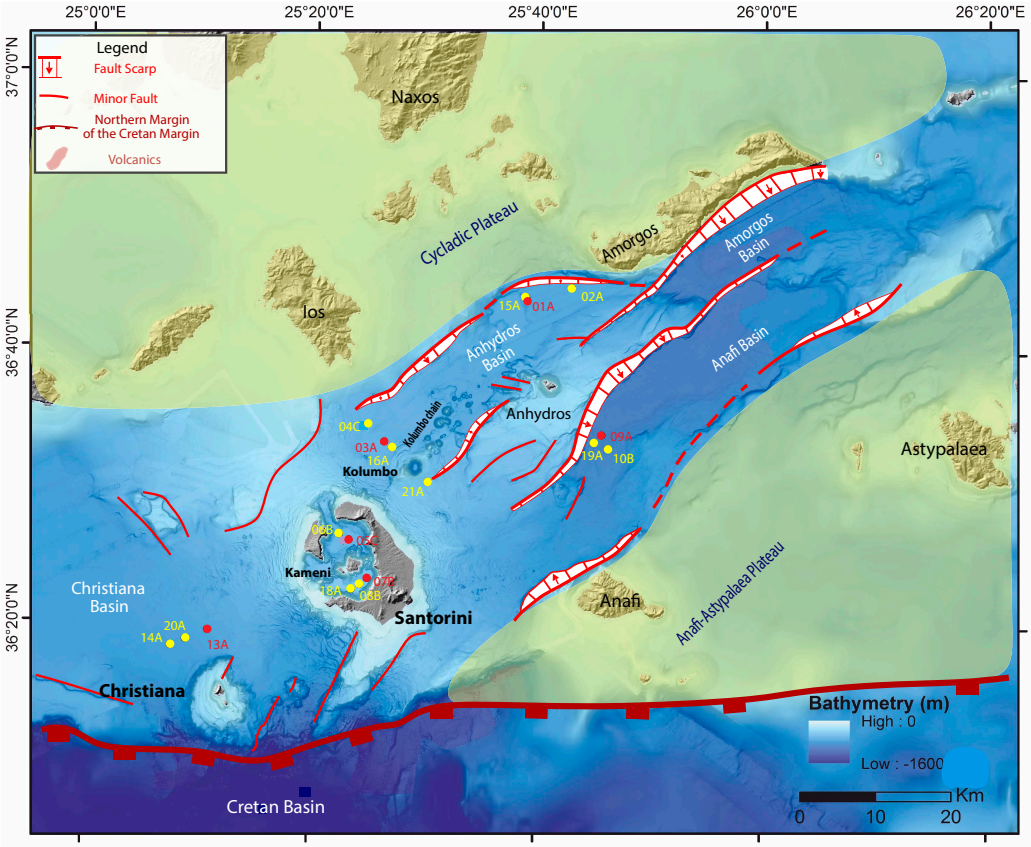

Figure F1. CSK volcanic field and its host rift basins, with locations of Expedition 398 proposed primary (red dots) and alternate (yellow dots) sites.

inside the Santorini caldera have allowed recognition of several intracaldera layers that will be sampled by drilling (Johnston et al., 2015). Seafloor volcanic products, hydrothermal deposits, and bacterial mounds have been sampled (Hanert, 2002; Camilli et al., 2015), and the surface biosphere documented (Oulas et al., 2016; Polymenakou et al., 2021). Deep-sea ash layers have been sampled by gravity coring across the Eastern Mediterranean (Figure **F2B**), and many have been correlated with onshore products. The resulting marine ash stratigraphy extends back to 200 ka, includes eight ash deposits from Santorini, and has enabled estimation of the ages and masses of many of the tephra layers (Satow et al., 2015; Wulf et al., 2020; Kutterolf et al., 2021a, 2021b). An issue of the professional earth science magazine *Elements* summarizing our current knowledge of the South Aegean volcanic arc was published recently (Druitt and Vougioukalakis, 2019).

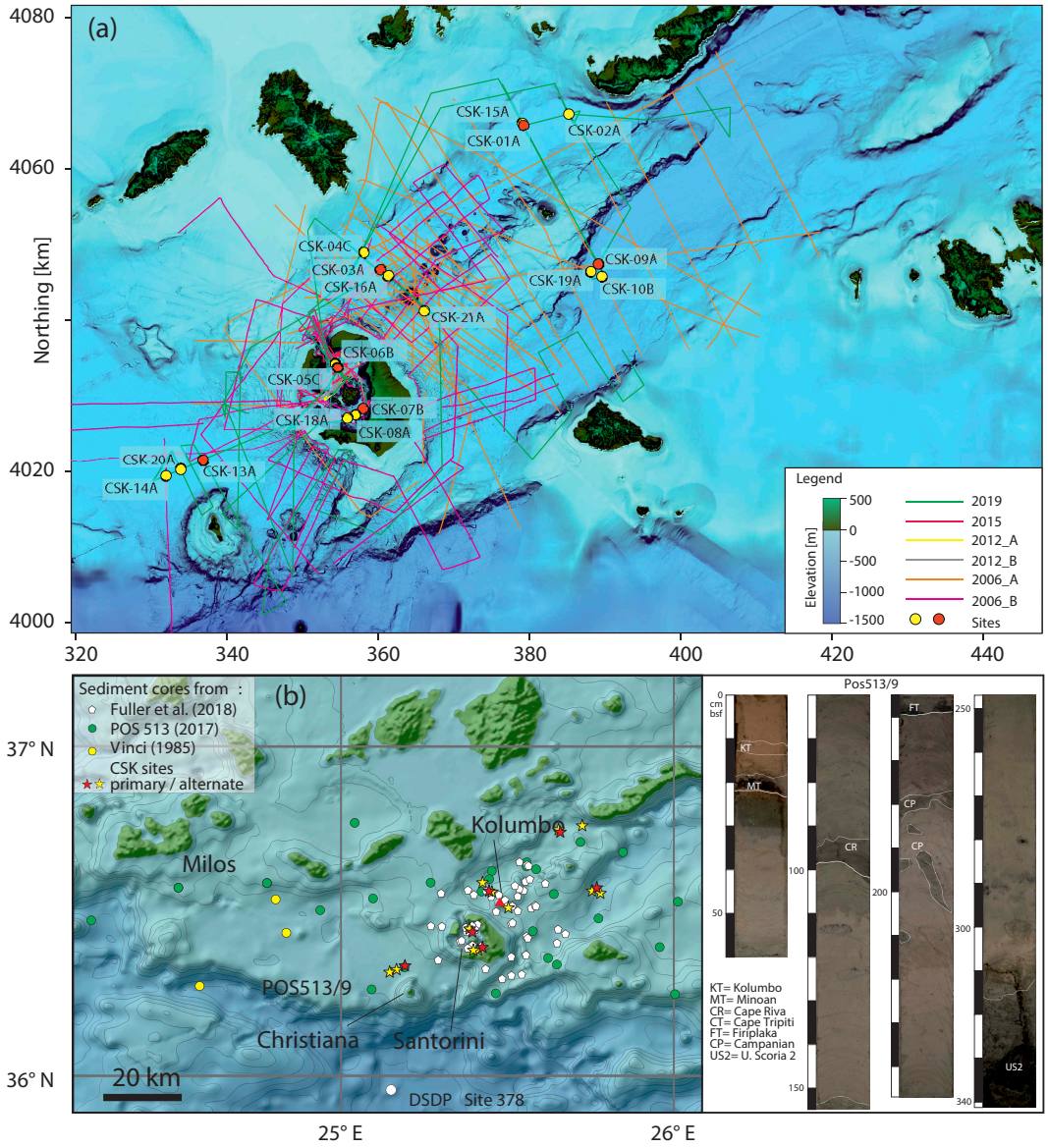

Figure F2. A. Available seismic lines in and around CSK volcanic field, with Expedition 398 proposed sites. B. Shallow gravity and box coring carried out to date near volcanic field and gravity core example illustrating lithologies present in upper few meters of marine sediments (Kutterolf et al., 2021a).

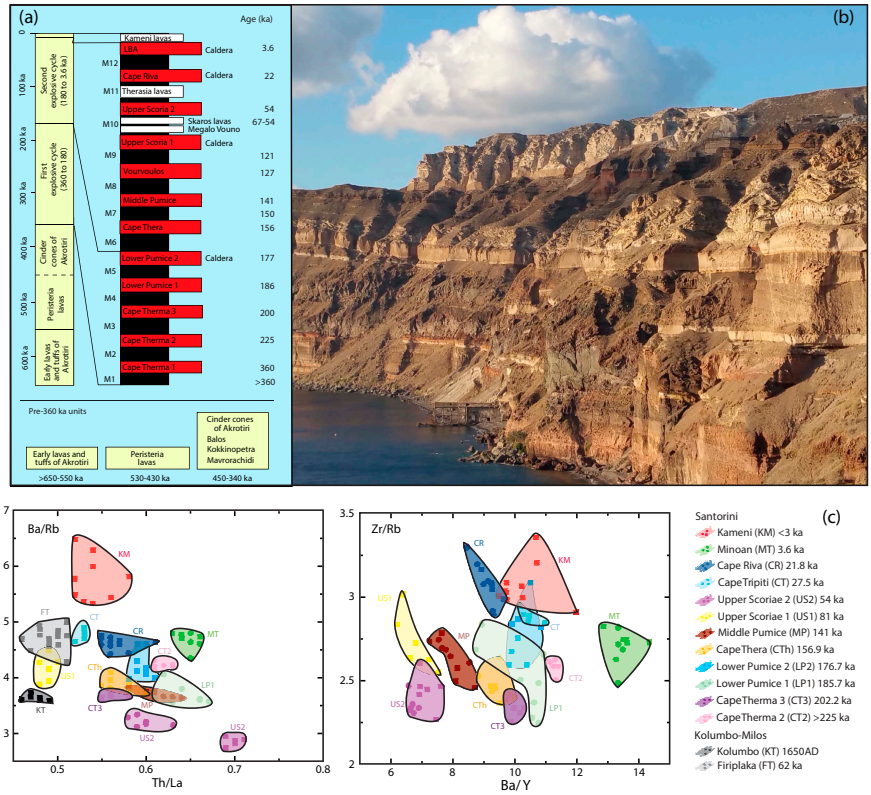

Figure F3. A. Santorini Volcano chronostratigraphy, showing Plinian eruptions (red) and inter-Plinian periods (black and white). Most of the Plinian eruptions poured pyroclastic flows and showered fallout tephra into surrounding marine basins. Eruption ages taken from Druitt et al. (1999), Fabbro et al. (2013), and Wulf et al. (2020). B. Lavas and tuffs from Santorini eruptions preserved onshore in caldera cliffs. Lateral equivalents of many of these tuffs are expected to be encountered in marine cores. C. Juvenile glasses of many of the CSK volcanic field (and neighboring Milos Volcano) eruptions can be distinguished based on their trace element signatures (modified from Kutterolf et al., 2021a).

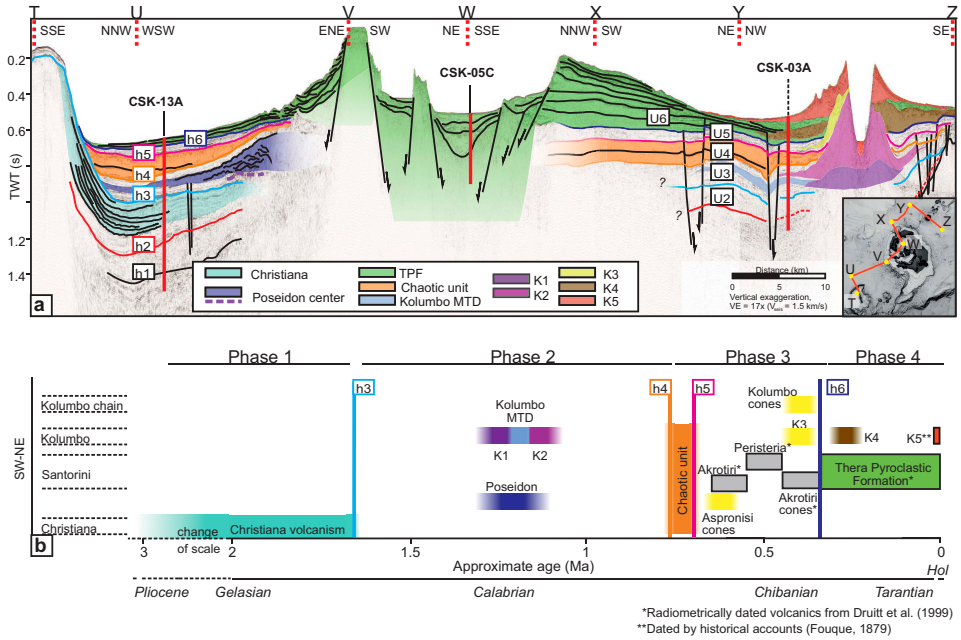

Figure F4. A. Composite seismic profile across CSK volcanic field, from Christiana to Kolumbo, showing three primary sites. Bases of Seismic Units U1–U6 are defined by Reflectors h1–h6, respectively. Kolumbo Volcano products are divided into five seismically defined units (K1–K5). TPF = Thera Pyroclastic Formation of Santorini (<360 ka). B. Interpretation of chronostratigraphic context of different seismic units. Modified from Preine et al. (2022).

3. Background

3.1. Geological setting

The Hellenic volcanic arc owes its existence to subduction of the African plate beneath the European plate, and was initiated in the Pliocene (Pe-Piper and Piper, 2005; Shaw and Jackson, 2010). The subducted slab descends at an angle of 10°–30°, and the back-arc Aegean region has been in extension since the Pliocene because of slab rollback (Jolivet et al., 2013; Papazachos, 2019). The convergence rate along the arc is 35 ± 8 mm/y, which is split into 5–10 mm/y of relative motion between the Eastern Mediterranean and the Aegean and ~25 mm/y of slab rollback. Back-arc extension has thinned the Aegean continental crust, creating horsts and grabens (Le Pichon and Kreemer, 2010; Royden and Papanikolaou, 2011) (Figure **F1**). The Hellenic subduction system has one of the oldest (coolest) slabs and lowest convergence rates on Earth (Syracuse et al., 2010).

The island arc consists of five volcanic fields (Druitt and Vougioukalakis, 2019): Sousaki, Aegina-Poros-Methana, Milos, CSK, and Kos-Nisyros-Yali, from west to east. The CSK volcanic field lies in the center of the arc on 18–20 km of thinned continental crust (Makris et al., 2013). It is located in a rift zone 100 km long and 45 km wide, with three main northeast–southwest-oriented marine basins and Pliocene–Quaternary sedimentary fills up to ~1 km thick (Piper and Perissoratis, 2003; Nomikou et al., 2016b, 2018) (Figures **F1**, **F4**, **F5**). The Anhydros Basin contains the Kolumbo volcanic chain, whereas the Amorgos and Anafi (also called "Santorini-Anafi") Basins lack volcanoes. The Anhydros and Anafi Basins each contain six seismic stratigraphic units (here named Units B1–B6 from the base up), separated by onlap surfaces (Figure **F5**), whereas the Amorgos Basin only contains Units B3–B6 (Nomikou et al., 2018). Thickness variations of the units record initial symmetric rifting (Units B1–B3) followed by northwest-tilted, more asymmetric rifting (Units B4–B6). Rifting began at 3.8–5.3 Ma in the Pliocene and is proceeding at about 2.5 mm/y (Nomikou et al., 2018).

The Christiana Basin is a broad, fault-bounded basin at the southwest entrance of the rift zone (Figure **F6**) that contains Pliocene–Quaternary sediments and volcaniclastics, with six major units (U1–U6) (Preine et al., 2022).

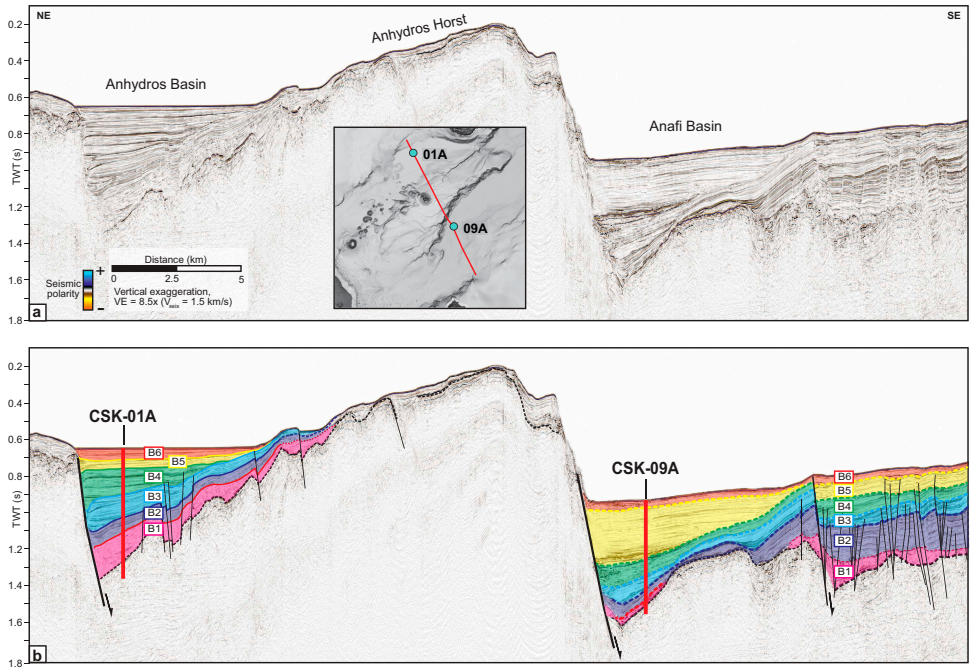

Figure F5. A–B. Locations and seismic context of primary Sites CSK-01A and CSK-09A in Anhydros and Santorini-Anafi Basins northeast of Santorini. Basin fills have six seismic stratigraphic units (B1–B6), following Nomikou et al. (2018).

The Santorini caldera is a complex 11 km × 7 km structure caused by at least four collapse events over the last 200,000 y, the last of which was the LBA eruption (Druitt and Francaviglia, 1992). It has a northern basin 390 m deep, a southern basin 280 m deep, and is connected to the sea via three breaches (Figure **F7A**) (Nomikou et al., 2014). The caldera's volcano-sedimentary fill is about 1 km thick (Budetta et al., 1984). The Kameni Islands are the subaerial summit of a 470 m high intracaldera edifice formed since the LBA eruption.

Volcanism at Santorini began at 650 ka with submarine and then subaerial effusive activity and became highly explosive at 360 ka (Thera Pyroclastic Formation; Figure **F3**). There have since been at least 12 Plinian eruptions (and approximately 100 less intense explosive eruptions), many of which generated high ash plumes and pyroclastic flows that entered the sea (Druitt et al., 1999). The LBA eruption in 1630 BCE discharged several tens of cubic kilometers of silicic magma as fallout and pyroclastic flows (Sparks and Wilson, 1990; Druitt, 2014), and the resulting subsidence deepened an already existing caldera (Athanassas et al., 2016). After the caldera had collapsed, the sea broke through the northwest breach, carving out a 2 km wide submarine channel (Nomikou et al., 2016a). Kameni Volcano has had nine subaerial effusive eruptions from 197 BCE to 1950, but bathymetry suggests a long previous submarine history (Pyle and Elliott, 2006; Nomikou et al., 2014).

Seismic profiles reveal three main units in the topmost caldera fill (here named Units S1–S3; Figure **F8**), interpreted most recently as follows (Johnston et al., 2015; Nomikou et al., 2016a):

- S1: Flat-lying sediments up to 40 m thick; mass wasting of the caldera cliffs;
- S2: Sediments up to 100 m thick that merge into the clastic apron of Kameni edifice; tuffs and hyaloclastites from the submarine phase of Kameni; and
- S3: Down-faulted deposits up to 250 m thick; uppermost levels of LBA intracaldera tuffs and/or sediments related to posteruptive flooding of the caldera.

Sub-S3 deposits lack layering on seismic images and are tentatively interpreted to be LBA intercaldera tuffs. Other less detailed interpretations have also been proposed (Perissoratis, 1995; Sakellariou et al., 2012).

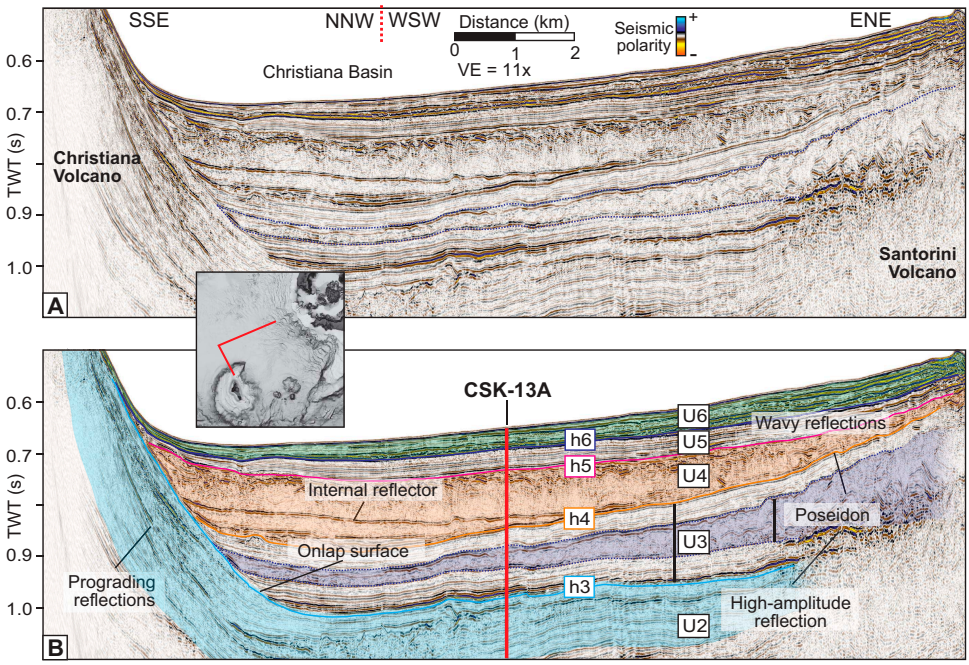

Figure F6. A–B. Location and seismic context of Site CSK-13A in Christiana Basin southwest of Santorini. Basin fill has six seismic stratigraphic units (U1–U6), each defined by prominent reflector (labeled h1–h6). Modified after Preine et al. (2022). VE = vertical exaggeration.

The low-density anomaly imaged by PROTEUS inside the caldera is a vertical cylinder 3.0 ± 0.5 km in diameter extending from 400 to 3000 mbsf of the northern basin of the caldera (Figure **F7**). It may be a large vent or collapse structure related to the Kameni Volcano, the LBA eruption, or earlier caldera-forming eruptions (Hooft et al., 2019). An episode of seismic unrest at Santorini from January 2011 to March 2012 was accompanied by up to 10 cm of inflation on Nea Kameni Island; it has been attributed to intrusion of magma 3–6 km beneath the caldera (Parks et al., 2015). The focus of uplift in 2011–2012 directly overlies the low-density anomaly (Figure **F7**), suggesting a relationship between them (Hooft et al., 2019). An upper crustal magma reservoir has been imaged by seismic tomography beneath Santorini and extending northeastward toward the Kolumbo Volcano (McVey et al., 2019).

The extinct Christiana Volcano produced lavas and tuffs of unknown ages (Aarburg and Frechen, 1999), but a particularly large ignimbrite found on neighboring islands is dated at 1.00 ± 0.05 Ma

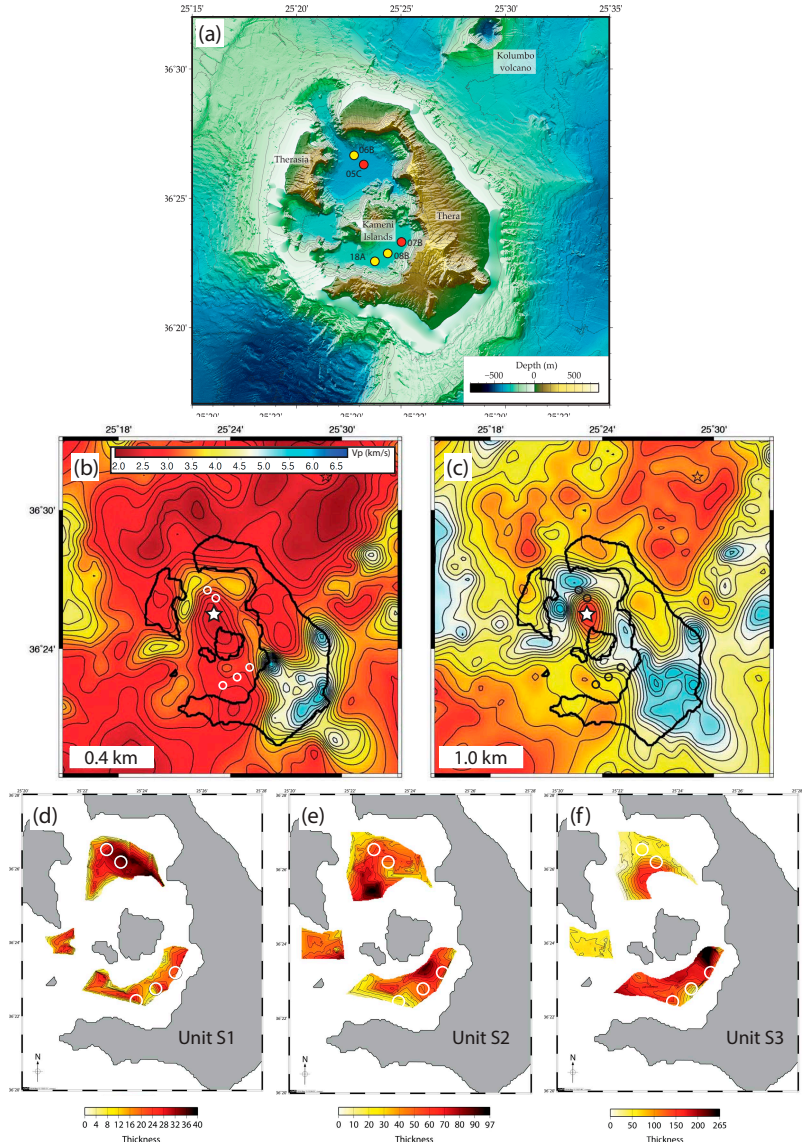

Figure F7. A. Bathymetric map of Santorini caldera (Nomikou et al., 2016b), showing drill sites (red = primary, yellow = alternate) and selected seismic lines. B, C. Horizontal sections (0.4 and 1.0 km depths) through low-velocity seismic anomaly in Santorini caldera (after Hooft et al., 2019). Anomaly forms vertical cylinder in 3-D extending 0.4–3 km (approximate) depth below caldera floor. Center of anomaly coincides with focus of caldera floor uplift during unrest in 2011–2012 (white star; Newman et al., 2012; Parks et al., 2015). Open circles = proposed primary and alternate drill sites. D–F. Thicknesses and areas of Seismic Units S1–S3 in Santorini caldera, calculated assuming mean sound velocity of 1900 m/s (from Johnston et al., 2015). Open circles = proposed primary and alternate drill sites.

(Keller et al., 2010). Geochemical and $^{40}Ar/^{39}Ar$ dating studies of onland Christiana volcanics are in progress (Vrije Universiteit, Amsterdam).

Kolumbo Volcano rises 480 m above the surrounding seafloor, with a 1.7 km diameter summit crater formed in 1650 (Nomikou et al., 2012; Carey et al., 2013). Seismic profiles across it reveal five units interpreted to be Kolumbo-derived volcaniclastics (Units K1–K5 from the base up), with Unit K5 representing the 1650 eruption (Hübscher et al., 2015) (Figure **F9**). The submarine cones northeast of Kolumbo postdate Unit K2 on seismic profiles (Figure **F4**); they are much smaller than Santorini or Kolumbo, and their products are not expected to be prominent in our drill cores.

Based on the compiled seismic data set, the entire CSK volcanic field evolved during four phases (Preine et al., 2022; Figure **F4**). Phase 1 initiated in the Pliocene with the formation of the Christiana Volcano. The formation of the current southwest–northeast trending rift system (Phase 2) was associated with the evolution of two distinct volcanic centers: the newly discovered Poseidon Center and the early Kolumbo Volcano. Phase 3 saw a period of widespread volcanic activity throughout the entire rift. The ongoing Phase 4 is confined to the Santorini caldera and Kolumbo Volcano.

3.2. Previous drilling

There have been two previous deep-drilling initiatives in or near the CSK volcanic field. Deep Sea Drilling Project (DSDP) Leg 42A Site 378 (344 mbsf) was drilled in the Cretan Basin 60 km south-southwest of Santorini in 1975; it penetrated Quaternary and upper and lower Pliocene sediments and bottomed in Messinian evaporites (upper Miocene) but recovered few volcaniclastics (Hsü et al., 1978). Land-based drilling in the Santorini caldera was carried out in 1987–1988 on the Kameni Islands to 201 m penetration, but the volcanics were variably altered and stratigraphic control was poor (Arvanitides et al., 1988).

Numerous shallow gravity cores have been sampled around and east of the volcanic field (Wulf et al., 2020; Kutterolf et al., 2021a, 2021b). These cores have intersected many fallout tephra layers and also some distal flow deposits from Santorini, Kolumbo, and other Mediterranean volcanoes. These cores provide samples of the types of sedimentary and volcanic lithologies to be expected in deep drilling (Figure **F2B**).

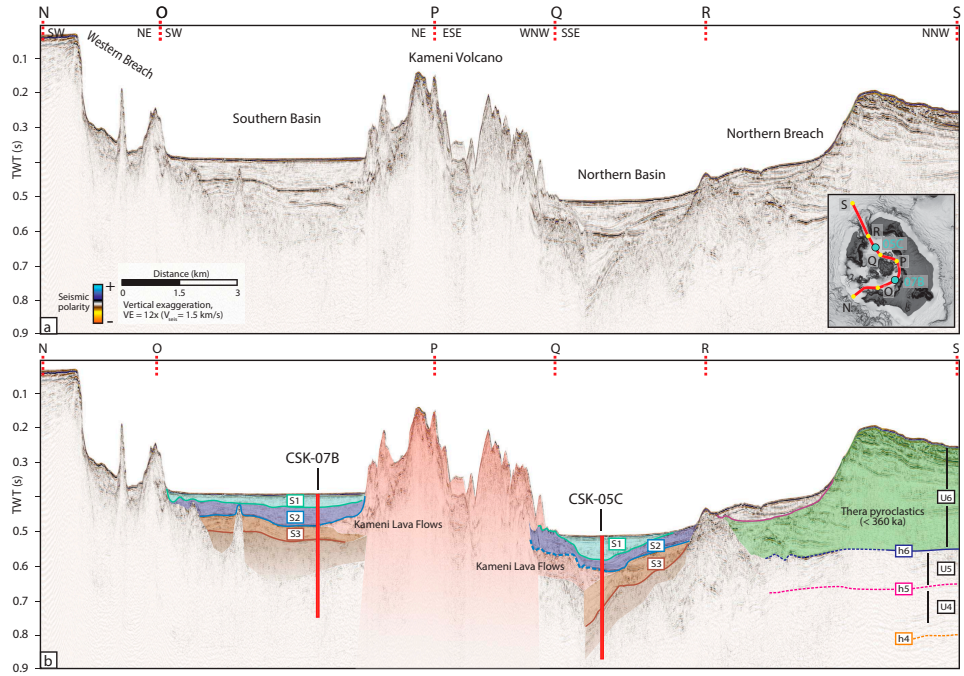

Figure F8. A–B. Locations and seismic context of Sites CSK-05C and CSK-07B in northern and southern caldera basins of Santorini, respectively. Basin fills have three seismic stratigraphic units (S1–S3) recognized by Johnston et al. (2015).

3.3. Seismic studies/site survey data

The supporting site survey data for Expedition 398 are archived at the IODP Site Survey Data Bank (**https://ssdb.iodp.org/SSDBquery/SSDBquery.php**; select P932 for proposal number).

A dense network of multichannel seismic (MCS) and single-channel seismic reflection profiles (campaigns in 2006–2015; Figure **F2A**) from collaborating groups and publications have been interpreted in detail in the Santorini caldera (based on the volcanic history recorded on land; Johnston et al., 2015) and in the basins northeast of Santorini, as well as to the southwest in the Christiana Basin (Sigurdsson et al., 2006; Hübscher et al., 2015; Nomikou et al., 2016a, 2016b, 2018; Tsampouraki-Kraounaki et al., 2018). A further 620 km of new, high-quality MCS profiles was shot in October 2019 on the German ship R/V *Poseidon* (Cruise POS538) under the leadership of Dr. Jens Karstens from GEOMAR Helmholtz Centre for Ocean Research Kiel (Preine et al., 2022). All profiles, which sum to 3350 km in length, were recorded with different sources and streamers and were merged into a homogeneous data set at the University of Hamburg (Germany). We adopted a velocity model based on MCS profiles and refined it using the diffraction-extraction technique (Schwarz and Gajewski, 2017). These velocities are lower than those based on tomography but are probably more accurate at shallow depths. As shown by Preine et al. (2022), a reliable traveltime to depth conversion even of the single-channel seismic data is now possible, which will allow for trustworthy core-seismic integration. At greater depth, velocity models are based on tomography (Hooft et al., 2019). All proposed primary drilling sites are situated at (or very close to) the intersections of MCS profiles.

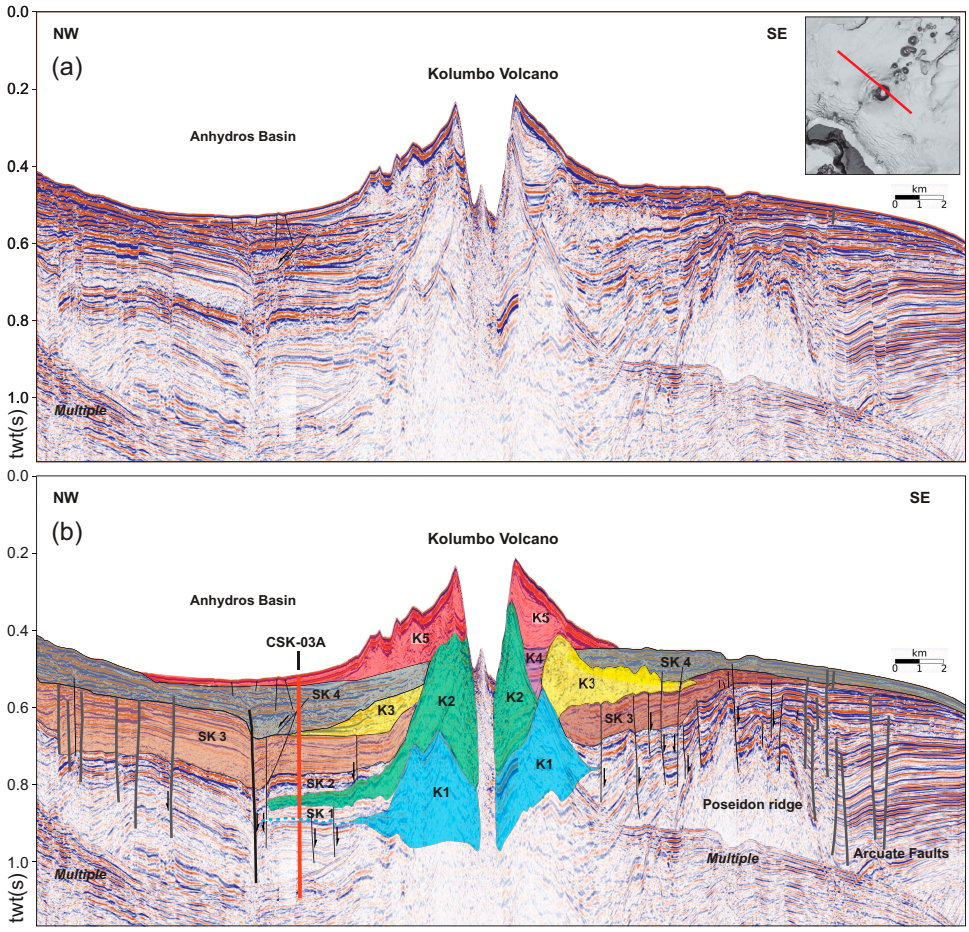

Figure F9. A–B. Northwest–southeast interpreted MCS profile (from Hübscher et al., 2015), showing edifice of Kolumbo Volcano formed during 1650 eruption (Unit K5) and buried edifices from older eruptions of same volcano (Units K1–K4). Units SK1–SK4 are volcano-sedimentary packages expected to contain Santorini-derived volcaniclastics. Primary Site CSK-03A will penetrate Units K5 and SK1–SK4, as well as thin lateral continuations of Units K1–K3.

In addition to the seismic survey and interpretations, fault distributions and throws have been mapped northeast of Santorini (Nomikou et al., 2016b; Hooft et al., 2017), and two-way traveltime (TWT) isopach maps have been constructed for each rift basin. During the 2015 PROTEUS cruise (Hooft et al., 2019), 3.5 kHz subbottom profiling, gravity, and magnetic data were recorded. High-resolution multibeam bathymetry is available inside and outside the Santorini caldera (Nomikou et al., 2014, 2016a; Hooft et al., 2017), as are isolated heat-flow measurements (Hannington et al., 2018).

Shallow sediments at or close to the drill sites provide initial sediment properties and tephrochronostratigraphic interpretations (Kutterolf et al., 2021a, 2021b). A large database of radiometric ages (K-Ar, $^{40}Ar/^{39}Ar$, and ^{14}C) and whole-rock chemical analyses exist for onland volcanic deposits from the CSK centers, particularly Santorini, along with glass major and trace element analyses for marine ash layers back to 200 ka (e.g., Druitt et al., 1999; Wulf et al., 2020; Kutterolf et al., 2021a, 2021b).

4. Scientific objectives

4.1. Objective 1: arc volcanism in an active rift environment

Leading hypothesis: the CSK volcanic field has developed in a complex manner through time.

Analysis of existing seismic profiles northeast and southwest of Santorini have led to an interpretation of the development of the volcanic field in space and time (Figure **F4**). This interpretation invokes (in chronological order) the development of the Christiana Volcano (late Pliocene), followed by Kolumbo Seismic Units K1 and K2 and an offshore submarine center (Poseidon; early Quaternary), a chaotic mass transport deposit (MTD) of unknown origin, deposits from the Akrotiri and Peristeria Volcanoes, the Kolumbo eruption corresponding to Unit K3 and Kolumbo submarine cones (0.65–0.35 Ma), and the post-0.35 Ma explosive products of Santorini (Thera Pyroclastic Formation) and Kolumbo eruptions corresponding to Units K4 and K5.

We will test this hypothesis using cores from all sites to reconstruct a complete volcanic stratigraphy of the CSK volcanic field since rift inception in the Pliocene, consistent with both onshore and offshore constraints. Were there earlier, now-buried volcanic centers in the area? How are large eruptions distributed spatially and temporally along the volcanic field? What is the enigmatic chaotic submarine Unit U4 (Figure **F4**) observed seismically by Preine et al. (2022)? How do eruptive styles at individual centers evolve through time? Using seismic profiles linked to the cores, we will estimate eruptive volumes and fluxes for the different eruptive centers and for the CSK field as a whole.

Eruption products will be preserved in the rift basins not only as tephra fallout but also as turbidites channeled down the basin axes from volcanoes upslope (e.g., Schmincke and Sumita, 1998). Using criteria for recognizing eruption-related turbidites (Table **T1**), we will correlate primary volcaniclastic beds based on chemical and textural criteria between cores, as well as link core material to the source volcano using onland (subaerial Christiana; Santorini) and drilled (submarine Kolumbo) near-source sequences. Bed-to-bed and seismic unit-to-unit correlation between cores will use major and trace element compositions of juvenile blocks or lapilli, glasses, crystal-hosted glass inclusions (e.g., Brandl et al., 2017), and phenocrysts. Pyroclast textures (e.g., vesicle abundances, sizes, and shapes) and accidental lithic assemblages will aid in correlation, as will physical properties measured aboard *JOIDES Resolution*. Correlation of volcaniclastics to source volcanoes will exploit established chemical and mineralogical differences between the different volcanic centers, extending chemical correlation databases already developed for the <0.2 Ma tephra layers (Figure **F3C**; Kutterolf et al., 2021a, 2021b). Tephra fall layers from other circum-Mediterranean volcanoes will serve as marker beds (Satow et al., 2015; Wulf et al., 2020). Absolute dates of cored volcanic layers based on (1) published onshore ages, (2) published ages of marine tephra fall layers, and (3) new radiometric age determinations on suitably fresh drilled pyroclasts (Table **T1**) will refine the volcanic chronostratigraphy. The results will contribute to existing facies models for explosive volcanoes in marine settings (e.g., Schmincke and Sumita, 1998).

4.2. Objective 2: the volcano-tectonic connection

Leading hypothesis: rifting has exerted a control on spatial and temporal development of volcanism in the CSK volcanic field, with links between major crustal tectonic events and eruption history.

Studies of Miocene plutons, fault patterns along the modern-day arc, and relationships between regional seismicity and caldera unrest at Santorini in 2011–2012 all hint at intimate relationships

Table T1. Selection of methods related to primary objectives, Expedition 398.

Criteria for interpretation of turbidites and debris flows (Objective 1, 2, and 4)	
Primary, eruption-generated turbidite	Homogeneity of juvenile components. Texture similar to onland deposits with lithic and pumice grading. Consistency with onland or upslope eruption stratigraphy. Consistency with onland or upslope eruption lithic assemblage. Use of particle textures to distinguish subaerial from submarine eruption (Schindlbeck et al., 2013; Freundt et al., 2021).
Secondary, reworked eruption-generated turbidite	Homogeneity of juvenile components. Texture similar to onland deposits with lithic and pumice grading. Possibly more heterogeneity than primary turbidite. Repetition in the sequence. Inconsistency with onland or upslope stratigraphy.
Seismogenic (or tsunamigenic) turbidite	Polylithologic. No magmatic component, or multiple populations of magmatic components. Possible presence of fault-scarp-derived lithologies. May overlie onlap surface on seismic profile.
Establishment of a chronostratigraphy (Objectives 1 and 2)	
Biostratigraphy	Microfossil assemblages will be used to construct a biostratigraphic framework, similar to that using the calcareous nannofossils *Ceratolithus tricorniculatus* and *Gephyrocapsa oceanica* in DSDP Hole 378 of the Cretan Basin.
Radiometric dating	Some primary core volcaniclastic beds will be dated directly by K-Ar or $^{40}Ar/^{39}Ar$ methods on large juvenile clasts (groundmass separates), if sufficiently fresh.
Oxygen isotope stratigraphy	Oxygen isotope stratigraphy of planktonic foraminifers will be established and correlated with the existing 5 My orbitally tuned and millennially resolved eastern Mediterranean ^{18}O stacks (Wang et al., 2010; Grant et al., 2012).
Sapropel stratigraphy	Sapropel occurrences will be matched to astronomically tuned sapropel cycles (Rohling et al., 2015; Grant et al., 2016), the sequences and ages of which are known to within 1000 years in the Mediterranean back to the Pliocene (target curve La2004; Laskar et al., 2004).
Reversal-based magnetostratigraphy	Provided sediments carry a strong natural remanent magnetization, geomagnetic polarity reversal-based magnetostratigraphy (Papanikolaou et al., 2011; Roberts et al., 2013) would target the Brunhes/Matuyama boundary at 0.78 My, the Jaramillo Subchron (1.068–0.987 My), and the Olduvai Subchron (1.778–1.945 My). All onland eruption products of Santorini are <0.65 My and are normally magnetized.
Relative paleointensity	Relative magnetic paleointensity (RPI) records will be compared with well-established global RPI records such as SINT2000 (Valet et al., 2005) and PISO1500 (Channell et al., 2009), validated to 2.0 and 1.5 My, respectively, while being aware of potential complications (Roberts et al., 2013).
Textural characterization (Objectives 1, 2, 4, and 5)	
Magma fragmentation mechanisms	Particles fragmented by bubble exsolution and growth have highly vesicular textures, whereas those produced by water-melt interaction have surface quench cracking, blocky shapes with stepped fractures or moss-like features (Zimanowski et al., 2015). Crystal and bubble size distributions will allow estimation of histories of magma ascent and bubble nucleation and growth (Giachetti et al., 2010; Rotella et al., 2015).
Turbidite types; tsunami deposits	Combined high-resolution textural (CT-scan) and geochemical (μ-XRF core scanner) characterization of turbidites will allow distinguishing of different types of turbidites. The same method could be applied to primary tsunami deposits (if preserved in the sedimentary record).
Deposit emplacement temperature	If chemical remanence is taken into account, thermal remanent magnetism studies of lithic clasts in submarine mass flow deposits enable estimation of emplacement temperatures (Bardot and McClelland, 2000) and distinction close to the shoreline between debris flow (<100°C) and subaqueous pyroclastic flow (>100°C) deposits.
Chemical, petrologic, and isotopic characterization (Objective 4)	
Magma petrogenesis and crustal interaction	Chemical (major and trace elements) data on suitably fresh juvenile samples, with radiogenic (Sr, Nd, Pb, Hf, and U-Th) and stable (O) isotopic analyses on selected samples, will enable us to track parental magma composition and degree of crustal assimilation in space and time since the Pliocene using classical geochemical approaches (Francalanci et al., 1995; Vaggelli et al., 2009; Klaver et al., 2016b). The role of deep-crustal amphibole in magma genesis will be tracked by the presence/absence of phenocrystic amphibole, and by trace element signatures of amphibole involvement (low Y and low Dy/Yb; Davidson et al., 2007).
Magma pre-eruptive storage depths	Variations of magma storage depths will be constrained using mineral barometry (Putirka, 2008) and the volatile contents of crystal-hosted melt inclusions (Druitt et al., 2016) if suitably unaltered.

between Aegean volcanism and crustal tectonics (Kokkalas and Aydin, 2013; Feuillet, 2013; Rabillard et al., 2018; Heath et al., 2021). We will test the leading hypothesis by (1) reconstructing the histories of subsidence and tectonics of the Anhydros, Anafi, and Christiana Basins from our drill cores and seismic records, (2) integrating them with our volcanic chronostratigraphy, and (3) seeking relationships between CSK volcanism and major crustal tectonic events.

We will reconstruct the sedimentary and subsidence histories of the basins using sediment-focused chronostratigraphic techniques: biostratigraphy, oxygen isotope and sapropel records, magnetostratigraphy, and relative magnetic paleointensity (Table **T1**) while noting that high sedimentation rates (order of magnitudes of 0.1 mm/y in the rift basins, 1 cm/y in the caldera, and >1 m/y for eruption units) and slumping may complicate use of these methods. Inclusion of the volcanic record will then build a detailed, rift-wide stratigraphy with multiple independent age markers, enabling construction of a Bayesian age model for each basin (Lougheed and Obrochta, 2019). Benthic foraminifers from fine-grained sediments (low-energy environments where the likelihood of microfossil reworking is reduced) will provide estimates of paleowater depth and, via integration with seismic profiles and chronologic data, time-integrated basin subsidence rates (Pallikarakis et al., 2018). Benthic foraminifers can predict water depths as deep as 850 m with accuracies of ±50 m in the Mediterranean back to the early Pleistocene (Avnaim-Katav et al., 2016; Milker et al., 2017).

Major rifting events in the basins will be recognized on seismic profiles principally from onlap surfaces (five of which have been recognized to date in the Anhydros and Anafi Basins; Figure **F5**) and levels of fault termination, assisted by predominant microfault directions logged in the cores. The presence of thick seismogenic turbidites (Goldfinger, 2011; Polonia et al., 2013; Sumner et al., 2013; Table **T1**) and/or homogenites (slumping of hemipelagic muds; Beck et al., 2007) in the cores may record large-magnitude seismic events and tsunamis.

By exploiting downhole seismic velocity measurements, we will match our core stratigraphies to seismic profiles and generate a time series of intercorrelated volcanic and tectonic histories of the basins that will be used to seek relationships between volcanism and major tectonic events. When did volcanism start relative to rifting? Do large tectonic events recorded by the five main onlap surfaces in the Anhydros and Anafi Basins or any prominent seismogenic sedimentary beds correlate with (1) activation of the different volcanic centers, (2) changes in eruptive style (e.g., the onset of major explosive activity at Santorini at 360 ka), or (3) particularly large explosive eruptions? In particular, did the change from symmetric (Basin Units B1–B3) to more asymmetric (Units B4–B6) rifting northeast of Santorini coincide with a change in the rate or type of volcanism at any of the CSK centers? Can we relate the reconstruction of rift development and volcanism to published histories of Hellenic subduction, slab rollback, and back-arc extension (Jolivet et al., 2013)?

We will also investigate how sea level modulates volcanic activity, although this will be challenging. There is already evidence for a sea level influence on Mediterranean volcanism (McGuire et al., 1997; Sternai et al., 2017; Satow et al., 2021). Our proposed drill core–based eruption time series will enable us to push these investigations into the Pliocene and exploit existing sea level curves back to 5 Ma (Grant et al., 2012, Rohling et al., 2014). Approximate paleodepth data from benthic foraminifers may help quantify the eustatic and regional tectonic contributions to sea level variations.

4.3. Objective 3: arc magmatism in a region of extending crust

Leading hypothesis: rift-driven crustal thinning influences magma petrogenesis through its effects on magma storage, differentiation, and contamination in the crust.

Magmas of the CSK field have ascended through 18–20 km of rifted continental crust, which has influenced their chemical and isotopic evolution (Bailey et al., 2009; Elburg et al., 2014). Primitive basaltic melts rise into the crust, where they evolve to intermediate and silicic compositions through fractional crystallization, crustal melting/assimilation, and magma mixing (Cashman et al., 2017). Crustal differentiation pathways vary significantly in the CSK field (Mortazavi and Sparks, 2004; Klaver et al., 2016a). Some silicic magmas such as those of Christiana, Santorini

(>550 ka), and Kolumbo show evidence (low Y, high Ba/Y, and low Dy/Yb) of interaction with amphibole-rich regions in the lower crust (amphibole "sponge" of Davidson et al., 2007), whereas others (Santorini < 550 ka) lack such evidence and differentiate by fractional crystallization of anhydrous minerals (Francalanci et al., 2005). The factors governing formation of an amphibole sponge, or lack of it, are debated (Smith, 2014; Klaver et al., 2018). At the CSK volcanic field, variations in the stability of amphibole cannot be attributed to differences in major element compositions or water contents of the primary magmas, so external factors may be responsible. It is likely that the structure of the rifted crust governs the polybaric ascent history of the CSK magmas, with evolving faults, density interfaces, and rheological transitions (Jolivet et al., 2013) controlling levels of magma storage and differentiation (Flaherty et al., 2018), as observed in the exhumed Miocene magmatic complexes of the Aegean (Rabillard et al., 2018).

Estimates from rift cross sections (Nomikou et al., 2018) suggest 10%–20% of horizontal extension since the late Pliocene, corresponding to 2–4 km of crustal thinning. This progressive rifting and thinning of the continental crust beneath and around the CSK volcanoes allows us to test the leading hypothesis. Most of the volcaniclastics in our basin drill holes will probably be from explosive eruptions of intermediate or silicic magmas. We will investigate magma genesis using major, trace, and multi-isotopic data on suitably fresh rocks. Volatile contents of crystal-hosted melt inclusions and mineral-barometry techniques will be used to quantify magma storage depths during ascent prior to eruption (Table **T1**). These data will constrain how mantle source characteristics and heterogeneity (Bailey et al., 2009; Klaver et al., 2016b), degree of magma contamination by the crust, and the role of lower crustal amphibole have varied in space and time since the Pliocene across the volcanic field.

4.4. Objective 4: unraveling an iconic caldera-forming eruption

Leading hypothesis: the LBA caldera-forming eruption shed large volumes of tsunami-generating pyroclastic flows into the sea, forming marine deposits up to 80 m thick.

The LBA eruption of Santorini has attracted attention for many decades (Friedrich 2009), and the onland products have been studied in detail (Sparks and Wilson, 1990; Druitt, 2014). More recently, seismic studies have imaged the LBA products both outside (Sigurdsson et al., 2006) and inside (Johnston et al., 2015) the caldera, although their firm identification on seismic profiles is problematic because of the many other eruptions and tuffs with which they can be confused. Full understanding of this famous eruption awaits deep drilling, although new interpretations based on the new 2019 seismic profiles are already ongoing (J. Karstens, pers. comm., 2021).

The eruption began with phases of Plinian fallout and violent phreatomagmatic explosions, followed by outpouring of hot pyroclastic flows into the sea. The eruption caused collapse of the present-day caldera, but whether collapse took place during or after the eruption is not known (Sparks and Wilson, 1990). Tsunamis that impacted the coasts of the Eastern Mediterranean and northern Crete (Bruins et al., 2008) may have been generated by the entry of pyroclastic flows into the sea (Nomikou et al., 2016a). Impacts of these waves on ports, shipping, and trade have been implicated in weakening the Minoan civilization on Crete prior to its collapse (Bruins et al., 2008).

LBA tuffs accumulated outside the caldera are inferred from seismic profiles to be up to 80 m thick and have an estimated volume in the range of 30–60 km^3 (dense-rock equivalent; Pyle, 1990; Sigurdsson et al., 2006). Drilling will enable us to test the leading hypothesis by coring the LBA deposits both outside and inside the caldera and by groundtruthing the seismic profiles using downhole measurements of seismic velocities. Conventional gravity coring is not sufficient for this purpose because the LBA deposits are far too thick. Outside the caldera, drilling will penetrate the LBA submarine pyroclastic flows at primary Sites CSK-03A and CSK-13A, testing the published seismic interpretation. This will in turn enable refined volume estimates for the flows, feeding into models of tsunami impact on the Bronze Age Aegean world (Novikova et al., 2011). Textural and paleomagnetic (thermal remanent magnetism; Table **T1**) analysis of the flow deposits will characterize the transformation of (hot) subaerially erupted pyroclastic flows into (cold) debris flows and turbidity currents upon entry into the sea (Schmincke and Sumita, 1998; Kutterolf et al., 2014).

Inside the Santorini caldera, we will drill to 234 mbsf in the northern caldera basin (Site CSK-05C) and to 360 mbsf in the southern basin (Site CSK-07B). Seismic Units S1 (cliff mass wasting), S2 (Kameni volcaniclastics), and S3 (possible flood deposit) in the caldera have a combined thickness of 185 m at Site CSK-05C and 218 m at Site CSK-07B (Figure **F7D–F7F**). Thus, our anticipated drilling will penetrate the top of the sub-S3 unit that is thought to possibly be intracaldera LBA tuffs. By drilling into the LBA tuffs in the caldera, we will be able to estimate their minimum volume, which we can then combine with volume estimates for LBA deposits onshore and offshore (outside of the caldera) to make a new, much more precise (minimum) estimate of the erupted volume.

We will also identify the deposits from different eruptive phases in the caldera fill and correlate them using textural and chemical criteria with the well-studied onland sequences (Druitt, 2014). The relative thicknesses of pyroclastic flow deposits inside and outside the caldera will tell us whether the caldera collapsed during or after the eruption (Sparks and Wilson, 1990; Druitt, 2014): pyroclastic flows can pond to great depths inside calderas if collapse takes place during eruption, but not if it occurs afterward (Lipman, 1997).

4.5. Objective 5: volcanic hazards from submarine silicic eruptions

Leading hypothesis: shallow-marine explosive eruptions of water-rich silicic magmas driven mainly by magmatic degassing, and with dispersion by fallout and density currents, have occurred repeatedly in the neighborhood of Santorini.

A potential future hazard at Santorini is a submarine eruption of the Kameni or Kolumbo Volcanoes similar to the one in 1650 but probably not as large. Better understanding of the dynamics of such eruptions will enable us to improve risk mitigation strategies in this highly populated and densely visited part of the Eastern Mediterranean (Vougioukalakis et al., 2016).

Three-quarters of global volcanism occurs under the sea, but the dynamics of submarine eruptions is poorly understood, particularly those of water-rich silicic magmas at island arcs (White et al., 2015, Carey et al., 2018). Possible tephra production mechanisms in the submarine realm include explosive fragmentation by bubble growth (magmatic explosive eruption), explosive fragmentation by water-magma interaction (phreatomagmatic explosive eruption), and autoclastic fragmentation (effusive eruption and hyaloclastite formation). The exact mechanisms likely depend on magma composition, magma volatile content, magma flux, and water depth (Rotella et al., 2015).

Studies of the 1650 Kolumbo eruption products show that the eruption was driven mainly by primary degassing of the water-rich silicic magma, but with a component of phreatomagmatic fragmentation, and that the deposits were emplaced by a combination of subaerial plumes, submarine plumes, and density currents (Cantner et al., 2014; Fuller et al., 2018). Drilling at Site CSK-03A will enable us to traverse the products of at least three earlier explosive eruptions of Kolumbo (Seismic Units K1–K3). We will use combined petrological, chemical, and textural studies (Table **T1**) to compare these earlier submarine eruptions to the one in 1650, test the leading hypothesis, and arrive at a general model for this rarely accessible type of submarine volcanism. Use of textural criteria for magmatic versus phreatomagmatic fragmentation (Table **T1**) will allow us to better understand the interplay of these processes as the Kolumbo cone grew through successive eruptions, with implications for tsunami genesis (Ulvrova et al., 2016).

Inside the Santorini caldera (Sites CSK-05C and CSK-07B), Seismic Unit S2 will provide access to a time series of postcaldera volcanism that dates back to the birth of Kameni after the LBA eruption to its emergence in 197 BCE. Using similar methods to those used at Kolumbo, we will reconstruct the history of eruption style (magmatic explosive, phreatomagmatic explosive, and/or effusive) during the growth of Kameni from 400 m water depth to the surface (sea level has changed <1 m over the past 3600 y). Has Kameni always been effusive, or has it had explosive submarine phases like Kolumbo that would need to be accounted for in hazard assessments? If so, did Kameni underwater eruptions exhibit the same dynamics as those of Kolumbo, given that both edifices erupt silicic magma?

The Kameni time series is also of petrological interest because it records the onset of a new caldera cycle following the LBA eruption (Pyle and Elliott, 2006). It is rare to have such a petrologic record of postcaldera volcanism at an arc caldera; the magmatic transition and long subsequent evolution of the new intracaldera volcano are seldom both preserved. Onland Kameni dacitic magmas and their mafic enclaves form a geochemical series that is lower in contents of incompatible elements (e.g., K, Rb, Nb, and Zr) than the LBA magma that preceded it and represent the arrival of a new magma batch from depth following the LBA eruption (Huijsmans et al., 1988; Zellmer and Turner, 2007). What compositions were the first Kameni magmas to erupt, and how have they evolved over the subsequent 3600 y? When did the changeover from residual LBA-type to Kameni-type magma take place, with what implications for posteruptive solidification of the LBA magma reservoir? Do barometric techniques such as the volatile contents of crystal-hosted melt inclusions (Druitt et al., 2016) record changes in magma storage depth over the lifetime of the Kameni Volcano? What are the implications for the mechanisms of postcaldera volcanism at Santorini and elsewhere?

4.6. Objective 6: transition from continental to marine environments in the southern Aegean

Drilling in the Christiana, Anhydros, and Anafi Basins (Sites CSK-13A, CSK-01A, and CSK-09A; Figures **F5**, **F6**) will enable us to pierce the entire basin stratigraphy and reach the basement unconformity (presubsidence land surface). This provides the opportunity to reconstruct the environmental histories of the basins from continental to deep marine stages, as well as the evolution of the Eastern Mediterranean paleoclimate, since the Pliocene. It will build on the ongoing analysis of cores from Site 378 in the Cretan Basin (Hsü et al., 1978) and will enable the establishment of a robust sedimentary reconstruction and time framework across the southern Aegean.

Uplift and erosion of the Aegean crust in the middle to late Miocene was followed by subsidence and marine transgression in the Pliocene and Quaternary. Seismic profiles at the Aegean margins reveal a gradual subsidence over 400,000 y (Lykousis et al., 2009). Commercial boreholes in the northern Aegean have revealed alluvial and lacustrine conditions in the Pliocene and early Pleistocene prior to marine transgression (Faugeres and Robert, 1976). However, the subsidence history in the southern Aegean is poorly known because of the paucity of offshore studies. We will build a high-resolution biostratigraphic framework for the recovered cores that along with stable isotope and alkenone profiles will provide a first-order bed-to-bed age control to be integrated into the chronological model of Objective 1 (Table **T2**). We will then extract a time series of paleoenvironmental data from the cores using assemblages of calcareous nannofossils, benthic foraminifers, dinoflagellates, and pollen, refined by stable oxygen and carbon isotopes, total organic carbon, major and trace elements, and organic biomarkers for selected depth intervals (Table **T2**).

4.7. Objective 7: biological systems reactions to volcanic eruptions and seawater acidification

The deep-marine biosphere hosts a large component of the world's microbial ecosystems, but little is known about them (Parkes et al., 2000; Schippers et al., 2005). Marine microbes have evolved to respond to environmental challenges, resulting in different survival mechanisms, growth strategies, and genetic adaptations. Knowing that the Santorini caldera harbors highly diverse, metabolically complex microbial communities (Oulas et al., 2016; Christakis et al., 2018), we will use core material from inside the caldera (Sites CSK-05C and CSK-07B) to characterize the living and fossilized subseafloor biological communities present. By applying the latest developments in analytical (geo)microbiology technologies, we will document the sizes, genetic variabilities, and metabolic functions of subsurface ecosystems to 300–400 m depth. We will also explore past anoxic events in the caldera subsurface, extant biological activity, and trace fossils of extinct seafloor life. Cores will offer potentially continuous records of (1) the impact of repeated eruptions of the Kameni Volcano, hydrothermal fluids, and seawater acidification on biological activity and (2) subsequent recolonization of the caldera floor (Danovaro et al., 2017).

Analytical methods will include cultivation experiments and state-of-the-art molecular omics study techniques to get a full picture of biological structural diversity, functional diversity, and

metabolic complexity (Table T2). Special emphasis will be given to the characterization of microbes associated with specific metabolic reactions and the identification of key metabolic processes. Effects of eruption-associated water acidification will be studied using synchrotron X-ray tomography for 3-D reconstructions of calcareous nannofossils (coccolithophores; Hönisch et al., 2012; Beuvier et al., 2019).

Table T2. Selection of methods and legal protocols relevant to Objectives 6 and 7, Expedition 398. MIS = marine isotope stage.

Paleoenvironmental analysis (Objective 6)	
Biostratigraphy	Microfossil assemblages, in particular calcareous nannofossils. At DSDP Site 378, the base of the marine sequence is dated as Early Pliocene (Biozone NN12) based on the presence of *Ceratolithus tricorniculatus*. The sequence extends up to NN19 based on the presence of *Gephyrocapsa oceanica*. (Athanasiou et al., 2015; Geraga et al., 2010; Gogou et al., 2016; Triantaphyllou et al., 2009a, 2009b, 2014, 2016, 2018.)
Calcareous nannofossils	Primary marine productivity; rapid response to variations in sea-surface temperature, sea-surface salinity, water column stratification, freshwater input, CO_2 variations affecting the carbonate system parameters. The abundance ratio between *Florisphaera profunda* (F) and *Emiliania huxleyi* (E) is used as a stratification index. *Helicosphaera* spp. (mainly *H. carteri*) together with *Braarudosphaera bigelowii* are used as indicators of salinity decrease. Previous studies of *Emiliania huxleyi* in the modern Aegean Sea provided strong evidence for seasonal variation in coccolith size, morphology, and calcification associated with carbonate system variations. (Triantaphyllou et al., 2016.)
Benthic foraminifers	Proxies for deepwater circulation and oxygenation, nutrient fluxes; approx. water paleodepth. Dysoxic to oxic bottom waters are characterized by a high abundance of benthic foraminiferal species tolerating surface sediment and/or pore water oxygen depletion (e.g., *Chilostomella mediterranensis* and *Globobulimina affinis*), and the presence of *Uvigerina mediterranea*, which thrives in oxic mesotrophic-eutrophic environments. (Triantaphyllou et al., 2009b, 2014; Avnaim-Katav et al., 2016; Milker et al., 2017.)
Dinoflagellates	Qualitative and comparative estimates of paleotemperature, paleosalinity, primary production, nutrient levels, bottom water anoxic/oxic conditions. The temperature index warm/cold (W/C) is derived from the warm-water dinocyst assemblage *Tuberculodinium vancampoae, Tectatodinium pellitum, S. nephroides, I. patulum, I. aculeatum, Pyxidinopsis reticulata, O. israelianum, Spiniferites mirabilis, S. hyperacanthus*, and the cold-water assemblage *N. labyrinthus* and *P. dalei*. (Geraga et al., 2010; Triantaphyllou et al., 2009a, 2016.)
Planktonic foraminifers	Powerful tool for estimation of past sea-surface temperatures and salinities; reconstructions of past water masses and circulation using the modern analog technique (MAT). Increased abundance of *Globigerina bulloides* suggests enhanced productivity in the water column. (Kouli et al., 2012, 2015.)
Pollen	Parameters such as terrestrial vegetation cover, humidity, runoff, and sediment influx are defined using Aegean pollen-based indices. Pollen data patterns organized in assemblage zones elucidate the occurrence - alternation of different vegetation types in time and contribute to estimation of climatic parameters such as humidity (H-index = AP/St, where AP is arboreal taxa excluding *Pinus* and St is steppic taxa) and relative temperature (T-index = cool temperate/(sum of temperate and Mediterranean taxa). (Rohling et al., 2014, 2015.)
Stable oxygen and carbon isotopes	Oxygen isotopes for ^{18}O stratigraphy and sea-surface temperatures and salinities. Carbon isotopes for relative contributions of marine/terrigenous organic matter. Negative shifts in foraminiferal $\delta^{18}O$ indicate cooling events. (De Lange et al. 2008; Katsouras et al. 2010; Filippidi et al. 2016).
Total organic carbon (TOC); major and trace elements	Paleoproductivity (e.g., TOC and Ba/Al) and preservation; in the absence of considerable diagenetic alteration in the sediments, enrichments observed in redox-sensitive elements represent initial depositional conditions. (Athanasiou et al. 2017; Gogou et al. 2007; 2016; Triantaphyllou et al. 2016.)
Alkenone-derived SSTs and selected lipid biomarkers	Alkenone/Uk37 index-based sea-surface temperature (SST) reconstructions are fundamental. Pliocene alkenone-SST record in the Eastern Mediterranean documents the "warm Pliocene" period (~4.1–3.25 Ma) characterized by mean SST of c. 26°C. Distinct SST minima at ~3.9 Ma, 3.58 Ma and between 3.34 and 3.31 Ma, correspond to the MIS Gi16, MIS MG12, and MIS M2 global cooling episodes, before onset of the Northern Hemisphere glaciation. (Triantaphyllou et al., 2016.)
Biological analysis (Objective 7)	
Sampling and processing	Carried out on board the ship using sterile conditions.
Minimize contamination	Use of seawater from pristine offshore locations for drilling mud. Avoiding sewage dumping during drilling. Surface seawater, drilling fluids, and onboard wastewater monitored for microbes. Core exteriors cleaned and trimmed; samples taken from interior. (Lever 2013; Hirayama et al. 2015.)
Cultivation experiments	Different media, temperatures, aerobic/anaerobic conditions - targeting chemolithoautotrophic and heterotrophic microorganisms to isolate the most extreme and active microbes from the deep subsurface.
Molecular techniques	Illumina-based 16S and 18S rRNA gene surveys. 16S is an excellent marker gene for all prokaryotic communities including bacteria and archaea and 18S is the marker gene for microeukaryotic communities.
	Metagenomic analysis. Metagenomics is the analysis of all genes of all microorganisms present in a sample and allows identification of dominant metabolic processes. Illumina HiSeq will be used to produce thousands of sequencing reads and capture all potential metabolic processes.
	Metatranscriptomic is the analysis of gene expression of all microbes from a sample; we will attempt to isolate RNA, which allows the identification of the active communities and processes in the deep subsurface.
	Targeted proteomic techniques to get additional insights into metabolic complexity. Extraction and analysis of proteins related to anaerobic degradation of aromatic hydrocarbons with potential implications in the bioremediation field. Bioremediation is the process that uses microbes or enzymes to detoxify contaminated environments.
Legal issues and the Nagoya protocol	
All participants endorse that access to, and use of, genetic resources taken during the project should be consistent with the provisions of the Convention on Biological Diversity (CBD) taking into account their specifications by the Bonn Guidelines on Access to Genetic Resources and the Fair and Equitable Sharing of Benefits arising from their Utilization, and, where appropriate, the Nagoya Protocol on Access to Genetic Resources and the Fair and Equitable Sharing of Benefits arising from their Utilization (NP, not yet in force), as well as with the United Nations Convention on the Law of the Sea (UNCLOS). All participants commit to abiding by the requirements of the Nagoya Protocol (**https://treaties.un.org/doc/Publication/MTDSG/Volume%20II/Chapter%20XXVII/XXVII-8-b.en.pdf**). Within the scope of this commitment, all biological samples related to Objective 7 will be studied in collaboration with the Institute of Marine Biology, Biotechnology and Aquaculture (IMBBC) at the Hellenic Centre for Marine Research (HCMR) in Heraklion, Crete, where they will be used for research purposes only.	

Study of drill cores and pore fluids will investigate the relationship between extant or fossilized subseafloor microbial communities and subseafloor biogeochemical and mineralization processes, particularly the relative importance of Fe released from hydrothermal activity in sustaining subseafloor biomes (Templeton, 2011).

It is assured that the access, distribution, and study of microbial samples taken during Expedition 398 will be implemented in full compliance with the Nagoya Protocol (Table **T2**).

5. Drilling and coring strategy

Expedition 398 will include coring and logging operations in the eastern Aegean Sea. The coring program encompasses six primary sites and twelve alternate sites in ~300–700 m water depth. Two primary (Sites CSK-05C and CSK-07B) and five alternate sites are located inside the Santorini caldera, one primary (Site CSK-03A) and three alternate sites cover the slope of the submarine Kolumbo Volcano, and the other primary (Sites CSK-01A, CSK-09A, and CSK-13A) and alternate sites target the surrounding basins (Figure **F1**). The proposed primary and alternate sites are described further below. All sites are located in Greek territorial waters. The final operations plan and number of sites to be cored is contingent upon the overall *JOIDES Resolution* operations schedule (**http://iodp.tamu.edu/scienceops/index.html**), the outcome of requests for territorial permission to occupy these sites, and any operational risks (see **Risks and contingency**).

Addressing the various scientific objectives requires a coring strategy of multiple holes at each site (outlined in Tables **T3** and **T4** for primary and alternate sites, respectively). In a first step, every drill site will be established using the advanced piston corer (APC)/half-length APC (HLAPC) system (see **http://iodp.tamu.edu/tools**) to penetrate to refusal and deploy nonmagnetic core barrels in the initial hole (Hole A). Refusal is expected to occur in indurated sediments around 150 mbsf. Further deepening will be achieved with the extended core barrel (XCB) system (**http://iodp.tamu.edu/tools**) in the same hole and is expected to reach the target depth at Sites CSK-03A and CSK-09A. To achieve an optimum in stratigraphic completeness, a second hole (Hole B) using the same coring strategy is planned at Sites CSK-01A, CSK-03A, CSK-13A, and CSK-09A. Depending on time constraints, a spot coring strategy (i.e., alternation of coring and drilling without core recovery) may need to be implemented in Hole B at Site CSK-09A to complement stratigraphic gaps from Hole A at this site. A third hole (Hole C) using the APC/HLAPC/XCB coring strategy is planned for Site CSK-03A to ensure recovery of the most complete stratigraphic succession and to overcome the more challenging sediment formation conditions at the slope of the submarine Kolumbo Volcano. Sites CSK-01A and CSK-13A have the deepest drilling target depths (>765 mbsf), including intersection of continental acoustic basement; thus, Hole C at these sites requires deployment of the rotary core barrel (RCB) coring system (**http://iodp.tamu.edu/tools**). Penetration of more challenging rock formations, expected in the deeper caldera stratigraphy, require Hole B at the two Santorini caldera sites (CSK-05C and CSK-07B) to be established with the RCB coring system to reach the respective drilling target depths. The preliminary operations plan for Expedition 398 is shown in Table **T3**. Figure **F10** displays the associated operations schematic for all primary sites.

The APC coring system ensures recovery of not only the least disturbed, most complete sediment stratigraphy and tephrostratigraphy but also the cleanest possible cores for addressing microbiology and sediment geochemistry with minimized seawater contamination (House et al., 2003; Lever et al., 2006; Schindlbeck et al., 2016). XCB coring will still produce intermediate-quality cores suitable for stratigraphic tasks and for some microbiology and most geochemistry sampling and analysis purposes, if necessary, especially because multiple holes are drilled.

At each site outside the Santorini caldera, cores from Hole A will be dedicated to stratigraphy, micropaleontology, structural geology, and lithology. In the caldera, Hole A will also serve as a pilot hole for microbial sampling. Hole B cores will be subject to pore water and solid-phase geochemistry analyses. At the intracaldera sites, the deeper cored section of Hole B will also be subject to microbial sampling. Cores recovered from Hole C will be used mainly for the deeper

stratigraphy, lithology, and mineralogy where the RCB coring tool is used, as well as for complementing structural and micropaleontological analyses at the Kolumbo Volcano site.

All full-length APC cores will be oriented using the Icefield MI-5 core orientation tool. Time-efficient temperature measurements will be taken in Hole A and, if applicable or necessary, in Hole B using the advanced piston corer temperature (APCT-3) tool, which is contained inside the APC coring shoe. In sediments that are too consolidated to deploy the APCT-3 tool, additional temperature measurements may be taken using the Sediment Temperature 2 (SET2) tool or sediment temperature pressure tool (SETP), which may include selected depth intervals drilled by the XCB coring system. If temperature monitoring in holes indicates downhole temperatures exceeding the ratings of both the APCT-3 and SET2/SETP tools (100°C; see **http://iodp.tamu.edu/tools/logging**), the deployment of an ultrahigh-temperature probe will be required (see **Wireline logging/Downhole measurements strategy** and **Risks and contingency**).

Table T3. Operations plan and time estimates for primary sites, Expedition 398. mbsl = meters below sea level. EPSP = Environmental Protection and Safety Panel.

Site	Location (latitude, longitude)	Seafloor depth (mbsl)	Operations description	Transit (days)	Drilling/ Coring (days)	Logging (days)
Tarragona			Begin expedition 5.0	Port call days		
			Transit ~1256 nmi to CSK-01A @ 10.5 kt	5.0		
CSK-01A	36.729300°N	489	Hole A - APC/HLAPC to refusal - XCB to 610 mbsf	0	3.3	0.0
EPSP	25.648200°E		Hole B - APC/HLAPC to refusal - XCB to 610 mbsf	0	3.3	0.0
to 765 mbsf			Hole C - Drill ahead to 575 mbsf - RCB from 575 to 765 mbsf - Log with triple combo, FMS-sonic, and VSI	0	3.1	1.6
			Subtotal days on site: 11.3			
			Transit ~14 nmi to CSK-03A @ 10.5 kt	0.1		
CSK-03A	36.554900°N	397	Hole A - APC/HLAPC to refusal - XCB to 566 mbsf	0	2.8	0.0
EPSP	25.439800°E		Hole B - APC/HLAPC to refusal - XCB to 566 mbsf	0	2.8	0.0
to 566 mbsf			Hole C - APC/HLAPC to refusal - XCB to 566 mbsf - Log with triple combo, FMS-sonic, and VSI	0	2.6	1.3
			Subtotal days on site: 9.5			
			Transit ~21 nmi to CSK-13A @ 10.5 kt	0.1		
CSK-13A	36.324300°N	489	Hole A - APC/HLAPC to refusal - XCB to 675 mbsf	0	3.3	0.0
EPSP	25.182600°E		Hole B - APC/HLAPC to refusal - XCB to 675 mbsf	0	3.3	0.0
to 857 mbsf			Hole C - Drill ahead to 575 mbsf - RCB from 575 to 857 mbsf - Log with triple combo, FMS-sonic, and VSI	0	3.6	1.8
			Subtotal days on site: 12.1			
			Transit ~12 nmi to CSK-05C @ 10.5 kt	0.0		
CSK-05C	36.437500°N	384	Hole A - APC/HLAPC/XCB to refusal	0	0.6	0.0
EPSP	25.378900°E		Hole B - Drill ahead to 130 mbsf - RCB from 130 to 234 mbsf - Log with triple combo, FMS-sonic, and VSI	0	1.1	1.0
to 234 mbsf						
			Subtotal days on site: 2.8			
			Transit ~4 nmi to CSK-07B @ 1.5 kt	0.1		
CSK-07B	36.388950°N	292	Hole A - APC/HLAPC/XCB to refusal	0	0.8	0.0
EPSP	25.417130°E		Hole B - Drill ahead to 175 mbsf - RCB Core to 360 mbsf - Log with triple combo, FMS-sonic, and VSI	0	2.4	1.0
to 360 mbsf						
			Subtotal days on site: 4.2			
			Transit ~35 nmi to CSK-09A @ 10.5 kt	0.1		
CSK-09A	36.565600°N	694	Hole A - APC/HLAPC to refusal - XCB to 595 mbsf	0	3.3	0.0
EPSP	25.761300°E		Hole B - APC/HLAPC to refusal - XCB to 595 mbsf - Log with triple combo, FMS-sonic, and VSI	0	3.3	1.3
to 595 mbsf						
			Subtotal days on site: 7.9			
			Transit ~81 nmi to Heraklion @ 10.5 kt	0.3		
Heraklion			End expedition	5.7	39.6	8.0

Port call days:	5.0	Total operating days:	52.8
Subtotal days on site:	47.8	Total expedition days:	57.8

Table T4. Time estimates for alternate sites, Expedition 398. mbsl = meters below sea level. EPSP = Environmental Protection and Safety Panel.

Site	Location (latitude, longitude)	Seafloor depth (mbsl)	Operations description	Drilling/ Coring (days)	LWD/ MWD log (days)
CSK-02A	36.743800°N	488	Hole A - APC/HLAPC/XCB to 553 mbsf	2.9	0.0
EPSP	25.714600°E		Hole B - APC/HLAPC/XCB to 553 mbsf	2.9	0.0
to 553 mbsf			Hole C - APC/HLAPC/XCB to 553 mbsf - Log with triple combo, FMS-sonic, and VSI	2.5	1.0
			Subtotal days on site: 9.3		
CSK-04C	36.575200°N	400	Hole A - APC/HLAPC/XCB to 581 mbsf	2.8	0.0
EPSP	25.414600°E		Hole B - APC/HLAPC/XCB to 581 mbsf	2.8	0.0
to 581 mbsf			Hole C - APC/HLAPC/XCB to 581 mbsf - Log with triple combo, FMS-sonic, and VSI	2.4	1.1
			Subtotal days on site: 9.0		
CSK-06B	36.442300°N	383	Hole A - APC/HLAPC/XCB to refusal	0.6	0.0
EPSP	25.375200°E		Hole B - Drill ahead to 130 mbsf - RCB to 360 mbsf - Log with triple combo, FMS-sonic, and VSI	1.5	1.1
to 360 mbsf					
			Subtotal days on site: 3.2		
CSK-08B	36.381610°N	293	Hole A - APC/HLAPC/XCB to refusal	0.8	0.0
EPSP	25.406060°E		Hole B - Drill ahead to 175 mbsf - RCB to 375 mbsf - Log with triple combo, FMS-sonic, and VSI	1.4	1.2
to 375 mbsf					
			Subtotal days on site: 3.4		
CSK-10B	36.550700°N	680	Hole A - APC/HLAPC/XCB to 363 mbsf	2.0	0.0
EPSP	25.766800°E		Hole B - APC/HLAPC/XCB to 363 mbsf	2.0	0.0
to 363 mbsf			Hole C - APC/HLAPC/XCB to 363 mbsf - Log with triple combo, FMS-sonic, and VSI	1.9	0.9
			Subtotal days on site: 6.8		
CSK-14A	36.304900°N	523	Hole A - APC/HLAPC/XCB to 675 mbsf or to refusal	4.0	0.0
EPSP	25.128600°E		Hole B - APC/HLAPC/XCB to 675 mbsf or to refusal	3.8	0.0
to 756 mbsf			Hole C - Drill ahead to 575 mbsf - RCB to 756 mbsf - Log with triple combo, FMS-sonic, and VSI	2.6	1.6
			Subtotal days on site: 12.0		
CSK-15A	36.732000°N	490	Hole A - APC/HLAPC/XCB to 610 mbsf	3.3	0.0
EPSP	25.646300°E		Hole B - APC/HLAPC/XCB to 610 mbsf	3.3	0.0
to 800 mbsf			Hole C - Drill ahead to 575 mbsf - RCB to 800 mbsf - Log with triple combo, FMS-sonic, and VSI	3.1	1.6
			Subtotal days on site: 11.3		
CSK-16A	36.548000°N	372	Hole A - APC/HLAPC/XCB to 565 mbsf	2.7	0.0
EPSP	25.451700°E		Hole B - APC/HLAPC/XCB to 565 mbsf	2.7	0.0
to 565 mbsf			Hole C - APC/HLAPC/XCB to 565 mbsf - Log with triple combo, FMS-sonic, and VSI	2.3	1.0
			Subtotal days on site: 8.8		
CSK-18A	36.375500°N	291	Hole A - APC/HLAPC/XCB to refusal	0.8	0.0
EPSP	25.394200°E		Hole B - Drill ahead to 175 mbsf - RCB to 380 mbsf - Log with triple combo, FMS-sonic, and VSI	1.4	1.2
to 380 mbsf					
			Subtotal days on site: 3.4		
CSK-19A	36.556300°N	688	Hole A - APC/HLAPC to refusal - XCB to 740 mbsf	4.4	0.0
EPSP	25.750300°E		Hole B - APC/HLAPC/XCB to 740 mbsf (spot coring) - Log with triple combo, FMS-sonic, and VSI	2.5	1.6
to 740 mbsf					
			Subtotal days on site: 8.5		
CSK-20A	36.312700°N	515	Hole A - APC/HLAPC/XCB to 675 mbsf or to refusal	3.8	0.0
EPSP	25.150100°E		Hole B - APC/HLAPC/XCB to 675 mbsf or to refusal	3.6	0.0
to 909 mbsf			Hole C - Drill ahead to 575 mbsf - RCB to 909 mbsf - Log with triple combo, FMS-sonic, and VSI	3.4	1.8
			Subtotal days on site: 12.7		
CSK-21A	36.506800°N	309	Hole A - APC/HLAPC/XCB to 630 mbsf	3.0	0.0
EPSP	25.505300°E		Hole B - APC/HLAPC/XCB to 630 mbsf	3.0	0.0
to 630 mbsf			Hole C - APC/HLAPC/XCB to 630 mbsf - Log with triple combo, FMS-sonic, and VSI	2.6	1.1
			Subtotal days on site: 9.6		

If borehole conditions permit, downhole wireline logging is planned in Hole B (Sites CSK-05C, CSK-07B, and CSK-09A) or C (Sites CSK-01A, CSK-03A, and CSK-13A) at each site upon completion of coring. For this purpose, the corresponding hole will be conditioned, filled with logging mud, and logged according to the logging strategy (see **Wireline logging/Downhole measurements strategy**).

5.1. Proposed drill sites

Two of the six proposed primary drill sites (and three of the twelve alternate sites) are located inside the Santorini caldera. Three primary sites (and six alternate sites) target the adjacent Christiana, Anhydros, and Anafi Basins, whereas one additional primary site and three alternate sites are proposed for the slope of the submarine Kolumbo Volcano (Figure **F1**). Sites were initially selected based on a dense network of MCS and single-channel seismic reflection profiles from collaborating groups and publications (Figure **F2A**). All site-specific bathymetric maps and seismic line positions are displayed in **Site summaries**.

5.2. Anhydros Basin site

Proposed primary Site CSK-01A and alternate Site CSK-15A are located ~10 km southeast from the Amorgos Island, whereas alternate Site CSK-02A is only 5 km away (Figures **F1**, **F5**, **AF1**, **AF2**, **AF3**). All sites are situated in the Anhydros Basin at water depths of around 490 meters below sea level (mbsl). The drill sites target the Pliocene–Quaternary volcano-sedimentary fill of the Anhydros Basin to the depth of the Alpine basement. CSK sites in the Anhydros Basin are located downstream of the Kolumbo Volcano and the submarine terminus of the LBA pyroclastic flows. They are expected to yield volcaniclastics from Kolumbo eruptions and large Santorini eruptions but not smaller Santorini eruptions because of flow blocking by the Kolumbo volcanic chain.

Primary Site CSK-01A lies near the basin axis (Figure **AF1**) and should record the entire histories of Santorini and Kolumbo within the proposed drilling target depth of 765 mbsf. The anticipated lithologies are undisturbed hemipelagic muds, volcaniclastics, turbidites, and finally continental basement rocks (Mesozoic limestones, schists, and/or granites; Kilias et al., 2013). A gravity core, recovered 7 km to the east, indicates that the uppermost sediments on site will consist of hemipelagic muds with ~8 cm/ky sedimentation rate and several interbedded, fine–coarse ash layers from Santorini, as well as sapropels (Core POS513-15; Kutterolf et al., 2021a, 2021b). The aim is to use deeper coring (and seismic profiles) to reconstruct the volcanic, sedimentary, and tectonic histories of the basin and to access a near-continuous time series of volcanism in the area since rift inception. The site will transect and characterize all six seismic packages of the Anhydros rift basin from the Pliocene to the present day (Units B1–B6) and the major onlap surfaces between them (Figure **F5**). For alternate Site CSK-02A, which is located closer to Amorgos, the sedimen-

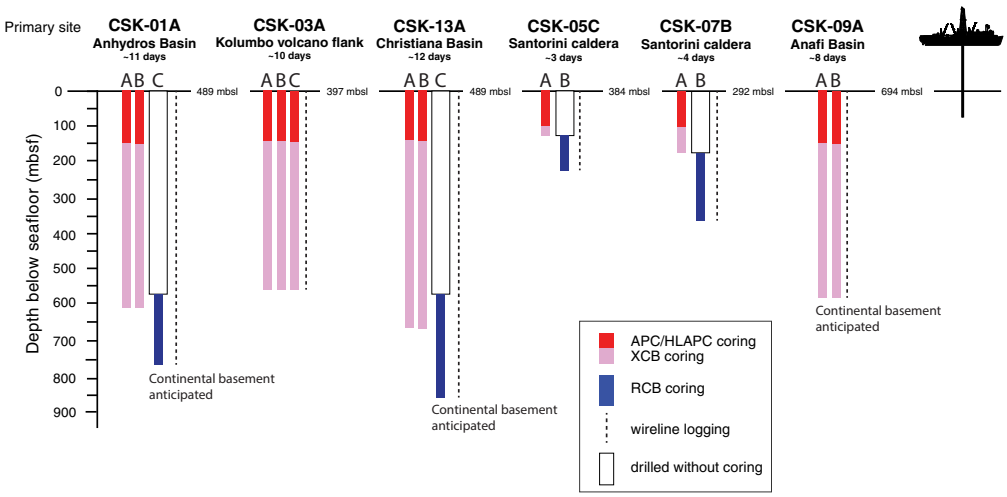

Figure F10. Operations schematics for primary sites, Expedition 398.

tary fill is condensed, resulting in a target depth of 553 mbsf, including basement (Figure **AF2**). In contrast, alternate Site CSK-15A has only a slightly deeper target depth (800 mbsf; Figure **AF3**) than adjacent Site CSK-01A. Coring at the sites in the Anhydros Basin will address science Objectives 1–4 and 6. Anhydros Basin operations will be complemented by drilling in the Anafi Basin to accomplish the fullest sampling of the submarine volcanic record because each basin taps a different sediment distributary branch of the CSK system.

5.3. Kolumbo Volcano flank site

Proposed primary Site CSK-03A and alternate Sites CSK-16A and CSK-04C are located 4–7 km northwest of the submarine Kolumbo caldera on its flank in the Anhydros Basin at water depths of ~370–400 mbsl, with Site CSK-04C targeting the most distal deposits if the more proximal sites are not successful (Figures **F1**, **F9**, **AF4**, **AF5**, **AF6**). In contrast, alternate Site CSK-21A is only 2 km away on its southeastern flank at a water depth of ~300 mbsl (Figure **AF7**). The target depths of all sites range from ~565 (Sites CSK-03A and CSK-16A) to 581 (Site CSK-04C) to 630 mbsf (Site CSK-21A). Seismic profiles across the Kolumbo edifice reveal five units interpreted to be Kolumbo-derived volcaniclastics (Units K1–K5 from the base up), with Unit K5 representing the 1650 eruption (Hübscher et al., 2015) (Figure **F9**). The submarine cones northeast of Kolumbo postdate Unit K2 on seismic profiles (Figure **F4**), but their products are not expected to be prominent in our drill cores.

The aim of drilling on the flanks of Kolumbo is to penetrate the different seismically recognized volcanic eruption units from that volcano (Units K1, K2, K3, or K5 or their thin, lateral equivalents), as well as many eruption units from Santorini and traces from the submarine cones northeast of Kolumbo. This will enable characterization of the products of the Kolumbo eruptions, as well as construction of a coherent stratigraphy for Santorini and the submarine Kolumbo volcanic chain together; this will then feed into scientific Objectives 1–6. The alternate sites are placed at different distances from the Kolumbo vent to avoid possible coarse, bouldery volcaniclastic facies of Seismic Units K1–K5. The anticipated lithologies are volcaniclastics, muds, and turbidites. Primary Site CSK-03A lies at the foot of the Kolumbo edifice; it will allow us to drill Units K1, K2, K3, and K5 and therefore nearly the entire history of the Kolumbo Volcano within the proposed drilling target depth of 566 mbsf (Figure **AF4**). Four intercalated seismic units (SK1–SK4; probably hemipelagic muds and volcaniclastics) will contain the products of Santorini eruptions, including potentially those of smaller magnitude than recorded at the more distal basin sites (Figure **F9**). Gravity cores recovered ~9 km to the west contain ash-to-lapilli pyroclastic layers from the Kolumbo 1650 and LBA eruptions intercalated within hemipelagic sediments (clayey silt to sandy silt). Sediments 15 and 9 km to the northwest and south, respectively, contain the typical tuffaceous hemipelagic muds of the region deposited at sedimentation rates of 5–8 cm/ky (Cores POS513-14, POS513-26, and POS513-20; Kutterolf et al., 2021a, 2021b).

Three alternate sites have been identified in the event of difficulties at the primary site. Alternate Site CSK-16A is located 1 km southeast of primary Site CSK-03A on the flank of Kolumbo and covers similar objectives in the slightly thicker seismic units at the same target depths. Drilling and coring using a strategy similar to that for Site CSK-03A are planned to 565 mbsf to penetrate four of the five identified seismic units associated with the Kolumbo Volcano and additionally recover intercalated stratigraphic sequences bearing pyroclastic deposits from Santorini (Figures **F9**, **AF6**).

The proximal location of south-southeast flank alternate Site CSK-21A to the vent of the Kolumbo Volcano ensures penetration of three Kolumbo-related seismic units (K1, K3, and K5) and two interbedded seismic units (SK3 and SK4) that are foreseen to contain Santorini deposits within the target depth of 630 mbsf (Figure **AF7**).

The third alternate site, CSK-04C, is located 3 km northwest of primary Site CSK-03A at the base of the Kolumbo edifice (Figures **F1**, **AF5**). The site has a target depth of 581 mbsf and is the backup plan if all other Kolumbo sites encounter too many difficulties by drilling into the proximal volcaniclastic sequences of the Kolumbo Volcano. Although this site penetrates all four seismic units

containing eruption products of Santorini (Units SK1–SK4), it only penetrates the uppermost unit from Kolumbo (Unit K5; Figure **AF5**).

5.4. Christiana Basin site

Primary drill Site CSK-13A and alternate Sites CSK-14A and CSK-20A are located ~4 km north to northwest of Christiana Island and 18–20 km southwest of Santorini (Figures **F1**, **F6**, **AF8**, **AF9**, **AF10**). All sites are situated in the Christiana Basin at water depths of 500–520 mbsl. The drill sites target the Pliocene–Quaternary volcano-sedimentary fill of the Christiana Basin. This basin is deeper than the Anhydros and Anafi Basins; its volcano-sedimentary fill potentially records the earlier volcanic history of the CSK volcanic field (including the products of Christiana and early Santorini), as well as younger Santorini and possibly Milos. The extinct Christiana Volcano produced lavas and tuffs of unknown ages (Aarburg and Frechen, 1999), but a particularly large ignimbrite found on neighboring islands is tentatively dated at 1.00 ± 0.05 Ma (Keller et al., 2010).

Primary Site CSK-13A will pass through Units U1–U6, including volcaniclastics from both Santorini and Christiana, to the first few meters of prevolcanic basement at the 857 mbsf target depth (Figure **AF8**). It will address scientific Objectives 1–4 and 6 (Figure **F6**). The anticipated lithologies are hemipelagic muds, volcaniclastics, turbidites, pumiceous tuffs, debris flows, and continental basement rocks (Mesozoic limestones, schists, and/or granites; Kilias et al., 2013). A gravity core recovered 7 km to the south-southwest indicates that the uppermost sediments on site will be characterized by hemipelagic muds (~6 cm/ky sedimentation rate) and several interbedded, fine- to medium-grained ash layers from Santorini and Milos (Core POS513-9; Figure **F2B**; Kutterolf et al., 2021a, 2021b).

The overall aim here is to use the deeper coring (and seismic profiles) to reconstruct the volcanic, sedimentary, and tectonic histories of the Christiana and Milos Volcanoes, complement the Santorini volcanic record of the northeastern basins, and therefore access a near-continuous time series of volcanism west of Santorini since rift inception.

Although alternate Site CSK-20A has a slightly deeper target depth of 909 mbsf and encounters the same seismic units as primary Site CSK-13A at similar thicknesses, the sedimentary fill at alternate Site CSK-14A, which is closer to the rim of Christiana Basin, is condensed (Figures **AF8**, **AF9**, **AF10**). This results in a target depth of only 756 mbsf, including basement. Alternate Site CSK-14A is therefore an option to reduce operational time if necessary while still ensuring the recovery of the entire stratigraphic sequence at a slightly lower resolution.

5.5. Santorini caldera sites

Proposed primary drill Site CSK-05C and alternate Site CSK-06B are sited 1 km apart in the northern basin of the Santorini caldera at a water depth of ~380 mbsl (Figures **F1**, **F7**, **F8**, **AF11**, **AF12**). Complementary primary drill Site CSK-07B and its two alternate Sites CSK-08B and CSK-18A are located south of the Kameni intracaldera volcano in the southern caldera basin at water depths of ~290 mbsl; these sites complete the drilling initiative in the Santorini caldera (Figures **F1**, **F7**, **F8**, **AF13**, **AF14**, **AF15**). Both primary caldera sites will sample intracaldera Seismic Units S1–S3, test the published correlations between the two caldera basins, penetrate below Unit S3 (Figure **F8**), and address scientific Objectives 1, 4, 5, and 7. The seismic units probably consist of muds and sands from cliff mass wasting (Unit S1), compacted (possibly lithified) sandy volcaniclastics from Kameni Volcano (Unit S2), and consolidated coarse blocky tuffs, landslide debris, and/or flood gravels (Unit S3). The goals are to groundtruth the different seismic units; document the processes, products, and potential impacts of the LBA eruption; reconstruct the eruptive history of Kameni Volcano; and penetrate below Unit S3. The combined approach of drilling in the northern and southern caldera basins will enable us to test several hypotheses regarding the LBA caldera-forming eruption of Santorini. By drilling both caldera basins and exploiting our dense seismic reflection coverage, we will gain access to the 3-D architecture of the entire caldera fill and will better understand the relative roles of downfaulting and downsagging in the LBA caldera collapse (Acocella, 2007). We will also target the question of why the northern basin is 100 m deeper than the southern one, with a thicker Unit S1 but thinner Unit S3, and if the northern caldera basin already existed prior to the LBA eruption, as proposed (Athanassas et al., 2016). Finally, we will be

able to test whether Unit S3 consists of flood debris from the caldera-flooding event (Nomikou et al., 2016a) or represents LBA intracaldera tuffs (Johnston et al., 2015). Although we will not drill into the cylindrical low-density seismic anomaly that extends from 400 to 3000 mbsf beneath the northern caldera basin (PROTEUS seismic tomography experiments; Hooft et al., 2019), characterization of the layers above it will place constraints on its stratigraphic and structural relationships with the shallow (<400 m) intracaldera fill. Because the axis of the anomaly coincides with the focus of uplift in 2011–2012 (Figure **F7**), we may also get a better understanding of the mechanisms of caldera unrest. The northern primary Site CSK-05C is located north of this low-velocity seismic anomaly and centered on the focus of caldera floor uplift during the unrest period in 2011–2012 (Figure **AF11**). This site will also be used for the microbiological work of Objective 7 and has a target depth of 234 mbsf. Alternate Site CSK-06B is located 1 km north-northwest of Site CSK-05C and covers the edge of the 2011–2012 caldera floor uplift with a target depth of 360 mbsf (Figure **AF12**). We expect at both sites lithologies consisting of muds, turbidites, debris flows, volcaniclastics, coarse breccias, gravels, unwelded and welded tuffs, and lavas.

Primary Site CSK-07B is located in the southern basin of the Santorini caldera. Besides penetration of intracaldera Seismic Units S1–S3, it also aims to core well below Unit S3 with a target depth of 360 mbsf (Figure **AF13**). Two alternate sites, CSK-08B and CSK-18A, with target depths of ~380 mbsf address the same drilling objectives and are located 1.5 and 3 km southwest of primary Site CSK-07B, respectively (Figures **AF14**, **AF15**).

Recent heat flow measurements gave 506–1496 mW/m^2 in the northern caldera basin and 8064 mW/m^2 in the southern caldera basin (Hannington et al., 2018), which is higher than the 56–63 mW/m^2 measured far from the volcanoes in the Anhydros Basin (and consistent with regional values of 60–80 mW/m^2; Kalyoncuoglu et al., 2013). However, no high-temperature hydrothermal system has been recognized in the caldera. Only low-temperature hydrothermal areas (60°–100°C on Nea Kameni; 18°–20°C on the caldera floor) and pools of CO_2-rich bottom water (Tassi et al., 2013; Camilli et al., 2015) have been identified.

5.6. Anafi Basin site

Primary Site CSK-09A and alternate Sites CSK-10B and CSK-19A are located ~10 km southeast of Anhydros Island in the Anafi Basin (Figures **F1**, **F5**, **AF16**, **AF17**, **AF18**) at water depths of 680–705 mbsl. The aim at all of these sites is to penetrate the entire volcano-sedimentary fill of this basin as far as the Alpine basement. The basin potentially records the full volcanic history of Santorini (and any older centers) since rift inception but probably contains few eruptive products from Kolumbo. Drilling will enable reconstruction of the volcanic, sedimentary, and tectonic histories of the Anafi Basin, allowing us to compare its evolution with that of the Anhydros Basin.

Site CSK-09A lies near the basin axis (Figure **F5**). Its proposed drilling target depth of 595 mbsf ensures intersection of all six seismic units (B1–B6) (Figures **F5**, **AF16**). The anticipated lithologies are undisturbed hemipelagic muds, volcaniclastics, and turbidites, as well as a couple of meters of continental basement rocks (Mesozoic limestones, schists, and/or granites; Kilias et al., 2013). A gravity core retrieved 14 km to the northeast indicates that the uppermost sediments on site consist of hemipelagic muds with an average sedimentation rate of 6 cm/ky and several interbedded, fine- to very coarse grained ash/fine lapilli layers from Santorini, as well as sapropels (Core POS513-14; Kutterolf et al., 2021a, 2021b).

Alternate Site CSK-19A has a much deeper target depth of 740 mbsf. It is situated directly on the basin axis and will therefore penetrate the uncondensed stratigraphy of the basin covering all six seismic units (Figure **AF18**). Alternate Site CSK-10B, in contrast, will recover a more condensed sedimentary fill further away from the basin axis on a structural high, missing Seismic Units B1–B3, and therefore resulting in a reduced target depth of 363 mbsf, including continental basement (Figure **AF17**).

6. Wireline logging/Downhole measurements strategy

Downhole wireline logging will be critical to characterize subseafloor lithologies and their structures, particularly regarding extrapolation to complete sections in deeper depth intervals where XCB and RCB coring may retrieve cores of lower recovery in stiff sediments and boulder deposits. We intend to deploy the available standard suites of downhole logging tools (**http://iodp.tamu.edu/tools/logging**) at all proposed drill sites, including the triple combination ("triple combo") and Formation MicroScanner (FMS)-sonic tool strings extended by the borehole seismics tool string equipped with the Versatile Seismic Imager (VSI) to collect active seismic data for integration of borehole and surface seismic data. The logging tools will be run in the final hole at each site. However, coring is the top priority for every site, and the scheduled logging program may be modified or abandoned if the coring objectives are not met in the allotted time. Furthermore, the actual deployment of the logging tools will depend on downhole temperatures, which will be determined prior to each planned logging run by using (1) the APCT-3 (soft sediments) and SET2/SETP (consolidated sediments) tools (**http://iodp.tamu.edu/tools/logging**) and, if necessary, (2) an ultrahigh-temperature probe—the Elevated Temperature Borehole Sensor (ETBS) memory tool (borehole fluid temperature measurement)—in open boreholes established within sediment formations that are too rigid to deploy the SET2/SETP tool or once the temperature environment indicates values exceeding 80°C. In any case, priority will be given to minimizing the risk to the logging tools (see **Risks and contingency**). The triple combo tool string consists of the logging equipment head-mud temperature (LEH-MT) sonde, Accelerator Porosity Sonde (APS), Hostile Environment Litho-Density Sonde (HLDS), Hostile Environment Natural Gamma Ray Sonde–Enhanced Digital Telemetry Cartridge (HNGS-EDTC), High-Resolution Laterolog Array (HRLA)/Phasor Dual Induction-Spherically Focused Resistivity Tool (DIT), and Magnetic Susceptibility Sonde (MSS) (Figure **F11**). The FMS-sonic tool string consists of the Dipole Sonic Imager (DSI) tool (acoustic velocity) and FMS (resistivity imaging), including the LEH-MT and HNGS-EDTC (Figure **F11**). The VSI is usually combined with the EDTC that includes not only telemetry but also a basic gamma ray sensor (Figure **F11**). The VSI is used for check shot surveys (to obtain a depth-traveltime relation) and zero-offset vertical seismic profile (VSP) experiments (to obtain seismograms at the site). The configuration of the tool (i.e., number of sensor packages,

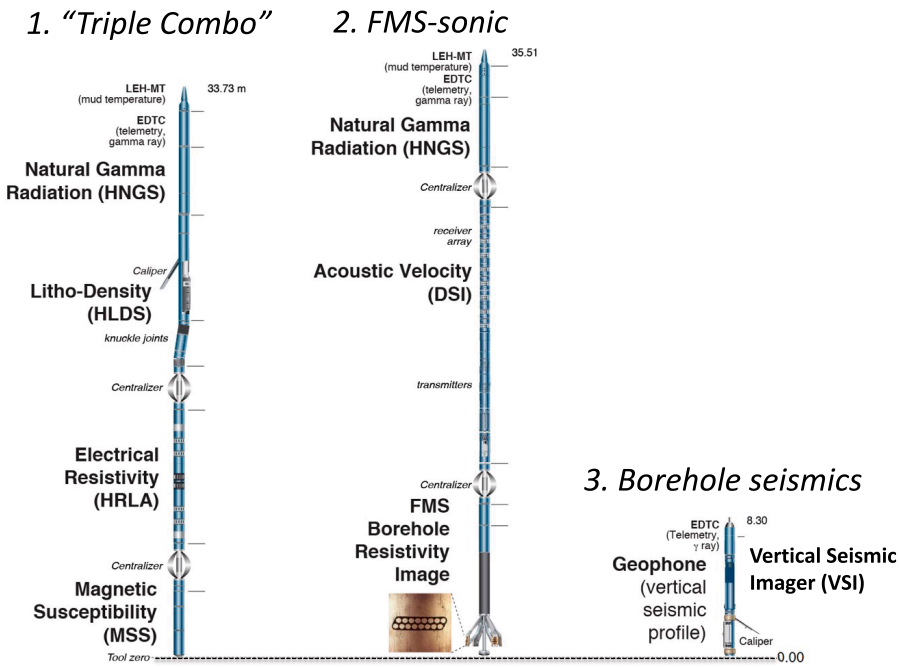

Figure F11. Triple combo, FMS-sonic, and VSI downhole logging tool strings (see **http://iodp.tamu.edu/tools/logging**) intended for use during Expedition 398 wireline logging. For borehole fluid temperature below 85°C, all logging tools can be safely deployed. For higher temperatures up to 140°–170°C (depending on the tool), temperature-sensitive tools need to be removed from the tool suites and resulting shortened tool strings can be deployed.

sensor spacing, and type of connection [stiff or flexible]) varies to provide the maximum versatility of the array.

Ideally, we will always implement three downhole deployments with different logging tool strings. The first run will always contain the triple combo tool string that measures density, neutron porosity, resistivity, and natural gamma radiation (NGR), along with borehole diameter (caliper log). The caliper log provided by the density tool will allow an assessment of hole conditions and the potential for success of subsequent logging runs. NGR data gathered by the triple combo may prove useful for correlation with NGR measurements taken from the cores on the ship. The second logging run use the FMS-sonic tool string that measures NGR, sonic velocity, and oriented high-resolution electrical resistivity images, along with borehole diameter. The NGR data will be used to depth match the different logging runs. The compressional velocity logs can be combined with the density logs to generate synthetic seismograms for detailed seismic-log correlations. A third run at each site will consist of a check shot survey with the VSI to acquire a zero-offset VSP. The objective is to establish a direct link between lithostratigraphic depths in the borehole and reflectors in the seismic profiles. The necessary seismic source pulse for the check shots will be provided by generator-injector air guns deployed by crane. Their deployment is subject to compliance with the IODP marine mammal protection policy; thus, the check shot survey would have to be postponed or canceled if policy conditions are not met.

The downhole logging data will be sent to the Lamont-Doherty Earth Observatory Borehole Research Group at Columbia University (New York, United States) for processing during the expedition and returned to the shipboard downhole logging scientists for interpretation within days upon completion of the downhole logging runs at a given site.

If we encounter hydrothermal deposits or fluid recharge/discharge downhole, we will attempt the recovery of borehole hydrothermal fluids. Their sampling at depth will be implemented by deployment of the water sampler temperature probe (WSTP) in soft to semiconsolidated sediments at temperatures ≤85°C. At higher temperatures or in consolidated sediments and basement, we will run the high-temperature resistant Kuster Flow Through Sampler (FTS) (**http://www.sword-tek.com/yahoo_site_admin/assets/docs/Kuster_FTS.314194716.pdf**), which is rated for a maximum of 232°C. Successful recovery of borehole hydrothermal fluids will aid studies of current hydrothermal activity, including its potential impact on subseafloor microbial communities in the Santorini caldera.

Detailed information on all logging tools outlined here can be retrieved from **http://iodp.tamu.edu/tools/logging**.

7. Risks and contingency

Three different coring systems (APC, XCB, and RCB) will be available to complement each other and ensure meeting the scientific objectives. For planning purposes, APC/HLAPC refusal depth is estimated at 150 mbsf (Tables **T3**, **T4**), although this depth may be exceeded at some sites. APC refusal is conventionally determined in two ways: (1) a complete stroke (as determined from the standpipe pressure after the shot) is not achieved because the formation is too hard and (2) excess force of >445 kN (equivalent to a mass of >45,360 kg/>100,000 lb) is required to pull the core barrel out of the formation because the sediment is too cohesive or "sticking." In cases where a significant stroke can be achieved but excessive force cannot retrieve the barrel, the core barrel can be "drilled over" (i.e., after the inner core barrel is successfully shot into the formation, the bit is advanced to some depth to free the APC barrel). In all A and B holes outside the caldera and in Hole C at Site CSK-03A, we have the option to deploy the XCB system to advance the hole (Tables **T3**, **T4**) if APC/HLAPC refusal occurs before the target depth is reached. The implementation of RCB coring will mitigate the risks imposed on exceeding the operational limits for the XCB coring system and is preferred to intersect the continental basement. Therefore, if some depths at solely APC/HLAPC/XCB sites are unattainable using the XCB system, another hole penetrating very firm sediments or very coarse, bouldery, and heterogeneous deposits will be drilled separately with the RCB system (**http://iodp.tamu.edu/tools**) to reach the target depth without recovery of

redundant sediments that are already available from APC/HLAPC and XCB coring. This strategy will already be applied to Hole B at Sites CSK-05C and CSK-07B as well as Hole C at Sites CSK-01A and CSK-13A.

Drilling and logging operations in active rift basins and in a caldera bear some risks and present challenges to achieving the expedition objectives. Unstable hole conditions can occur, negatively impacting core recovery or even leading to abandonment of a hole. In particular, drilling a heterogeneous succession of sediments and coarser volcaniclastics in the basins, with fracturing and paleofault zones as well as unconformities, most likely present in deeper intervals, may lead to problems with the borehole stability and a stuck bottom-hole assembly, resulting in lost time and possible loss of equipment. At the caldera sites, one can expect inevitable bouldery deposits and lavas to cause the same problems. Therefore, additional hardware will be available on board the ship to alleviate any losses. Extra time may be required for hole remediation (i.e., cleaning and stabilizing the hole). Moreover, hole instability may prevent downhole logging operations or lead to the untimely stop of a logging run.

To prevent an unstable hole from collapsing in its uppermost section (~1–3 m) or if an unforeseen reentry is necessary, a free-fall funnel can be deployed as a seafloor cone. This device is assembled around the drill string and then dropped to the seafloor. If a hole needs to be stabilized across tens of meters of depth range, it must be terminated and another hole needs to be established by installing a drill-in casing string. Its length then covers the depth range of instability. Such casing is attached to a hydraulic release tool (HRT) reentry system that is deployed upon assembly on board the ship. Subsequently, the casing is drilled into the seabed and coring starts below where the casing ends. The loss of a mud motor and/or underreamer while drilling in any required short casing string is always possible. A second mud motor and spare underreamers will be available. Particularly in the Santorini caldera, multiple holes may be required to find an area with stable (sub)seafloor conditions (cf. IODP Expedition 376 at the caldera of Brothers Volcano; de Ronde et al., 2019). Unpredictable borehole conditions and concomitant efforts on hole remediation may take a considerable amount of time, which is difficult to plan for in the operations schedule (Tables **T3**, **T4**). In particular, caldera deposits have yielded low recovery (≤20%) during previous expeditions (e.g., de Ronde et al., 2019), which may handicap sampling objectives.

At the caldera sites, there is also the possibility of encountering excess fluid pore pressures due to the given proximity of, for example, Site CSK-05C to the focus of a deep intrusion related to the seismic unrest of 2011–2012. So far, however, we do not expect the pore water concentrations of hydrocarbons to exceed the given limits for drilling. Also, no high temperatures in basin or caldera sediments are anticipated that would require extra precautions during operations. Plastic core liners can be used at in situ temperatures >200°C without melting because of virtually steady-state drilling fluid (seawater) circulation, as demonstrated by Integrated Ocean Drilling Program Expedition 331 (Expedition 331 Scientists, 2011) and Expedition 376 (de Ronde et al., 2019), and if necessary, aluminum core liners can replace the plastic liner to recover cores from high-temperature rocks and indurated sediments.

In contrast to drilling, the subseafloor temperature environment may bear a significant risk for logging operations. Because drilling fluid (seawater) will not be circulated during logging operations, there will be no considerable cooling of the hole at this time. Given the temperature gradients known so far, we do not expect downhole fluid and/or formation temperatures too high to use the standard logging suites. However, we are aware of this potential challenge and will monitor the formation and borehole fluid temperatures at each site to avoid problems during downhole logging. The downhole temperature measurements (APCT-3, SET2/SETP, and ETBS) implemented in Hole A at all sites will determine which logging tool string suite can be deployed (see **Wireline logging/Downhole measurements strategy**). If we encounter high temperatures at one or more sites, we can use the shorter high-temperature triple combo (HTTC) string that can be assembled for these purposes. It was deployed successfully during Expedition 376 (de Ronde et al., 2019) and consists of the HLDS/HNGS-EDTC/LEH-MT logging tools (Figure **F11**). Such a shortened tool string can be run without flasking at elevated borehole fluid temperatures (85°–140°C) using a conventional, low- to medium-temperature wireline cable that is permanently available on the ship.

Inclement weather always poses issues because rough seas and the resultant heave may adversely impact drilling or logging operations. For example, core quality and recovery can be negatively influenced or logging tools may not be deployable. The Expedition 398 schedule coincides with the season in the year (autumn/winter) when 80% of the time winds are below 20 kt and waves >2 m are limited to 2–3 days per month (**https://de.wisuki.com/statistics/5884/santorini**). Thus, operational delays triggered by weather are possible but do not seem to be crucial. The currently scheduled contingency time to make up for delays caused by operational issues or weather is 3.2 days (Table **T3**).

8. Sampling and data sharing strategy

Shipboard and shore-based researchers should refer to the IODP Sample, Data, and Obligations Policy and Implementation Guidelines posted online at **http://www.iodp.org/top-resources/program-documents/policies-and-guidelines**. This document outlines the policy for distributing IODP samples and data to research scientists, curators, and educators. The document also defines the obligations that sample and data recipients incur. The Sample Allocation Committee (SAC; composed of Co-Chief Scientists, Expedition Project Manager/Staff Scientist, and IODP Curator on shore and curatorial representative on board the ship) will work with the entire scientific party to formulate a formal expedition-specific sampling plan for shipboard and post-expedition sampling.

Every member of the science party is obligated to carry out scientific research for the expedition and publish the results. All shipboard scientists and any potential shore-based scientists are required to submit a detailed research plan and associated sample/data requests using the IODP Sample and Data Request Management System (at **http://iodp.tamu.edu/curation/samples.html**) before the beginning of Expedition 398. Based on sample requests (shipboard and shore based) submitted by a certain deadline, the SAC will prepare a tentative sampling plan, which will be revised on the ship as dictated by core recovery and expedition objectives. The sampling plan will be subject to modification depending on the actual material recovered and collaborations that may evolve between scientists during the expedition. Modification of the strategy during the expedition and within the moratorium must be approved by the SAC.

Shipboard sampling will include samples taken for shipboard analyses and ephemeral personal samples for postexpedition research (e.g., microbial samples). We expect shipboard samples to be taken for volcanological, geochemical, petrophysical, and microbiological measurements. We will attempt to take nonephemeral personal samples for postexpedition research on board the ship as well. However, it is likely that time constraints will prevent this effort from being completed. Thus, a postexpedition sampling party is going to be held within 4–6 months of the end of the expedition at the IODP Bremen Core Repository (BCR) of the Center for Marine Environmental Sciences (MARUM) at the University of Bremen (Germany). Sampling of whole-round samples are restricted to Hole B at any given site if two APC/HLAPC/XCB holes are planned. If some critical intervals are recovered, there may be considerable demand for samples from a limited amount of cored low-recovery material. These intervals may require special handling (e.g., separate shipboard sampling party), a higher sampling density, reduced sample size, pooled sampling, or continuous core sampling by a single investigator. A dedicated sampling plan coordinated by the SAC may be required before critical intervals are sampled.

The minimum permanent archive will be the standard archive half of each core. All sample frequencies and sizes must be justified on a scientific basis and will depend on core recovery, the full spectrum of other requests, and the expedition objectives. Some redundancy of measurement is unavoidable, but minimizing the duplication of measurements among the shipboard science party and identified shore-based collaborators will be a factor in evaluating sample requests.

The BCR will receive the working- and archive-half core sections from Expedition 398 for permanent storage. Prior to storage at the BCR, all archive-half core sections will be shipped to the IODP Gulf Coast Repository (GCR) at Texas A&M University (College Station, Texas, United States) for

implementation of programmed X-ray fluorescence (XRF) core scanning over a 60 day period after the end of Expedition 398 beginning on 24 April 2023 and ending on 22 June.

All Expedition 398 data and samples will be protected by a 1 y moratorium period that will start at the end of the expedition/postexpedition sampling party. During this moratorium, all data and samples will be available only to the expedition shipboard scientists and approved shore-based participants.

9. Expedition scientists and scientific participants

The current list of participants for Expedition 398 can be found at **http://iodp.tamu.edu/science-ops/expeditions/hellenic_arc_volcanic_field.html**.

References

Aarburg, S., and Frechen, M., 1999. Die pyroklastischen Abfolgen der Christiana-Inseln (Süd-Ägäis, Griechenland). In Becker-Haumann, R., and Frechen, M. (Eds.) Terrestrische Quartargeologie. 260–276.

Acocella, V., 2007. Understanding caldera structure and development: an overview of analogue models compared to natural calderas. Earth-Science Reviews, 85(3–4):125–160. **https://doi.org/10.1016/j.earscirev.2007.08.004**

Acocella, V., and Funiciello, F., 2010. Kinematic setting and structural control of arc volcanism. Earth and Planetary Science Letters, 289(1–2):43–53. **https://doi.org/10.1016/j.epsl.2009.10.027**

Arvanitides, N., Galanopoulos, V., Kalogeropoulos, S., Skamnelos, G., Papavassiliou, C., Paritsis, S., and Boström, K., 1988. Drilling at Santorini Volcano, Greece. Eos, Transactions of the American Geophysical Union, 69(19):578–579. **https://doi.org/10.1029/88EO00166**

Athanasiou, M., Bouloubassi, I., Gogou, A., Klein, V., Dimiza, M.D., Parinos, C., Skampa, E., and Triantaphyllou, M.V., 2017. Sea surface temperatures and environmental conditions during the "warm Pliocene" interval (~4.1–3.2 Ma) in the eastern Mediterranean (Cyprus). Global and Planetary Change, 150:46–57. **https://doi.org/10.1016/j.gloplacha.2017.01.008**

Athanasiou, M., Triantaphyllou, M.V., Dimiza, M.D., Gogou, A., and Theodorou, G., 2015. Zanclean/Piacenzian transition on Cyprus (SE Mediterranean): calcareous nannofossil evidence of sapropel formation. Geo-Marine Letters, 35(5):367–385. **https://doi.org/10.1007/s00367-015-0414-6**

Athanassas, C.D., Bourlès, D.L., Braucher, R., Druitt, T.H., Nomikou, P., and Léanni, L., 2016. Evidence from cosmic ray exposure (CRE) dating for the existence of a pre-Minoan caldera on Santorini, Greece. Bulletin of Volcanology, 78(5):35. **https://doi.org/10.1007/s00445-016-1026-3**

Avnaim-Katav, S., Milker, Y., Schmiedl, G., Sivan, D., Hyams-Kaphzan, O., Sandler, A., and Almogi-Labin, A., 2016. Impact of eustatic and tectonic processes on the southeastern Mediterranean shelf during the last one million years: quantitative reconstructions using a foraminiferal transfer function. Marine Geology, 376:26–38. **https://doi.org/10.1016/j.margeo.2016.03.010**

Bachmann, O., and Huber, C., 2016. Silicic magma reservoirs in the Earth's crust. American Mineralogist, 101(11):2377–2404. **https://doi.org/10.2138/am-2016-5675**

Bailey, J.C., Jensen, E.S., Hansen, A., Kann, A.D.J., and Kann, K., 2009. Formation of heterogeneous magmatic series beneath north Santorini, South Aegean island arc. Lithos, 110(1):20–36. **https://doi.org/10.1016/j.lithos.2008.12.002**

Bardot, L., and McClelland, E., 2000. The reliability of emplacement temperature estimates using palaeomagnetic methods: a case study from Santorini, Greece. Geophysical Journal International, 143(1):39–51. **https://doi.org/10.1046/j.1365-246x.2000.00186.x**

Beck, C., Mercier de Lépinay, B., Schneider, J.-L., Cremer, M., Çağatay, N., Wendenbaum, E., Boutareaud, S., Ménot, G., Schmidt, S., Weber, O., Eris, K., Armijo, R., Meyer, B., Pondard, N., Gutscher, M.-A., Turon, J.L., Labeyrie, L., Cortijo, E., Gallet, Y., Bouquerel, H., Gorur, N., Gervais, A., Castera, M.H., Londeix, L., de Rességuier, A., and Jaouen, A., 2007. Late Quaternary co-seismic sedimentation in the Sea of Marmara's deep basins. Sedimentary Geology, 199(1–2):65–89. **https://doi.org/10.1016/j.sedgeo.2005.12.031**

Beuvier, T., Probert, I., Beaufort, L., Suchéras-Marx, B., Chushkin, Y., Zontone, F., and Gibaud, A., 2019. X-ray nanotomography of coccolithophores reveals that coccolith mass and segment number correlate with grid size. Nature Communications, 10(1):751. **https://doi.org/10.1038/s41467-019-08635-x**

Brandl, P.A., Hamada, M., Arculus, R.J., Johnson, K., Marsaglia, K.M., Savov, I.P., Ishizuka, O., and Li, H., 2017. The arc arises: the links between volcanic output, arc evolution and melt composition. Earth and Planetary Science Letters, 461:73–84. **https://doi.org/10.1016/j.epsl.2016.12.027**

Bruins, H.J., MacGillivray, J.A., Synolakis, C.E., Benjamini, C., Keller, J., Kisch, H.J., Klügel, A., and van der Plicht, J., 2008. Geoarchaeological tsunami deposits at Palaikastro (Crete) and the late Minoan IA eruption of Santorini. Journal of Archaeological Science, 35(1):191–212. **https://doi.org/10.1016/j.jas.2007.08.017**

Budetta, G., Condarelli, D., Fytikas, M., Kolios, N., Pascale, G., Rapolla, A., and Pinna, E., 1984. Geophysical prospecting on the Santorini Islands. Bulletin Volcanologique, 47(3):447–466. **https://doi.org/10.1007/BF01961218**

Camilli, R., Nomikou, P., Escartín, J., Ridao, P., Mallios, A., Kilias, S.P., Argyraki, A., Andreani, M., Ballu, V., Campos, R., Deplus, C., Gabsi, T., Garcia, R., Gracias, N., Hurtós, N., Magí, L., Mével, C., Moreira, M., Palomeras, N., Pot,

O., Ribas, D., Ruzié, L., Sakellariou, D., and the Caldera Science Team, 2015. The Kallisti Limnes, carbon dioxide-accumulating subsea pools. Scientific Reports, 5(1):12152. **https://doi.org/10.1038/srep12152**

Cantner, K., Carey, S., and Nomikou, P., 2014. Integrated volcanologic and petrologic analysis of the 1650AD eruption of Kolumbo submarine volcano, Greece. Journal of Volcanology and Geothermal Research, 269:28–43. **https://doi.org/10.1016/j.jvolgeores.2013.10.004**

Carey, R., Soule, S.A., Manga, M., White, J.D.L., McPhie, J., Wysoczanski, R., Jutzeler, M., Tani, K., Yoerger, D., Fornari, D., Caratori-Tontini, F., Houghton, B., Mitchell, S., Ikegami, F., Conway, C., Murch, A., Fauria, K., Jones, M., Cahalan, R., and McKenzie, W., 2018. The largest deep-ocean silicic volcanic eruption of the past century. Science Advances, 4(1):e1701121. **https://doi.org/10.1126/sciadv.1701121**

Carey, S., Nomikou, P., Bell, K.C., Lilley, M., Lupton, J., Roman, C., Stathopoulou, E., Bejelou, K., and Ballard, R., 2013. CO_2 degassing from hydrothermal vents at Kolumbo submarine volcano, Greece, and the accumulation of acidic crater water. Geology, 41(9):1035–1038. **https://doi.org/10.1130/G34286.1**

Cashman, K.V., Sparks, R.S.J., and Blundy, J.D., 2017. Vertically extensive and unstable magmatic systems: a unified view of igneous processes. Science, 355(6331):eaag3055. **https://doi.org/10.1126/science.aag3055**

Cembrano, J., and Lara, L., 2009. The link between volcanism and tectonics in the southern volcanic zone of the Chilean Andes: a review. Tectonophysics, 471(1–2):96–113. **https://doi.org/10.1016/j.tecto.2009.02.038**

Channell, J.E.T., Xuan, C., and Hodell, D.A., 2009. Stacking paleointensity and oxygen isotope data for the last 1.5 Myr (PISO-1500). Earth and Planetary Science Letters, 283(1–4):14–23. **https://doi.org/10.1016/j.epsl.2009.03.012**

Christakis, C.A., Polymenakou, P.N., Mandalakis, M., Nomikou, P., Kristoffersen, J.B., Lampridou, D., Kotoulas, G., and Magoulas, A., 2018. Microbial community differentiation between active and inactive sulfide chimneys of the Kolumbo submarine volcano, Hellenic Volcanic Arc. Extremophiles, 22(1):13–27. **https://doi.org/10.1007/s00792-017-0971-x**

Danovaro, R., Canals, M., Tangherlini, M., Dell'Anno, A., Gambi, C., Lastras, G., Amblas, D., Sanchez-Vidal, A., Frigola, J., Calafat, A.M., Pedrosa-Pàmies, R., Rivera, J., Rayo, X., and Corinaldesi, C., 2017. A submarine volcanic eruption leads to a novel microbial habitat. nature ecology & evolution, 1(6):144. **https://doi.org/10.1038/s41559-017-0144**

Davidson, J., Turner, S., Handley, H., Macpherson, C., and Dosseto, A., 2007. Amphibole "sponge" in arc crust? Geology, 35(9):787–790. **https://doi.org/10.1130/G23637A.1**

De Lange, G.J., Thomson, J., Reitz, A., Slomp, C.P., Speranza Principato, M., Erba, E., and Corselli, C., 2008. Synchronous basin-wide formation and redox-controlled preservation of a Mediterranean sapropel. Nature Geoscience, 1(9):606–610. **https://doi.org/10.1038/ngeo283**

de Ronde, C.E.J., Humphris, S.E., Höfig, T.W., Brandl, P.A., Cai, L., Cai, Y., Caratori Tontini, F., Deans, J.R., Farough, A., Jamieson, J.W., Kolandaivelu, K.P., Kutovaya, A., Labonté, J.M., Martin, A.J., Massiot, C., McDermott, J.M., McIntosh, I.M., Nozaki, T., Pellizari, V.H., Reyes, A.G., Roberts, S., Rouxel, O., Schlicht, L.E.M., Seo, J.H., Straub, S.M., Strehlow, K., Takai, K., Tanner, D., Tepley III, F.J., and Zhang, C., 2019. Expedition 376 summary. In de Ronde, C.E.J., Humphris, S.E., Höfig, T.W., and the Expedition 376 Scientists, Brothers Arc Flux. Proceedings of the International Ocean Discovery Program, 376: College Station, TX (International Ocean Discovery Program). **https://doi.org/10.14379/iodp.proc.376.101.2019**

Druitt, T.H., 2014. New insights into the initiation and venting of the Bronze-Age eruption of Santorini (Greece), from component analysis. Bulletin of Volcanology, 76(2):794. **https://doi.org/10.1007/s00445-014-0794-x**

Druitt, T.H., and Vougioukalakis, G.E. (Eds.), 2019. The South Aegean Volcanic Arc. Elements, 15(3). **http://elementsmagazine.org/past-issues/south-aegean-volcanic-arc/**

Druitt, T.H., Edwards, L., Mellors, R.M., Pyle, D.M., Sparks, R.S.J., Lanphere, M., Davies, M., and Barreirio, B., 1999. Santorini Volcano. Memoir - Geological Society of London, 19. **http://pubs.er.usgs.gov/publication/70094778**

Druitt, T.H., and Francaviglia, V., 1992. Caldera formation on Santorini and the physiography of the islands in the late Bronze Age. Bulletin of Volcanology, 54(6):484–493. **https://doi.org/10.1007/BF00301394**

Druitt, T.H., Mercier, M., Florentin, L., Deloule, E., Cluzel, N., Flaherty, T., Médard, E., and Cadoux, A., 2016. Magma storage and extraction associated with Plinian and Interplinian activity at Santorini Caldera (Greece). Journal of Petrology, 57(3):461–494. **https://doi.org/10.1093/petrology/egw015**

Duggen, S., Olgun, N., Croot, P., Hoffmann, L., Dietze, H., Delmelle, P., and Teschner, C., 2010. The role of airborne volcanic ash for the surface ocean biogeochemical iron-cycle: a review. Biogeosciences, 7(3):827–844. **https://doi.org/10.5194/bg-7-827-2010**

Elburg, M.A., Smet, I., and De Pelsmaeker, E., 2014. Influence of source materials and fractionating assemblage on magmatism along the Aegean arc, and implications for crustal growth. Geological Society Special Publication, 385(1):137–160. **https://doi.org/10.1144/SP385.1**

Expedition 331 Scientists, 2011. Site C0014. In Takai, K., Mottl, M.J., Nielsen, S.H., and the Expedition 331 Scientists, Proceedings of the Integrated Ocean Drilling Program. 331: Tokyo (Integrated Ocean Drilling Program Management International, Inc.). **https://doi.org/10.2204/iodp.proc.331.104.2011**

Fabbro, G.N., Druitt, T.H., and Scaillet, S., 2013. Evolution of the crustal magma plumbing system during the build-up to the 22-ka caldera-forming eruption of Santorini (Greece). Bulletin of Volcanology, 75(12):767. **https://doi.org/10.1007/s00445-013-0767-5**

Farner, M.J., and Lee, C.-T.A., 2017. Effects of crustal thickness on magmatic differentiation in subduction zone volcanism: a global study. Earth and Planetary Science Letters, 470:96–107. **https://doi.org/10.1016/j.epsl.2017.04.025**

Faugeres, L., and Robert, C., 1976. Etude sédimentologique et minéralogique de deux forages du golfe thermaïque (mer Egée). Géologie Méditerranéenne, 1976(3–4):209–218. **https://www.persee.fr/doc/geolm_0397-2844_1976_num_3_4_977**

Feuillet, N., 2013. The 2011–2012 unrest at Santorini rift: stress interaction between active faulting and volcanism. Geophysical Research Letters, 40(14):3532–3537. **https://doi.org/10.1002/grl.50516**

Filippidi, A., Triantaphyllou, M.V., and De Lange, G.J., 2016. Eastern-Mediterranean ventilation variability during sapropel S1 formation, evaluated at two sites influenced by deep-water formation from Adriatic and Aegean Seas. Quaternary Science Reviews, 144:95–106. **https://doi.org/10.1016/j.quascirev.2016.05.024**

Flaherty, T., Druitt, T.H., Tuffen, H., Higgins, M.D., Costa, F., and Cadoux, A., 2018. Multiple timescale constraints for high-flux magma chamber assembly prior to the Late Bronze Age eruption of Santorini (Greece). Contributions to Mineralogy and Petrology, 173(9):75. **https://doi.org/10.1007/s00410-018-1490-1**

Fouqué, F., 1879. Santorin et ses éruptions: Paris (G. Masson).

Francalanci, L., Varekamp, J., Vougioukalakis, G.E., Delant, M.J., Innocenti, F., and Manetti, P., 1995. Crystal retention, fractionation and crustal assimilation in a convecting magma chamber, Nisyros Volcano, Greece. Bulletin of Volcanology, 56:601–620. **https://doi.org/10.1007/BF00301465**

Francalanci, L., Vougioukalakis, G.E., Perini, G., and Manetti, P., 2005. A West-East traverse along the magmatism of the south Aegean volcanic arc in the light of volcanological, chemical and isotope data. In Fytikas, M. and Vougioukalakis, G.E. (Eds.), The South Aegean Active Volcanic Arc: Present Knowledge and Future Perspectives. Developments in Volcanology, 7: (Elsevier), 65–111. **https://doi.org/10.1016/S1871-644X(05)80033-6**

Freundt, A., Schindlbeck-Belo, J.C., Kutterolf, S., and Hopkins, J.L., 2021. Tephra layers in the marine environment: a review of properties and emplacement processes. In Di Capua, A., De Rosa, R., Kereszturi, G., Le Pera, E., Rosi, M. and Watt, S.F.L.. (Eds.), Volcanic Processes in the Sedimentary Record: When Volcanoes Meet the Environment. Geological Society Special Publication, 520. **https://doi.org/10.1144/SP520-2021-50**

Friedrich, W.L., 2009. Santorini: Volcano, Natural History, Mythology: Aarhus, Denmark (Aarhus University Press).

Fuller, S., Carey, S., and Nomikou, P., 2018. Distribution of fine-grained tephra from the 1650?CE submarine eruption of Kolumbo volcano, Greece. Journal of Volcanology and Geothermal Research, 352:10–25. **https://doi.org/10.1016/j.jvolgeores.2018.01.004**

Geraga, M., Ioakim, C., Lykousis, V., Tsaila-Monopolis, S., and Mylona, G., 2010. The high-resolution palaeoclimatic and palaeoceanographic history of the last 24,000years in the central Aegean Sea, Greece. Palaeogeography, Palaeoclimatology, Palaeoecology, 287(1):101–115. **https://doi.org/10.1016/j.palaeo.2010.01.023**

Giachetti, T., Druitt, T.H., Burgisser, A., Arbaret, L., and Galven, C., 2010. Bubble nucleation, growth and coalescence during the 1997 Vulcanian explosions of Soufrière Hills Volcano, Montserrat. Journal of Volcanology and Geothermal Research, 193(3):215–231. **https://doi.org/10.1016/j.jvolgeores.2010.04.001**

Gogou, A., Bouloubassi, I., Lykousis, V., Arnaboldi, M., Gaitani, P., and Meyers, P.A., 2007. Organic geochemical evidence of late glacial–Holocene climate instability in the north Aegean Sea. Palaeogeography, Palaeoclimatology, Palaeoecology, 256(1):1–20. **https://doi.org/10.1016/j.palaeo.2007.08.002**

Gogou, A., Triantaphyllou, M., Xoplaki, E., Izdebski, A., Parinos, C., Dimiza, M., Bouloubassi, I., Luterbacher, J., Kouli, K., Martrat, B., Toreti, A., Fleitmann, D., Rousakis, G., Kaberi, H., Athanasiou, M., and Lykousis, V., 2016. Climate variability and socio-environmental changes in the northern Aegean (NE Mediterranean) during the last 1500 years. Quaternary Science Reviews, 136:209–228. **https://doi.org/10.1016/j.quascirev.2016.01.009**

Goldfinger, C., 2011. Submarine paleoseismology based on turbidite records. Annual Review of Marine Science, 3(1):35–66. **https://doi.org/10.1146/annurev-marine-120709-142852**

Grant, K.M., Grimm, R., Mikolajewicz, U., Marino, G., Ziegler, M., and Rohling, E.J., 2016. The timing of Mediterranean sapropel deposition relative to insolation, sea-level and African monsoon changes. Quaternary Science Reviews, 140:125–141. **https://doi.org/10.1016/j.quascirev.2016.03.026**

Grant, K.M., Rohling, E.J., Bar-Matthews, M., Ayalon, A., Medina-Elizalde, M., Ramsey, C.B., Satow, C., and Roberts, A.P., 2012. Rapid coupling between ice volume and polar temperature over the past 150,000years. Nature, 491(7426):744–747. **https://doi.org/10.1038/nature11593**

Hanert, H.H., 2002. Bacterial and chemical iron oxide deposition in a shallow bay on Palaea Kameni, Santorini, Greece: microscopy, electron probe microanalysis, and photometry of in situ experiments. Geomicrobiology Journal, 19(3):317–342. **https://doi.org/10.1080/01490450290098405**

Hannington, M., Petersen, S., Nomikou, P., Wind, S., Heinath, V., Lange, S., Rothenbeck, M., Triebe, L., and Wenzlaff, E., 2018. RV POSEIDON Fahrtbericht / Cruise Report POS510 - ANYDROS: Rifting and Hydrothermal Activity in the Cyclades Back-arc Basin, Catania (Italy) – Heraklion (Greece) 06.03.-29.03.2017 GEOMAR Report, 43. **https://doi.org/10.3289/geomar_rep_ns_43_2018**

Heath, B.A., Hooft, E.E.E., Toomey, D.R., Paulatto, M., Papazachos, C.B., Nomikou, P., and Morgan, J.V., 2021. Relationship between active faulting/fracturing and magmatism around Santorini: seismic anisotropy from an active source tomography experiment. Journal of Geophysical Research: Solid Earth, 126(8):e2021JB021898. **https://doi.org/10.1029/2021JB021898**

Hirayama, H., Abe, M., Miyazaki, J., Sakai, S., Nagano, Y., and Takai, K., 2015. Data report: cultivation of microorganisms from basaltic rock and sediment cores from the North Pond on the western flank of the Mid-Atlantic Ridge, IODP Expedition 336. In Edwards, K.J., Bach, W., Klaus, A., and the Expedition 336 Scientists, Proceedings of the Integrated Ocean Drilling Program. 336: Tokyo (Integrated Ocean Drilling Program Management International, Inc.). **https://doi.org/10.2204/iodp.proc.336.204.2015**

Hönisch, B., Ridgwell, A., Schmidt, D.N., Thomas, E., Gibbs, S.J., Sluijs, A., Zeebe, R., Kump, L., Martindale, R.C., Greene, S.E., Kiessling, W., Ries, J., Zachos, J.C., Royer, D.L., Barker, S., Marchitto, T.M., Moyer, R., Pelejero, C., Ziveri, P., Foster, G.L., and Williams, B., 2012. The geological record of ocean acidification. Science, 335(6072):1058–1063. **https://doi.org/10.1126/science.1208277**

Hooft, E.E.E., Heath, B.A., Toomey, D.R., Paulatto, M., Papazachos, C.B., Nomikou, P., Morgan, J.V., and Warner, M.R., 2019. Seismic imaging of Santorini: subsurface constraints on caldera collapse and present-day magma recharge. Earth and Planetary Science Letters, 514:48–61. **https://doi.org/10.1016/j.epsl.2019.02.033**

Hooft, E.E.E., Nomikou, P., Toomey, D.R., Lampridou, D., Getz, C., Christopoulou, M.-E., O'Hara, D., Arnoux, G.M., Bodmer, M., Gray, M., Heath, B.A., and VanderBeek, B.P., 2017. Backarc tectonism, volcanism, and mass wasting

shape seafloor morphology in the Santorini-Christiana-Amorgos region of the Hellenic Volcanic Arc. Tectonophysics, 712–713:396–414. **https://doi.org/10.1016/j.tecto.2017.06.005**

House, C.H., Cragg, B.A., Teske, A., and the Leg 201 Scientific Party, 2003. Drilling contamination tests during ODP Leg 201 using chemical and particulate tracers. In D'Hondt, S.L., Jørgensen, B.B., Miller, D.J., et al., Proceedings of the Ocean Drilling Program, Initial Reports. 201: College Station, TX (Ocean Drilling Program). **https://doi.org/10.2973/odp.proc.ir.201.102.2003**

Hsü, K.J., Montadert, L., Bernoulli, D., Bizon, G., Cita, M., Erickson, A., Fabricius, F., Garrison, R.E., Kidd, R.B., Mélières, F., Müller, C., and Wright, R.C., 1978. Introduction and explanatory notes. In Hsü, K., Montadert, L., et al., Initial Reports of the Deep Sea Drilling Project. 42 (Part 1): Washington, DC (US Government Printing Office), 3–26. **https://doi.org/10.2973/dsdp.proc.42-1.101.1978**

Hübscher, C., Ruhnau, M., and Nomikou, P., 2015. Volcano-tectonic evolution of the polygenetic Kolumbo submarine volcano/Santorini (Aegean Sea). Journal of Volcanology and Geothermal Research, 291:101–111. **https://doi.org/10.1016/j.jvolgeores.2014.12.020**

Huijsmans, J.P.P., Barton, M., and Salters, V.J.M., 1988. Geochemistry and evolution of the calc-alkaline volcanic complex of santorini, Aegean Sea, Greece. Journal of Volcanology and Geothermal Research, 34(3–4):283–306. **https://doi.org/10.1016/0377-0273(88)90039-X**

Johnston, E.N., Sparks, R.S.J., Nomikou, P., Livanos, I., Carey, S., Phillips, J.C., and Sigurdsson, H., 2015. Stratigraphic relations of Santorini's intracaldera fill and implications for the rate of post-caldera volcanism. Journal of the Geological Society, 172(3):323–335. **https://doi.org/10.1144/jgs2013-114**

Jolivet, L., Faccenna, C., Huet, B., Labrousse, L., Le Pourhiet, L., Lacombe, O., Lecomte, E., Burov, E., Denèle, Y., Brun, J.-P., Philippon, M., Paul, A., Salaün, G., Karabulut, H., Piromallo, C., Monié, P., Gueydan, F., Okay, A.I., Oberhänsli, R., Pourteau, A., Augier, R., Gadenne, L., and Driussi, O., 2013. Aegean tectonics: strain localisation, slab tearing and trench retreat. Tectonophysics, 597–598:1–33. **https://doi.org/10.1016/j.tecto.2012.06.011**

Kalyoncuoglu, U.Y., Elitok, Ö., and Dolmaz, M.N., 2013. Tectonic implications of spatial variation of b-values and heat flow in the Aegean region. Marine Geophysical Research, 34(1):59–78. **https://doi.org/10.1007/s11001-013-9174-8**

Katsouras, G., Gogou, A., Bouloubassi, I., Emeis, K.-C., Triantaphyllou, M., Roussakis, G., and Lykousis, V., 2010. Organic carbon distribution and isotopic composition in three records from the eastern Mediterranean Sea during the Holocene. Organic Geochemistry, 41(9):935–939. **https://doi.org/10.1016/j.orggeochem.2010.04.008**

Keller, J., Dietrich, V., Reusser, E., Gertisser, R., and Aarburg, S., 2010. Recognition of a major ignimbrite in the early evolution of the Santorini Group: the Christiani Ignimbrite. Presented at the Cities on Volcanoes Conference, Tenerife, Spain, January 2010.

Kilias, S.P., Nomikou, P., Papanikolaou, D., Polymenakou, P.N., Godelitsas, A., Argyraki, A., Carey, S., Gamaletsos, P., Mertzimekis, T.J., Stathopoulou, E., Goettlicher, J., Steininger, R., Betzelou, K., Livanos, I., Christakis, C., Bell, K.C., and Scoullos, M., 2013. New insights into hydrothermal vent processes in the unique shallow-submarine arc-volcano, Kolumbo (Santorini), Greece. Scientific Reports, 3(1):2421. **https://doi.org/10.1038/srep02421**

Klaver, M., Blundy, J.D., and Vroon, P.Z., 2018. Generation of arc rhyodacites through cumulate-melt reactions in a deep crustal hot zone: evidence from Nisyros volcano. Earth and Planetary Science Letters, 497:169–180. **https://doi.org/10.1016/j.epsl.2018.06.019**

Klaver, M., Carey, S., Nomikou, P., Smet, I., Godelitsas, A., and Vroon, P., 2016a. A distinct source and differentiation history for Kolumbo submarine volcano, Santorini volcanic field, Aegean arc. Geochemistry, Geophysics, Geosystems, 17(8):3254–3273. **https://doi.org/10.1002/2016GC006398**

Klaver, M., Davies, G.R., and Vroon, P.Z., 2016b. Subslab mantle of African provenance infiltrating the Aegean mantle wedge. Geology, 44(5):367–370. **https://doi.org/10.1130/G37627.1**

Kokkalas, S., and Aydin, A., 2013. Is there a link between faulting and magmatism in the south-central Aegean Sea? Geological Magazine, 150(2):193–224. **https://doi.org/10.1017/S0016756812000453**

Kouli, K., Gogou, A., Bouloubassi, I., Triantaphyllou, M.V., Ioakim, C., Katsouras, G., Roussakis, G., and Lykousis, V., 2012. Late postglacial paleoenvironmental change in the northeastern Mediterranean region: combined palynological and molecular biomarker evidence. Quaternary International, 261:118–127. **https://doi.org/10.1016/j.quaint.2011.10.036**

Kouli, K., Rousakis, G., Bouloubassi, I., Gogou, A., Kyrikou, S., Ratopoulou, M., Triantaphyllou, M., Dimiza, M., Kapsimalis, V., and Lykousis, V., 2015. Palynological investigation of the marine core SK-3 (SW Aegean Sea): implications on the vegetation of the last Interglacial. Proceedings of the 11th Panhellenic Symposium on Oceanography and Fisheries, 2015:1009–1012.

Kutterolf, S., Freundt, A., Druitt, T.H., McPhie, J., Nomikou, P., Pank, K., Schindlbeck-Belo, J.C., Hansteen, T.H., and Allen, S., 2021a. The medial offshore record of explosive volcanism along the central to eastern Aegean Volcanic Arc, part 2: Tephra ages and volumes, eruption magnitudes and marine sedimentation rate variations. Geochemistry, Geophysics, Geosystems. **https://doi.org/10.1029/2021GC010011**

Kutterolf, S., Freundt, A., Hansteen, T.H., Dettbarn, R., Hampel, F., Sievers, C., Wittig, C., Allen, S., Druitt, T.H., McPhie, J., Nomikou, P., Pank, K., Schindlbeck-Belo, J.C., Wang, K.-L., Lee, H.-Y., and Friedrichs, B., 2021b. The medial offshore record of explosive volcanism along the central to eastern Aegean Volcanic Arc, part 1: Tephrostratigraphic correlations. Geochemistry, Geophysics, Geosystems. **https://doi.org/10.1029/2021GC010010**

Kutterolf, S., Jegen, M., Mitrovica, J.X., Kwasnitschka, T., Freundt, A., and Huybers, P.J., 2013. A detection of Milankovitch frequencies in global volcanic activity. Geology, 41(2):227–230. **https://doi.org/10.1130/G33419.1**

Kutterolf, S., Schindlbeck, J.C., Scudder, R.P., Murray, R.W., Pickering, K.T., Freundt, A., Labanieh, S., Heydolph, K., Saito, S., Naruse, H., Underwood, M.B., and Wu, H., 2014. Large volume submarine ignimbrites in the Shikoku

Basin: an example for explosive volcanism in the Western Pacific during the Late Miocene. Geochemistry, Geophysics, Geosystems, 15(5):1837–1851. **https://doi.org/10.1002/2014GC005263**

Laskar, J., Robutel, P., Joutel, F., Gastineau, M., Correia, A.C.M., and Levrard, B., 2004. A long-term numerical solution for the insolation quantities of the Earth. A&A, 428(1):261–285. **https://doi.org/10.1051/0004-6361:20041335**

Le Pichon, X., and Kreemer, C., 2010. The Miocene-to-Present kinematic evolution of the eastern Mediterranean and Middle East and its implications for dynamics. Annual Review of Earth and Planetary Sciences, 38(1):323–351. **https://doi.org/10.1146/annurev-earth-040809-152419**

Lever, M.A., 2013. Functional gene surveys from ocean drilling expeditions—a review and perspective. FEMS Microbiology Ecology, 84(1):1–23. **https://doi.org/10.1111/1574-6941.12051**

Lever, M.A., Alperin, M., Engelen, B., Inagaki, F., Nakagawa, S., Steinsbu, B.O., and Teske, A., 2006. Trends in basalt and sediment core contamination during IODP Expedition 301. Geomicrobiology Journal, 23(7):517–530. **https://doi.org/10.1080/01490450600897245**

Lipman, P.W., 1997. Subsidence of ash-flow calderas: relation to caldera size and magma-chamber geometry. Bulletin of Volcanology, 59(3):198–218. **https://doi.org/10.1007/s004450050186**

Lougheed, B.C., and Obrochta, S.P., 2019. A rapid, deterministic age-depth modeling routine for geological sequences with inherent depth uncertainty. Paleoceanography and Paleoclimatology, 34(1):122–133. **https://doi.org/10.1029/2018PA003457**

Loughlin, S.C., Sparks, S., Brown, S.K., Jenkins, S.F., and Vye-Brown, C. (Eds.), 2015. Global Volcanic Hazards and Risk: Cambridge, United Kingdom (Cambridge University Press). **https://doi.org/10.1017/CBO9781316276273**

Lykousis, V., Roussakis, G., and Sakellariou, D., 2009. Slope failures and stability analysis of shallow water prodeltas in the active margins of Western Greece, northeastern Mediterranean Sea. International Journal of Earth Sciences, 98(4):807–822. **https://doi.org/10.1007/s00531-008-0329-9**

Makris, J., Papoulia, J., and Yegorova, T., 2013. A 3-D density model of Greece constrained by gravity and seismic data. Geophysical Journal International, 194(1):1–17. **https://doi.org/10.1093/gji/ggt059**

McGuire, J., Plank, T., Barrientos, S., Becker, T., Brodsky, E., Cottrell, E., French, M., Fulton, P., Gomberg, J., Gulick, S., Haney, M., Melgar, D., Penniston-Dorland, S., Roman, D., Skemer, P., Tobin, H., Wada, I., and Wiens, D., 2017. The SZ4D Initiative: Understanding the Processes that Underlie Subduction Zone Hazards in 4D. Vision Document Submitted to the National Science Foundation. The IRIS Consortium. **http://www-udc.ig.utexas.edu/external/becker/sz4dmcs/ftp/sz4d.pdf**

McGuire, W.J., Howarth, R.J., Firth, C.R., Solow, A.R., Pullen, A.D., Saunders, S.J., Stewart, I.S., and Vita-Finzi, C., 1997. Correlation between rate of sea-level change and frequency of explosive volcanism in the Mediterranean. Nature, 389(6650):473–476. **https://doi.org/10.1038/38998**

McVey, B.G., Hooft, E.E.E., Heath, B.A., Toomey, D.R., Paulatto, M., Morgan, J.V., Nomikou, P., and Papazachos, C.B., 2019. Magma accumulation beneath Santorini volcano, Greece, from P-wave tomography. Geology, 48(3):231–235. **https://doi.org/10.1130/G47127.1**

Milker, Y., Weinkauf, M.F.G., Titschack, J., Freiwald, A., Krüger, S., Jorissen, F.J., and Schmiedl, G., 2017. Testing the applicability of a benthic foraminiferal-based transfer function for the reconstruction of paleowater depth changes in Rhodes (Greece) during the early Pleistocene. PloS One, 12(11):e0188447. **https://doi.org/10.1371/journal.pone.0188447**

Mortazavi, M., and Sparks, R.S.J., 2004. Origin of rhyolite and rhyodacite lavas and associated mafic inclusions of Cape Akrotiri, Santorini: the role of wet basalt in generating calcalkaline silicic magmas. Contributions to Mineralogy and Petrology, 146(4):397–413. **https://doi.org/10.1007/s00410-003-0508-4**

National Academies of Sciences, Engineering, and Medicine, 2017. Volcanic Eruptions and Their Repose, Unrest, Precursors, and Timing: Washington, DC (The National Academies Press). **https://doi.org/10.17226/24650**

Newman, A.V., Stiros, S., Feng, L., Psimoulis, P., Moschas, F., Saltogianni, V., Jiang, Y., Papazachos, C., Panagiotopoulos, D., Karagianni, E., and Vamvakaris, D., 2012. Recent geodetic unrest at Santorini Caldera, Greece. Geophysical Research Letters, 39(6):L06309. **https://doi.org/10.1029/2012GL051286**

Nomikou, P., Carey, S., Papanikolaou, D., Croff Bell, K., Sakellariou, D., Alexandri, M., and Bejelou, K., 2012. Submarine volcanoes of the Kolumbo volcanic zone NE of Santorini Caldera, Greece. Global and Planetary Change, 90-91:135–151. **https://doi.org/10.1016/j.gloplacha.2012.01.001**

Nomikou, P., Druitt, T.H., Hübscher, C., Mather, T.A., Paulatto, M., Kalnins, L.M., Kelfoun, K., Papanikolaou, D., Bejelou, K., Lampridou, D., Pyle, D.M., Carey, S., Watts, A.B., Weiß, B., and Parks, M.M., 2016a. Post-eruptive flooding of Santorini caldera and implications for tsunami generation. Nature Communications, 7(1):13332. **https://doi.org/10.1038/ncomms13332**

Nomikou, P., Hübscher, C., Papanikolaou, D., Farangitakis, G.P., Ruhnau, M., and Lampridou, D., 2018. Expanding extension, subsidence and lateral segmentation within the Santorini - Amorgos basins during Quaternary: implications for the 1956 Amorgos events, central - south Aegean Sea, Greece. Tectonophysics, 722:138–153. **https://doi.org/10.1016/j.tecto.2017.10.016**

Nomikou, P., Hübscher, C., Ruhnau, M., and Bejelou, K., 2016b. Tectono-stratigraphic evolution through successive extensional events of the Anydros Basin, hosting Kolumbo volcanic field at the Aegean Sea, Greece. Tectonophysics, 671:202–217. **https://doi.org/10.1016/j.tecto.2016.01.021**

Nomikou, P., Papanikolaou, D., Alexandri, M., Sakellariou, D., and Rousakis, G., 2013. Submarine volcanoes along the Aegean volcanic arc. Tectonophysics, 597-598:123–146. **https://doi.org/10.1016/j.tecto.2012.10.001**

Nomikou, P., Parks, M.M., Papanikolaou, D., Pyle, D.M., Mather, T.A., Carey, S., Watts, A.B., Paulatto, M., Kalnins, M.L., Livanos, I., Bejelou, K., Simou, E., and Perros, I., 2014. The emergence and growth of a submarine volcano: the Kameni islands, Santorini (Greece). GeoResJ, 1–2:8–18. **https://doi.org/10.1016/j.grj.2014.02.002**

Novikova, T., Papadopoulos, G.A., and McCoy, F.W., 2011. Modelling of tsunami generated by the giant Late Bronze Age eruption of Thera, south Aegean Sea, Greece. Geophysical Journal International, 186(2):665–680. **https://doi.org/10.1111/j.1365-246X.2011.05062.x**

Okal, E.A., Synolakis, C.E., Uslu, B., Kalligeris, N., and Voukouvalas, E., 2009. The 1956 earthquake and tsunami in Amorgos, Greece. Geophysical Journal International, 178(3):1533–1554. **https://doi.org/10.1111/j.1365-246X.2009.04237.x**

Oulas, A., Polymenakou, P.N., Seshadri, R., Tripp, H.J., Mandalakis, M., Paez-Espino, A.D., Pati, A., Chain, P., Nomikou, P., Carey, S., Kilias, S., Christakis, C., Kotoulas, G., Magoulas, A., Ivanova, N.N., and Kyrpides, N.C., 2016. Metagenomic investigation of the geologically unique Hellenic Volcanic Arc reveals a distinctive ecosystem with unexpected physiology. Environmental Microbiology, 18(4):1122–1136. **https://doi.org/10.1111/1462-2920.13095**

Pallikarakis, A., Triantaphyllou, M.V., Papanikolaou, I., Dimiza, M.D., Reicherter, K., and Migiros, G., 2018. Age constraints and paleoenvironmental interpretation of a borehole sedimentary sequence along the eastern part of the Corinth Isthmus, Greece. Journal of Coastal Research, 34(3):602–617. **https://doi.org/10.2112/JCOASTRES-D-16-00191.1**

Papanikolaou, M.D., Triantaphyllou, M.V., Platzman, E.S., Gibbard, P.L., Niocaill, C.M., and Head, M.J., 2011. A well-established early–middle Pleistocene marine sequence on south-east Zakynthos island, western Greece: magneto-biostratigraphic constraints and palaeoclimatic implications. Journal of Quaternary Science, 26(5):523–540. **https://doi.org/10.1002/jqs.1462**

Papazachos, C.B., 2019. Deep structure and active tectonics of the South Aegean Volcanic Arc. Elements, 15(3):153–158. **https://doi.org/10.2138/gselements.15.3.153**

Parkes, R.J., Cragg, B.A., and Wellsbury, P., 2000. Recent studies on bacterial populations and processes in subseafloor sediments: a review. Hydrogeology Journal, 8(1):11–28. **https://doi.org/10.1007/PL00010971**

Parks, M.M., Moore, J.D.P., Papanikolaou, X., Biggs, J., Mather, T.A., Pyle, D.M., Raptakis, C., Paradissis, D., Hooper, A., Parsons, B., and Nomikou, P., 2015. From quiescence to unrest: 20years of satellite geodetic measurements at Santorini volcano, Greece. Journal of Geophysical Research: Solid Earth, 120(2):1309–1328. **https://doi.org/10.1002/2014JB011540**

Pe-Piper, G., and Piper, D.J.W., 2005. The South Aegean active volcanic arc: relationships between magmatism and tectonics. In Fytikas, M., and Vougioukalakis, G.E. (Eds.), The South Aegean Active Volcanic Arc: Present Knowledge and Future Perspectives. Developments in Volcanology, 7: 113–133. **https://doi.org/10.1016/S1871-644X(05)80034-8**

Perissoratis, C., 1995. The Santorini volcanic complex and its relation to the stratigraphy and structure of the Aegean arc, Greece. Marine Geology, 128(1):37–58. **https://doi.org/10.1016/0025-3227(95)00090-L**

Piper, D.J.W., and Perissoratis, C., 2003. Quaternary neotectonics of the South Aegean arc. Marine Geology, 198(3–4):259–288. **https://doi.org/10.1016/S0025-3227(03)00118-X**

Polonia, A., Bonatti, E., Camerlenghi, A., Lucchi, R.G., Panieri, G., and Gasperini, L., 2013. Mediterranean megaturbidite triggered by the AD 365 Crete earthquake and tsunami. Scientific Reports, 3(1):1285. **https://doi.org/10.1038/srep01285**

Polymenakou, P.N., Nomikou, P., Zafeiropoulos, H., Mandalakis, M., Anastasiou, T.I., Kilias, S., Kyrpides, N.C., Kotoulas, G., and Magoulas, A., 2021. The Santorini volcanic complex as a valuable source of enzymes for bioenergy. Energies, 14(5):1414. **https://doi.org/10.3390/en14051414**

Preine, J., Karstens, J., Hübscher, C., Nomikou, P., Schmid, F., Crutchley, G.J., Druitt, T.H., and Papanikolaou, D., 2022. Spatio-temporal evolution of the Christiana-Santorini-Kolumbo volcanic field, Aegean Sea. Geology, 50(1):96–100. **https://doi.org/10.1130/G49167.1**

Putirka, K.D., 2008. Thermometers and Barometers for Volcanic Systems. Reviews in Mineralogy and Geochemistry, 69(1):61–120. **https://doi.org/10.2138/rmg.2008.69.3**

Pyle, D.M., 1990. New estimates for the volume of the Minoan eruption. In Hardy, D.A. (Ed.), Thera and the Aegean World III (Volume 2). London (Thera Foundation), 113–121.

Pyle, D.M., and Elliott, J.R., 2006. Quantitative morphology, recent evolution, and future activity of the Kameni Islands volcano, Santorini, Greece. Geosphere, 2(5):253–268. **https://doi.org/10.1130/GES00028.1**

Rabillard, A., Jolivet, L., Arbaret, L., Bessière, E., Laurent, V., Menant, A., Augier, R., and Beaudoin, A., 2018. Synextensional granitoids and detachment systems within cycladic metamorphic core complexes (Aegean Sea, Greece): toward a regional tectonomagmatic model. Tectonics, 37(8):2328–2362. **https://doi.org/10.1029/2017TC004697**

Roberts, A.P., Tauxe, L., and Heslop, D., 2013. Magnetic paleointensity stratigraphy and high-resolution Quaternary geochronology: successes and future challenges. Quaternary Science Reviews, 61:1–16. **https://doi.org/10.1016/j.quascirev.2012.10.036**

Rohling, E.J., Foster, G.L., Grant, K.M., Marino, G., Roberts, A.P., Tamisiea, M.E., and Williams, F., 2014. Sea-level and deep-sea-temperature variability over the past 5.3 million years. Nature, 508(7497):477–482. **https://doi.org/10.1038/nature13230**

Rohling, E.J., Marino, G., and Grant, K.M., 2015. Mediterranean climate and oceanography, and the periodic development of anoxic events (sapropels). Earth-Science Reviews, 143:62–97. **https://doi.org/10.1016/j.earscirev.2015.01.008**

Rotella, M.D., Wilson, C.J.N., Barker, S.J., Schipper, C.I., Wright, I.C., and Wysoczanski, R.J., 2015. Dynamics of deep submarine silicic explosive eruptions in the Kermadec arc, as reflected in pumice vesicularity textures. Journal of Volcanology and Geothermal Research, 301:314–332. **https://doi.org/10.1016/j.jvolgeores.2015.05.021**

Royden, L.H., and Papanikolaou, D.J., 2011. Slab segmentation and late Cenozoic disruption of the Hellenic arc. Geochemistry, Geophysics, Geosystems, 12(3):Q03010. **https://doi.org/10.1029/2010GC003280**

Sachpazi, M., Laigle, M., Charalampakis, M., Diaz, J., Kissling, E., Gesret, A., Becel, A., Flueh, E., Miles, P., and Hirn, A., 2016. Segmented Hellenic slab rollback driving Aegean deformation and seismicity. Geophysical Research Letters, 43(2):651–658. **https://doi.org/10.1002/2015GL066818**

Sakellariou, D., Rousakis, G., Sigurdsson, H., Nomikou, P., Katsenis, I., Crift Bell, K., and Carey, S., 2012. Seismic stratigraphy of Santorini's caldera: a contribution to the understanding of the Minoan eruption. Presented at the 10th Hellenic Symposium on Oceanography & Fisheries, May 2012.

Satow, C., Gudmundsson, A., Gertisser, R., Ramsey, C.B., Bazargan, M., Pyle, D.M., Wulf, S., Miles, A.J., and Hardiman, M., 2021. Eruptive activity of the Santorini Volcano controlled by sea-level rise and fall. Nature Geoscience, 14(8):586–592. **https://doi.org/10.1038/s41561-021-00783-4**

Satow, C., Tomlinson, E.L., Grant, K.M., Albert, P.G., Smith, V.C., Manning, C.J., Ottolini, L., Wulf, S., Rohling, E.J., Lowe, J.J., Blockley, S.P.E., and Menzies, M.A., 2015. A new contribution to the Late Quaternary tephrostratigraphy of the Mediterranean: Aegean Sea core LC21. Quaternary Science Reviews, 117:96–112. **https://doi.org/10.1016/j.quascirev.2015.04.005**

Schindlbeck, J.C., Kutterolf, S., Freundt, A., Alvarado, G.E., Wang, K.L., Straub, S.M., Hemming, S.R., Frische, M., and Woodhead, J.D., 2016. Late Cenozoic tephrostratigraphy offshore the southern Central American volcanic arc: 1. Tephra ages and provenance. Geochemistry, Geophysics, Geosystems, 17(11):4641–4668. **https://doi.org/10.1002/2016GC006503**

Schippers, A., Neretin, L.N., Kallmeyer, J., Ferdelman, T.G., Cragg, B.A., John Parkes, R., and Jørgensen, B.B., 2005. Prokaryotic cells of the deep sub-seafloor biosphere identified as living bacteria. Nature, 433(7028):861–864. **https://doi.org/10.1038/nature03302**

Schmincke, H.U., and Sumita, M., 1998. Volcanic evolution of Gran Canaria reconstructed from apron sediments: synthesis of VICAP project drilling. In Weaver, P.P.E., Schmincke, H.-U., Firth, J.V., and Duffield, W. (Eds.), Proceedings of the Ocean Drilling Program, Scientific Results. 157: College Station, TX (Ocean Drilling Program). **https://doi.org/10.2973/odp.proc.sr.157.135.1998**

Schwarz, B., and Gajewski, D., 2017. Accessing the diffracted wavefield by coherent subtraction. Geophysical Journal International, 211(1):45–49. **https://doi.org/10.1093/gji/ggx291**

Shaw, B., and Jackson, J., 2010. Earthquake mechanisms and active tectonics of the Hellenic subduction zone. Geophysical Journal International, 181(2):966–984. **https://doi.org/10.1111/j.1365-246X.2010.04551.x**

Sigurdsson, H., Carey, S., Alexandri, M., Vougioukalakis, G., Croff, K., Roman, C., Sakellariou, D., Anagnostou, C., Rousakis, G., Ioakim, C., Gogou, A., Missaridis, A., and Nomikou, P., 2006. Marine investigations of Greece's Santorini volcanic field. Eos Transactions American Geophysical Union, 37:342.

Sigurdsson, H.E. (Ed.), 2015. Encyclopedia of Volcanoes: New York (Elsevier). **https://doi.org/10.1016/C2015-0-00175-7**

Smith, D.J., 2014. Clinopyroxene precursors to amphibole sponge in arc crust. Nature Communications, 5(1):4329. **https://doi.org/10.1038/ncomms5329**

Sparks, R.S.J., and Wilson, C.J.N., 1990. The Minoan deposits: a review of their characteristics and interpretation. In Hardy, D.A. (Ed.), Thera and the Aegean World III (Volume 2). London (Thera Foundation), 89–99.

Sternai, P., Caricchi, L., Garcia-Castellanos, D., Jolivet, L., Sheldrake, T.E., and Castelltort, S., 2017. Magmatic pulse driven by sea-level changes associated with the Messinian salinity crisis. Nature Geoscience, 10(10):783–787. **https://doi.org/10.1038/ngeo3032**

Sumner, E.J., Siti, M.I., McNeill, L.C., Talling, P.J., Henstock, T.J., Wynn, R.B., Djajadihardja, Y.S., and Permana, H., 2013. Can turbidites be used to reconstruct a paleoearthquake record for the central Sumatran margin? Geology, 41(7):763–766. **https://doi.org/10.1130/G34298.1**

Syracuse, E.M., van Keken, P.E., and Abers, G.A., 2010. The global range of subduction zone thermal models. Physics of the Earth and Planetary Interiors, 183(1):73–90. **https://doi.org/10.1016/j.pepi.2010.02.004**

Tassi, F., Vaselli, O., Papazachos, C.B., Giannini, L., Chiodini, G., Vougioukalakis, G.E., Karagianni, E., Vamvakaris, D., and Panagiotopoulos, D., 2013. Geochemical and isotopic changes in the fumarolic and submerged gas discharges during the 2011–2012 unrest at Santorini caldera (Greece). Bulletin of Volcanology, 75(4):711. **https://doi.org/10.1007/s00445-013-0711-8**

Templeton, A.S., 2011. Geomicrobiology of iron in extreme environments. Elements, 7(2):95–100. **https://doi.org/10.2113/gselements.7.2.95**

Triantaphyllou, M., Baumann, K.-H., Karatsolis, B.-T., Dimiza, M.D., Psarra, S., Skampa, E., Patoucheas, P., Vollmar, N.M., Koukousioura, O., Katsigera, A., Krasakopoulou, E., and Nomikou, P., 2018. Coccolithophore community response along a natural CO_2 gradient off Methana (SW Saronikos Gulf, Greece, NE Mediterranean). PloS One. **https://doi.org/10.1371/journal.pone.0200012**

Triantaphyllou, M.V., Antonarakou, A., Kouli, K., Dimiza, M., Kontakiotis, G., Papanikolaou, M.D., Ziveri, P., Mortyn, P.G., Lianou, V., Lykousis, V., and Dermitzakis, M.D., 2009a. Late Glacial–Holocene ecostratigraphy of the southeastern Aegean Sea, based on plankton and pollen assemblages. Geo-Marine Letters, 29(4):249–267. **https://doi.org/10.1007/s00367-009-0139-5**

Triantaphyllou, M.V., Gogou, A., Bouloubassi, I., Dimiza, M., Kouli, K., Rousakis, G., Kotthoff, U., Emeis, K.C., Papanikolaou, M., Athanasiou, M., Parinos, C., Ioakim, C., and Lykousis, V., 2014. Evidence for a warm and humid mid-Holocene episode in the Aegean and northern Levantine Seas (Greece, NE Mediterranean). Regional Environmental Change, 14(5):1697–1712. **https://doi.org/10.1007/s10113-013-0495-6**

Triantaphyllou, M.V., Gogou, A., Dimiza, M.D., Kostopoulou, S., Parinos, C., Roussakis, G., Geraga, M., Bouloubassi, I., Fleitmann, D., Zervakis, V., Velaoras, D., Diamantopoulou, A., Sampatakaki, A., and Lykousis, V., 2016. Holocene climatic optimum centennial-scale paleoceanography in the NE Aegean (Mediterranean Sea). Geo-Marine Letters, 36(1):51–66. **https://doi.org/10.1007/s00367-015-0426-2**

Triantaphyllou, M.V., Ziveri, P., Gogou, A., Marino, G., Lykousis, V., Bouloubassi, I., Emeis, K.C., Kouli, K., Dimiza, M., Rosell-Melé, A., Papanikolaou, M., Katsouras, G., and Nunez, N., 2009b. Late Glacial–Holocene climate variability at the south-eastern margin of the Aegean Sea. Marine Geology, 266(1–4):182–197. **https://doi.org/10.1016/j.margeo.2009.08.005**

Tsampouraki-Kraounaki, K., and Sakellariou, D., 2018. Seismic stratigraphy and geodynamic evolution of Christiana Basin, South Aegean Arc. Marine Geology, 399:135–147. **https://doi.org/10.1016/j.margeo.2018.02.012**

Ulvrova, M., Paris, R., Nomikou, P., Kelfoun, K., Leibrandt, S., Tappin, D.R., and McCoy, F.W., 2016. Source of the tsunami generated by the 1650AD eruption of Kolumbo submarine volcano (Aegean Sea, Greece). Journal of Volcanology and Geothermal Research, 321:125–139. **https://doi.org/10.1016/j.jvolgeores.2016.04.034**

Vaggelli, G., Pellegrini, M., Vougioukalakis, G., Innocenti, S., and Francalanci, L., 2009. Highly Sr radiogenic tholeiitic magmas in the latest inter-Plinian activity of Santorini volcano, Greece. Journal of Geophysical Research: Solid Earth, 114(B6):B06201. **https://doi.org/10.1029/2008JB005936**

Valet, J.-P., Meynadier, L., and Guyodo, Y., 2005. Geomagnetic dipole strength and reversal rate over the past two million years. Nature, 435(7043):802–805. **https://doi.org/10.1038/nature03674**

Vougioukalakis, G., Sparks, R.S., Druitt, T., Pyle, D., Papazachos, C., and Fytikas, M., 2016. Volcanic hazard assessment at Santorini Volcano: a review and a synthesis in the light of the 2011–2012 Santorini unrest. Bulletin of the Geological Society of Greece, 50(1):274–283. **https://doi.org/10.12681/bgsg.11728**

Walter, T.R., and Amelung, F., 2007. Volcanic eruptions following M ≥ 9 megathrust earthquakes: implications for the Sumatra-Andaman volcanoes. Geology, 35(6):539–542. **https://doi.org/10.1130/G23429A.1**

Wang, P., Tian, J., and Lourens, L.J., 2010. Obscuring of long eccentricity cyclicity in Pleistocene oceanic carbon isotope records. Earth and Planetary Science Letters, 290(3–4):319–330. **https://doi.org/10.1016/j.epsl.2009.12.028**

White, J.D.L., Schipper, C.I., and Kano, K., 2015. Submarine explosive eruptions. In Sigurdsson, H. (Ed.), The Encyclopedia of Volcanoes (Second Edition). Amsterdam (Academic Press), 553–569. **https://doi.org/10.1016/B978-0-12-385938-9.00031-6**

Wulf, S., Keller, J., Satow, C., Gertisser, R., Kraml, M., Grant, K.M., Appelt, O., Vakhrameeva, P., Koutsodendris, A., Hardiman, M., Schulz, H., and Pross, J., 2020. Advancing Santorini's tephrostratigraphy: new glass geochemical data and improved marine-terrestrial tephra correlations for the past ~360 kyrs. Earth-Science Reviews, 200:102964. **https://doi.org/10.1016/j.earscirev.2019.102964**

Zellmer, G.F., and Turner, S.P., 2007. Arc dacite genesis pathways: evidence from mafic enclaves and their hosts in Aegean lavas. Lithos, 95(3):346–362. **https://doi.org/10.1016/j.lithos.2006.08.002**

Zimanowski, B., Büttner, R., Dellino, P., White, J.D.L., and Wohletz, K.H., 2015. Magma–water interaction and phreatomagmatic fragmentation. In Sigurdsson, H. (Ed.), The Encyclopedia of Volcanoes (Second Edition). Amsterdam (Academic Press), 473–484. **https://doi.org/10.1016/B978-0-12-385938-9.00026-2**

Site summaries

Site CSK-01A (Anhydros Basin)

Priority:	Primary
Position:	36.7293°N, 25.6482°E (36° 43.7580'N, 25° 38.8920' E) Central Anhydros Basin
Water depth (m):	489
Target drilling depth (mbsf):	765
Approved maximum penetration (mbsf):	to basement
Survey coverage (track map; seismic profile):	Intersection of MCS Lines HH06-15-REPROC (CDP 2746) and GEOMAR_P2002 (CDP 5572)
Objective(s):	Recover the plio-quaternary volcano-sedimentary fill of the Anhydros Basin, to the depth of the Alpine basement; characterize all six Pliocene to the present seismic packages (B1 to B6) of the Anhydros rift basin.
Coring program:	• Hole A: APC/XCB to 610 mbsf or refusal • Hole B: APC/XCB to 610 mbsf or refusal • Hole C: Drill down to 575 mbsf or depth of refusal; RCB to 765 mbsf and wireline log
Downhole measurements program:	Hole C: Wireline log with triple combo, FMS-sonic & VSI
Nature of rock anticipated:	hemipelagic muds, volcaniclastics, and turbidites

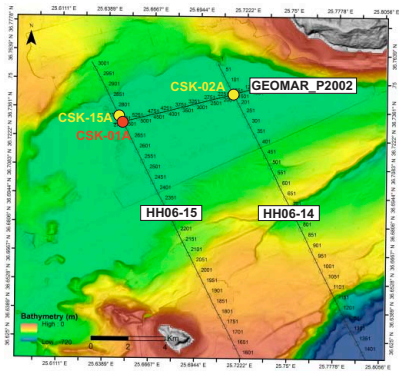

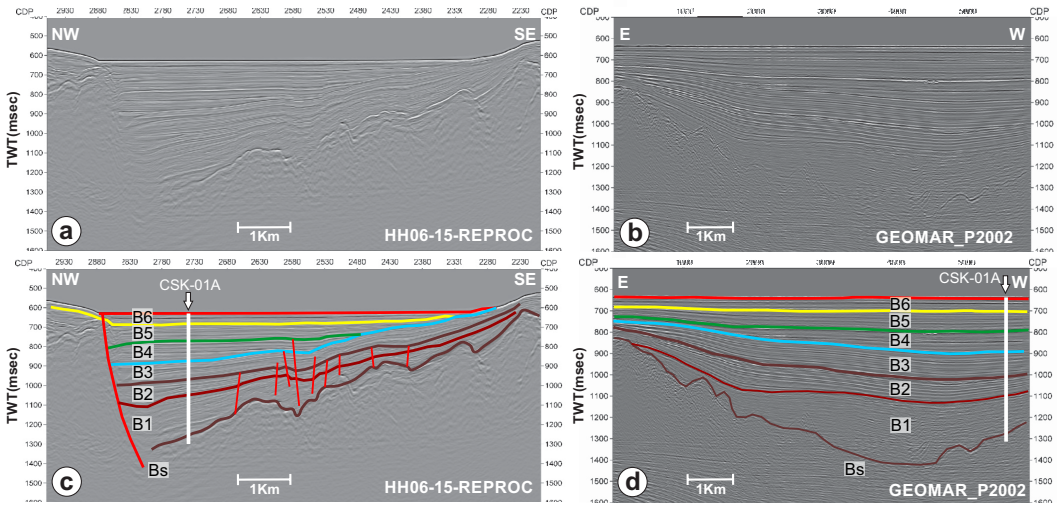

Figure AF1. Top: bathymetric map with location of proposed primary Site CSK-01A in Anhydros Basin. Bottom: (A, B) raw and (C, D) interpreted seismic sections at intersection of Lines GEOMAR_P2002 and HH06-15. CDP = common depth point.

Site CSK-02A (Anhydros Basin)

Priority:	Alternate
Position:	36.7438°N, 25.7146°E (36° 44.6280'N, 25° 42.8760' E) Eastern Anhydros Basin
Water depth (m):	488
Target drilling depth (mbsf):	553
Approved maximum penetration (mbsf):	to basement
Survey coverage (track map; seismic profile):	Intersection of MCS Lines HH06-14-REPROC (CDP 150) and GEOMAR_P2002 (CDP 1636)
Objective(s):	Recover the plio-quaternary volcano-sedimentary fill of the Anhydros Basin, to the depth of the Alpine basement; characterize all six Pliocene to the present seismic packages (B1 to B6) of the Anhydros rift basin.
Coring program:	• Hole A: APC/XCB to 553 mbsf • Hole B: APC/XCB to 553 mbsf • Hole C: APC/XCB to 553 mbsf and wireline log
Downhole measurements program:	Hole C: Wireline log with triple combo, FMS-sonic & VSI
Nature of rock anticipated:	hemipelagic muds, volcaniclastics, and turbidites

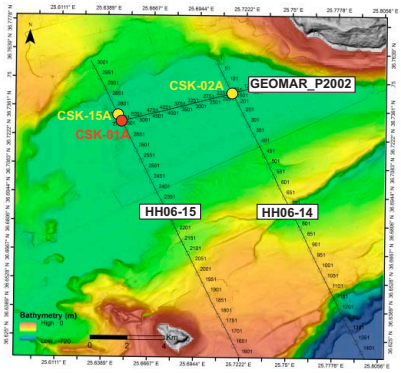

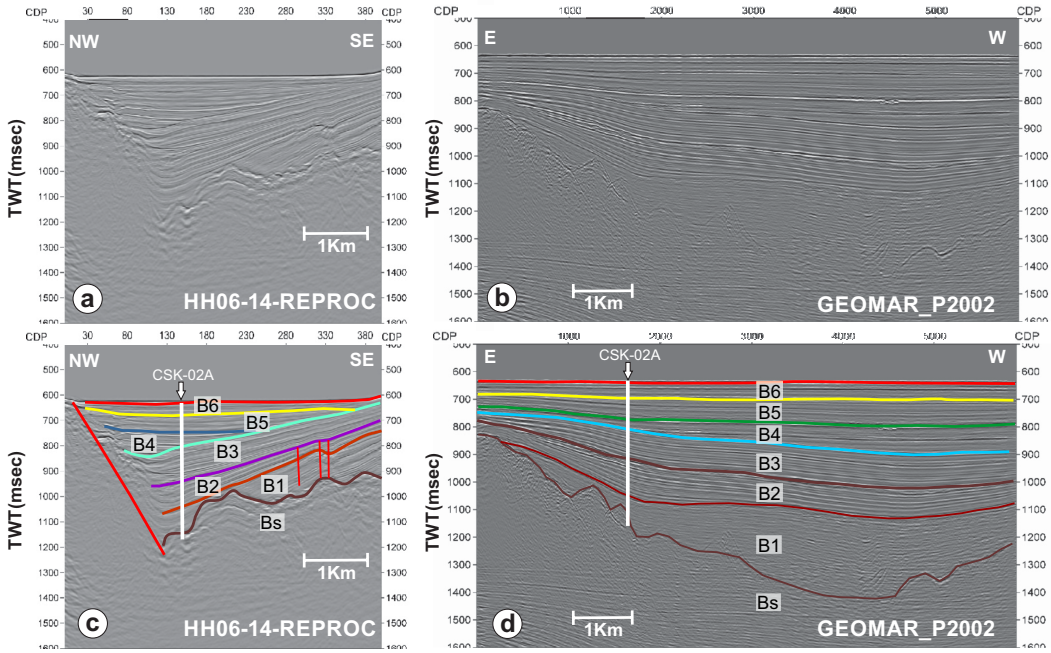

Figure AF2. Top: bathymetric map with location of proposed alternate Site CSK-02A in Anhydros Basin. Bottom: (A, B) raw and (C, D) interpreted seismic sections at intersection of Lines GEOMAR_P2002 and HH06-14.

Site CSK-15A (Anhydros Basin)

Priority:	Alternate
Position:	36.7320°N, 25.6463°E (36° 43.9200'N, 25° 38.7780' E) Central Anhydros Basin
Water depth (m):	490
Target drilling depth (mbsf):	800
Approved maximum penetration (mbsf):	to basement
Survey coverage (track map; seismic profile):	MCS Line HH06-15-REPROC (CDP 2770)
Objective(s):	Recover the plio-quaternary volcano-sedimentary fill of the Anhydros Basin, to the depth of the Alpine basement; characterize all six Pliocene to the present seismic packages (B1 to B6) of the Anhydros rift basin.
Coring program:	• Hole A: APC/XCB to 610 mbsf or to refusal • Hole B: APC/XCB to 610 mbsf or to refusal • Hole C: Drill down to 575 mbsf or depth of refusal; RCB to 800 mbsf and wireline log
Downhole measurements program:	Hole C: Wireline log with triple combo, FMS-sonic & VSI
Nature of rock anticipated:	hemipelagic muds, volcaniclastics, and turbidites

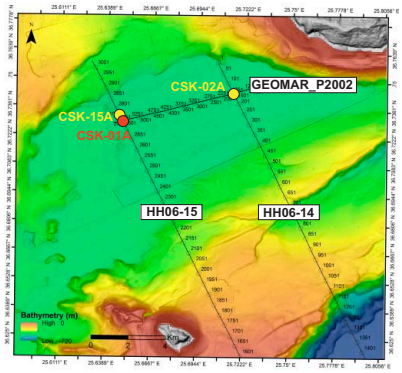

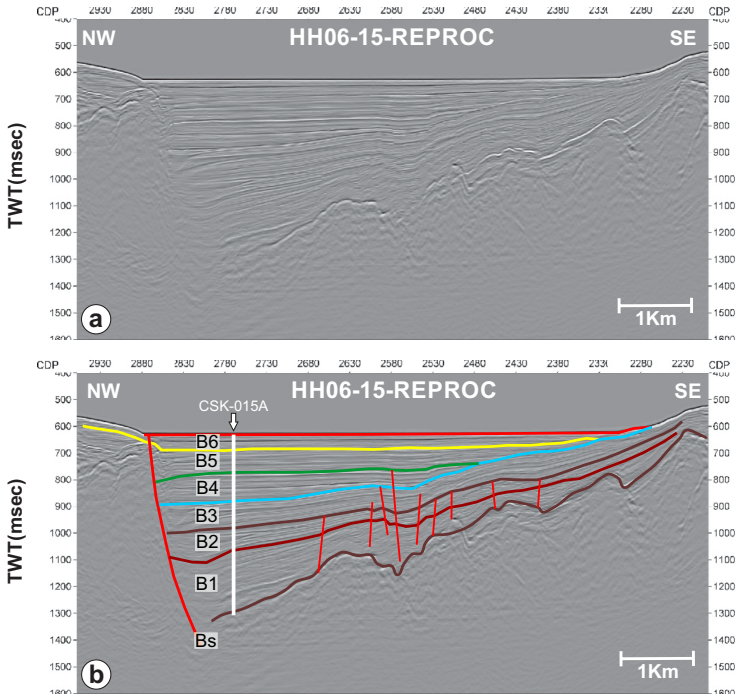

Figure AF3. Top: bathymetric map with location of proposed alternate Site CSK-15A in Anhydros Basin. Bottom: (A) raw and (B) interpreted seismic section along Line HH06-15, with Site CSK-15A situated just north of intersection with Line GEOMAR_P2002.

Site CSK-03A (Kolumbo)

Priority:	Primary
Position:	36.5549°N, 25.4398°E (36° 33.2940'N, 25° 26.3880' E) Northwestern flank Kolumbo volcano
Water depth (m):	397
Target drilling depth (mbsf):	566
Approved maximum penetration (mbsf):	566
Survey coverage (track map; seismic profile):	Intersection of MCS Lines HH06-34-REPROC (CDP 760) and HH06-22-REPROC (CDP 614)
Objective(s):	Recover the different seismically recognized units from Kolumbo (K1, K2, K3, K5 or their thin, lateral equivalents), as well as many eruption units from Santorini; characterize the products of Kolumbo eruptions; construct a coherent stratigraphy
Coring program:	• Hole A: APC/XCB to 566 mbsf • Hole B: APC/XCB to 566 mbsf • Hole C: APC/XCB to 566 mbsf and wireline log
Downhole measurements program:	Hole C: Wireline log with triple combo, FMS-sonic & VSI
Nature of rock anticipated:	hemipelagic muds, volcaniclastics, debris flow deposits, and turbidites

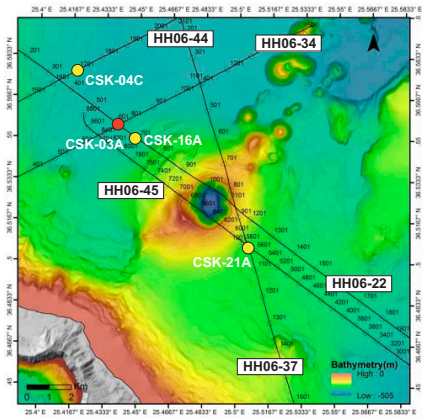

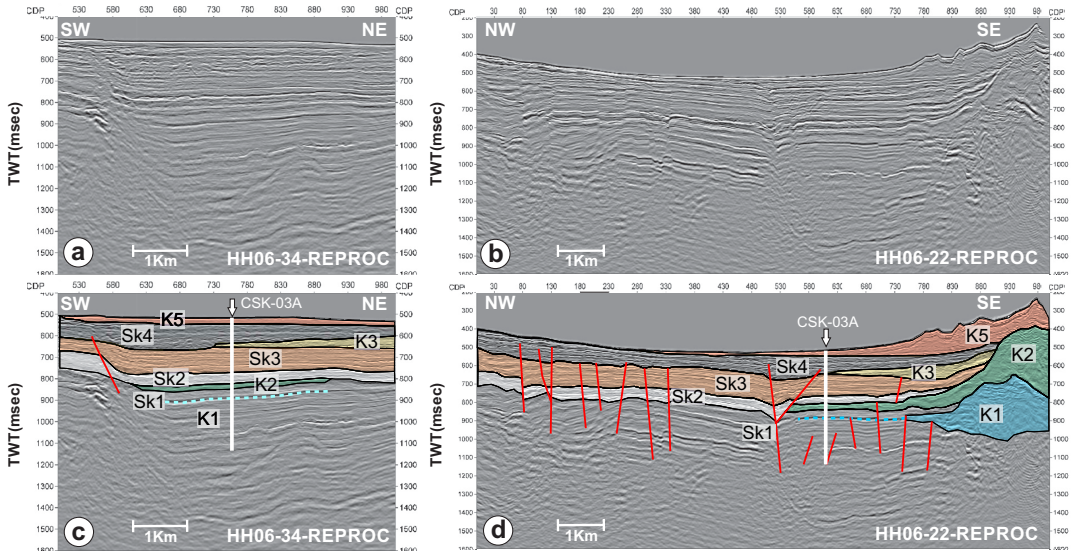

Figure AF4. Top: bathymetric map with location of proposed primary Site CSK-03A at northwestern flank of Kolumbo Volcano. Bottom: (A, B) raw and (C, D) interpreted seismic sections at intersection of Lines HH06-22 and HH06-34.

Site CSK-04C (Kolumbo)

Priority:	Alternate
Position:	36.5752°N, 25.4146°E (36° 34.5120'N, 25° 24.8760' E) Northwestern flank Kolumbo volcano
Water depth (m):	400
Target drilling depth (mbsf):	581
Approved maximum penetration (mbsf):	581
Survey coverage (track map; seismic profile):	MCS Line HH06-44-REPROC (CDP 1670)
Objective(s):	Recover the youngest seismically recognized unit from Kolumbo (K5) or the thin, lateral equivalents of older eruption units, as well as many eruption units from Santorini; characterize the products of Kolumbo eruptions; construct a coherent stratigraphy for Santorini and Kolumbo together.
Coring program:	• Hole A: APC/XCB to 581 mbsf • Hole B: APC/XCB to 581 mbsf • Hole C: APC/XCB to 581 mbsf and wireline log
Downhole measurements program:	Hole C: Wireline log with triple combo, FMS-sonic & VSI
Nature of rock anticipated:	hemipelagic muds, volcaniclastics, debris flow deposits, and turbidites

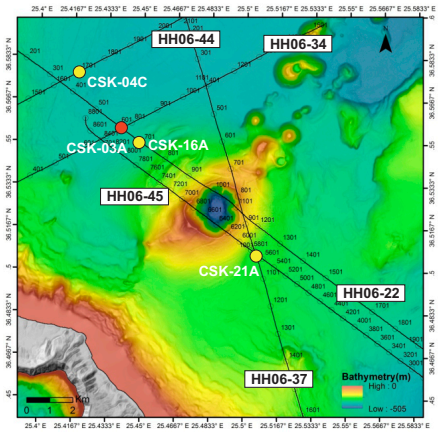

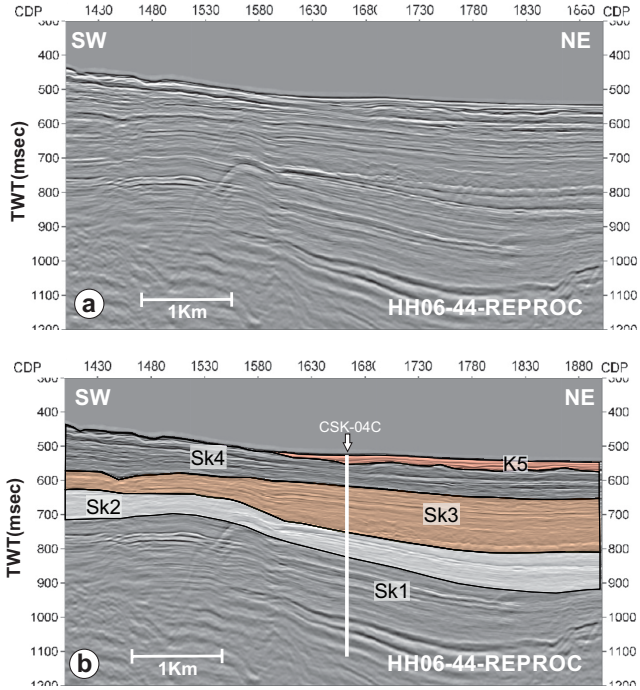

Figure AF5. Top: bathymetric map with location of proposed alternate Site CSK-04C at northwestern flank of Kolumbo Volcano. Bottom: (A) raw and (B) interpreted seismic section along Line HH06-44, with Site CSK-04C situated just northeast of intersection with Line HH06-22.

Site CSK-16A (Kolumbo)

Priority:	Alternate
Position:	36.5480°N, 25.4517°E (36° 32.8800'N, 25° 27.1020' E) Northwestern flank Kolumbo volcano
Water depth (m):	372
Target drilling depth (mbsf):	565
Approved maximum penetration (mbsf):	565
Survey coverage (track map; seismic profile):	MCS Line HH06-22-REPROC (CDP 722)
Objective(s):	Recover the different seismically recognized units from Kolumbo (K1, K2, K3, K5 or their thin, lateral equivalents), as well as many eruption units from Santorini; characterize the products of Kolumbo eruptions; construct a coherent stratigraphy for Santorini and Kolumbo together.
Coring program:	• Hole A: APC/XCB to 565 mbsf • Hole B: APC/XCB to 565 mbsf • Hole C: APC/XCB to 565 mbsf and wireline log
Downhole measurements program:	Hole C: Wireline log with triple combo, FMS-sonic & VSI
Nature of rock anticipated:	hemipelagic muds, volcaniclastics, debris flow deposits, and turbidites

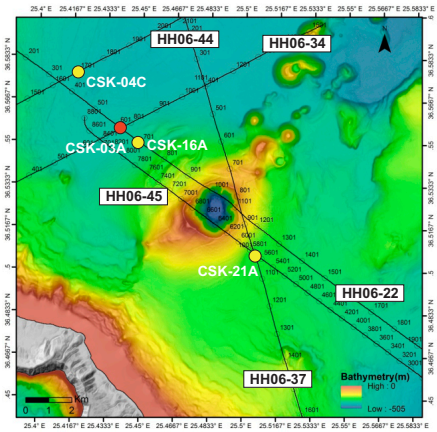

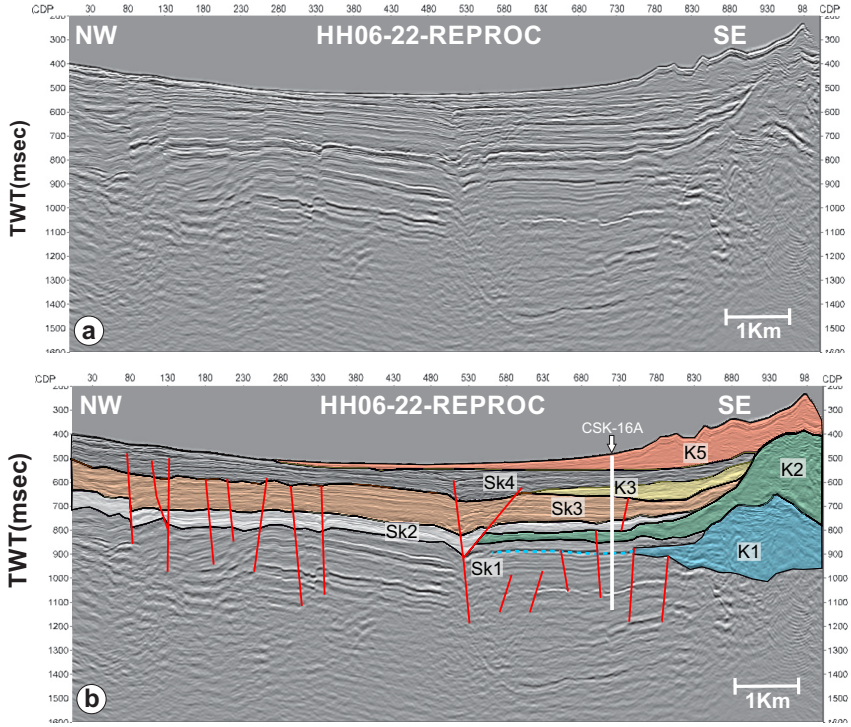

Figure AF6. Top: bathymetric map with location of proposed alternate Site CSK-16A at northwestern flank of Kolumbo Volcano. Bottom: (A) raw and (B) interpreted seismic section along Line HH06-22, with Site CSK-16A located just southeast of intersection with Line HH06-34 that marks location of Site CSK-03A.

Site CSK-21A (Kolumbo)

Priority:	Alternate
Position:	36.5068°N, 25.5053°E (36° 30.4080'N, 25° 30.3180' E) Southeastern flank Kolumbo volcano
Water depth (m):	309
Target drilling depth (mbsf):	630
Approved maximum penetration (mbsf):	630
Survey coverage (track map; seismic profile):	Intersetion of MCS Lines HH06-37-REPROC (CDP 1009) and HH06-45-REPROC (CDP 5727)
Objective(s):	Recover the different seismically recognized units from Kolumbo (K1, K3, K5 or their thin, lateral equivalents), as well as many eruption units from Santorini; characterize the products of Kolumbo eruptions; construct a coherent stratigraphy for Santorini and Kolumbo together.
Coring program:	• Hole A: APC/XCB to 630 mbsf • Hole B: APC/XCB to 630 mbsf • Hole C: APC/XCB to 630 mbsf and wireline log
Downhole measurements program:	Hole C: Wireline log with triple combo, FMS-sonic & VSI
Nature of rock anticipated:	hemipelagic muds, volcaniclastics, debris flow deposits, and turbidites

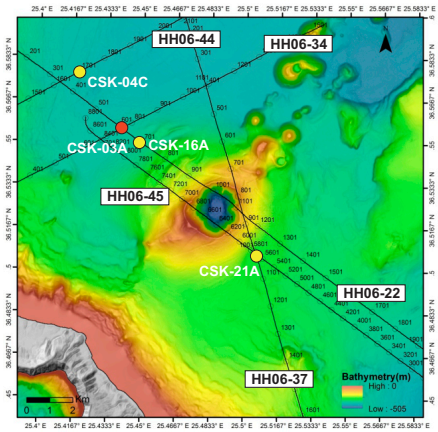

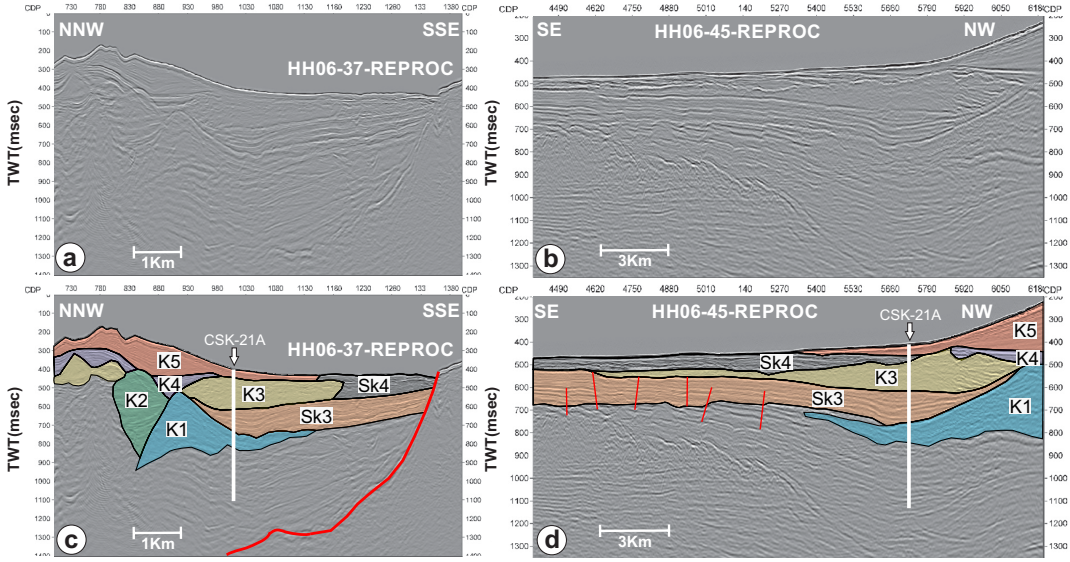

Figure AF7. Top: bathymetric map with location of proposed alternate Site CSK-21A at southeastern flank of Kolumbo Volcano. Bottom: (A, B) raw and (C, D) interpreted seismic sections at intersection of Lines HH06-37 and HH06-45.

Site CSK-13A (Christiana Basin)

Priority:	Primary
Position:	36.3243°N, 25.1826°E (36° 19 4580.'N, 25° 10.9560' E) Christiana basin
Water depth (m):	489
Target drilling depth (mbsf):	857
Approved max. penetration (mbsf)	to basement
Survey coverage (track map; seismic profile):	Intersection of MCS GEOMAR_P5009 (CDP 5042) and GEOMAR_P5006 (CDP 4431)
Objective(s):	Recover the plio-quaternary volcano-sedimentary fill of the Christiana Basin, to the depth of the Alpine basement; characterize the sediments and volcaniclastics comprising seismic units U1 to U6.
Coring program:	• Hole A: APC/XCB to 675 mbsf or to refusal • Hole B: APC/XCB to 675 mbsf or to refusal • Hole C: Drill down to 575 mbsf or depth of refusal; RCB to 857 mbsf and wireline log
Downhole measurements program:	Hole C: Wireline log with triple combo, FMS-sonic & VSI
Nature of rock anticipated:	hemipelagic muds, volcaniclastics, debris flow deposits, and turbidites

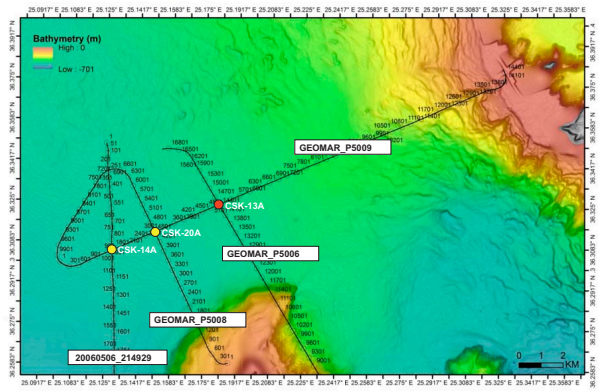

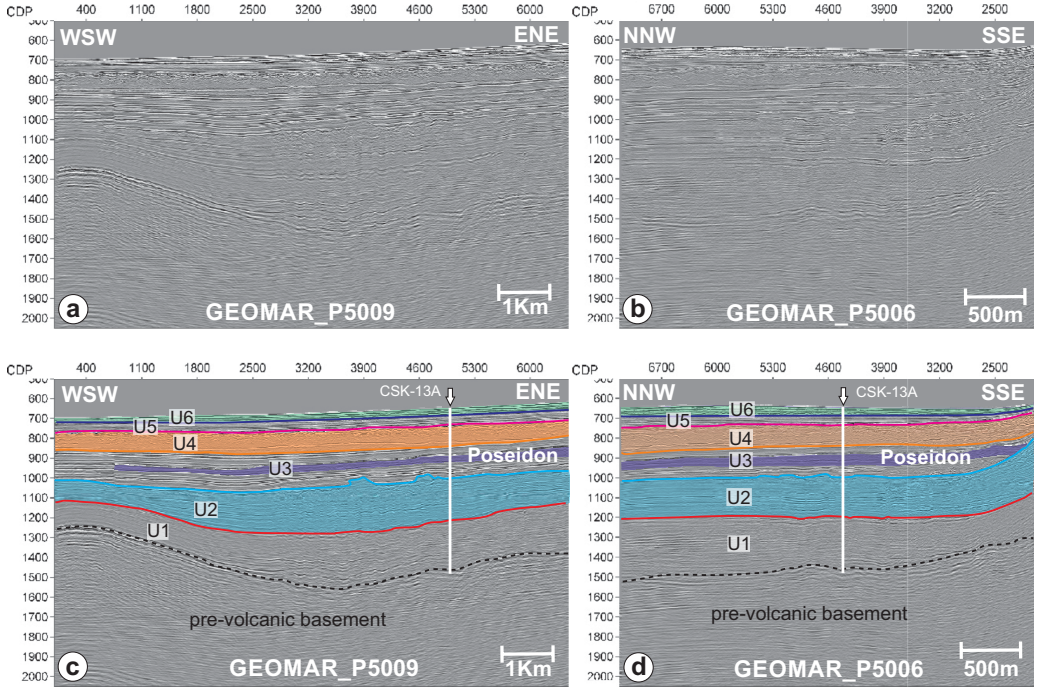

Figure AF8. Top: bathymetric map with location of proposed primary Site CSK-13A in Christiana Basin. Bottom: (A, B) raw and (C, D) interpreted seismic sections at intersection of Lines GEOMAR_P5006 and GEOMAR_P5009.

Site CSK-14A (Christiana Basin)

Priority:	Alternate
Position:	36.3049°N, 25.1286°E (36° 18.2940'N, 25° 07.7160' E) Christiana basin
Water depth (m)	523
Target drilling depth (mbsf):	756
Approved max. penetration (mbsf)	to basement
Survey coverage (track map; seismic profile):	Intersection of MCS GEOMAR_P5009 (CDP 1644) and 20060506_214929-REPROC (CDP 886)
Objective(s):	Recover the plio-quaternary volcano-sedimentary fill of the Christiana Basin, to the depth of the Alpine basement; characterize the sediments and volcaniclastics comprising seismic units U1 to U6.
Coring program:	• Hole A: APC/XCB to 675 mbsf or to refusal • Hole B: APC/XCB to 675 mbsf or to refusal • Hole C: Drill down to 575 mbsf or depth of refusal; RCB to 756 mbsf and wireline log
Downhole measurements program:	Hole C: Wireline log with triple combo, FMS-sonic & VSI
Nature of rock anticipated:	hemipelagic muds, volcaniclastics, debris flow deposits, and turbidites

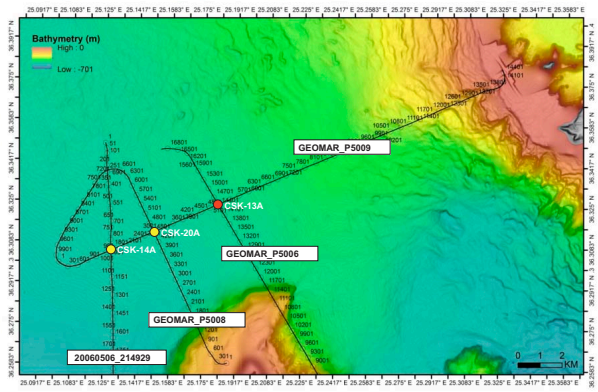

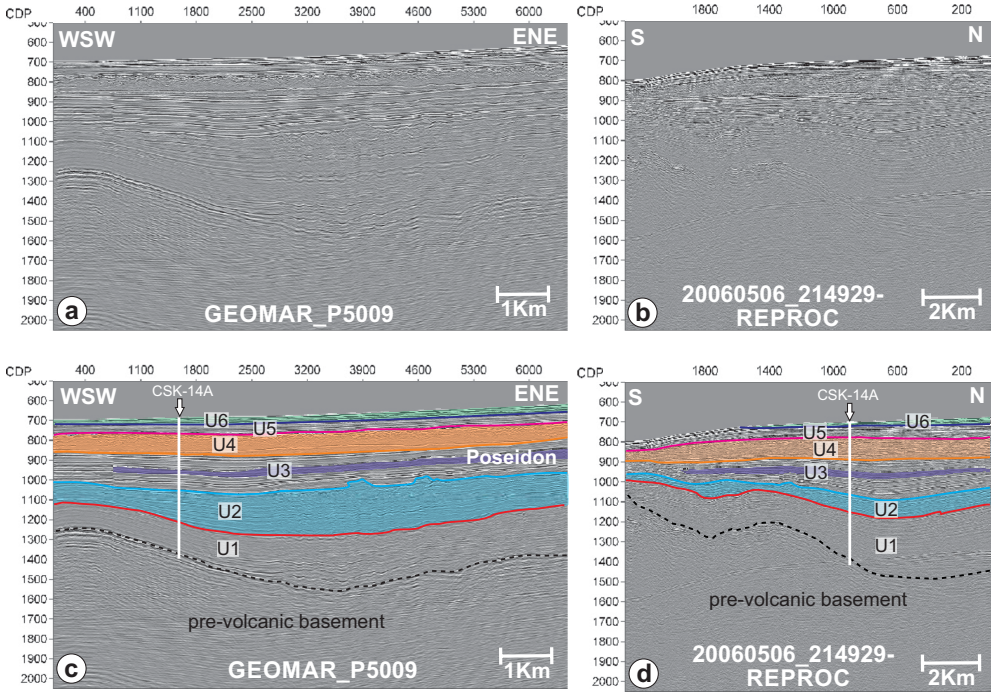

Figure AF9. Top: bathymetric map with location of proposed alternate Site CSK-14A in Christiana Basin. Bottom: (A, B) raw and (C, D) interpreted seismic sections at intersection of Lines 20060506_214929 and GEOMAR_P5009.

Site CSK-20A (Christiana Basin)

Priority:	Alternate
Position:	36.3127°N, 25.1501°E (36° 18.7620'N, 25° 09.0060' E) Christiana Basin
Water depth (m)	515
Target drilling depth (mbsf):	909
Approved max. penetration (mbsf)	to basement
Survey coverage (track map; seismic profile):	Intersection of MCS GEOMAR_P5009 (CDP 3013) and GEOMAR_P5008 (CDP 4521)
Objective(s):	Recover the plio-quaternary volcano-sedimentary fill of the Christiana Basin, to the depth of the Alpine basement; characterize the sediments and volcaniclastics comprising seismic units U1 to U6.
Coring program:	• Hole A: APC/XCB to 675 mbsf or to refusal • Hole B: APC/XCB to 675 mbsf or to refusal • Hole C: Drill down to 575 mbsf or depth of refusal; RCB to 909 mbsf and wireline log
Downhole measurements program:	Hole C: Wireline log with triple combo, FMS-sonic & VSI
Nature of rock anticipated:	hemipelagic muds, volcaniclastics, debris flow deposits, and turbidites

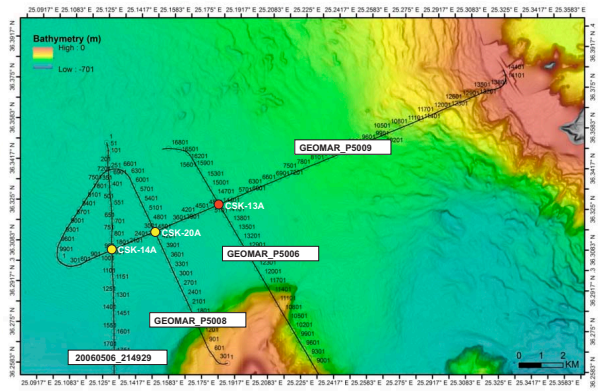

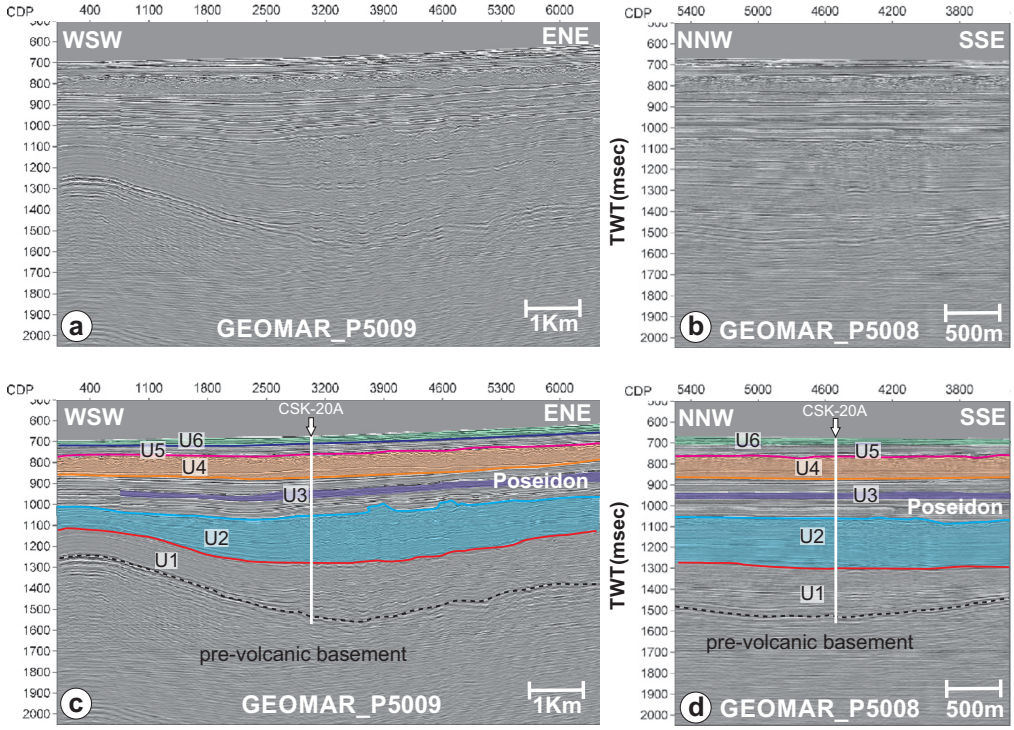

Figure AF10. Top: bathymetric map with location of proposed alternate Site CSK-20A in Christiana Basin. Bottom: (A, B) raw and (C, D) interpreted seismic sections at intersection of Lines GEOMAR_P5008 and GEOMAR_P5009.

Site CSK-05C (Santorini)

Priority:	Primary
Position:	36.4375°N, 25.3789°E (36° 26.2500'N, 25° 22.7340' E) Northern basin Santorini caldera
Water depth (m):	384
Target drilling depth (mbsf):	234
Approved maximum penetration (mbsf):	234
Survey coverage (track map; seismic profile):	MCS Line GEOMAR_P1006 (CDP 20245)
Objective(s):	Recover the intracaldera seismic units S1, S2, and S3 in order to characterise them, as well as to penetrate below unit S3 (probably intracaldera tuff of the LBA eruption) to elaborate, complementary with Sites in the Southern Caldera basin, on the collapse and caldera fill history of Santorini Caldera. These holes will also be used for the microbiological work of objective 7.
Coring program:	• Hole A: APC/XCB to refusal • Hole B: Drill down to 130 mbsf or to depth of refusal; RCB to 234 mbsf and wireline log
Downhole measurements program:	Hole B: Wireline log with triple combo, FMS-sonic & VSI
Nature of rock anticipated:	Coarse intracaldera sediments, breccias, landslide deposits, lavas, muds

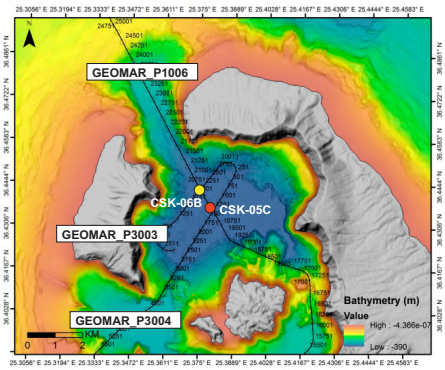

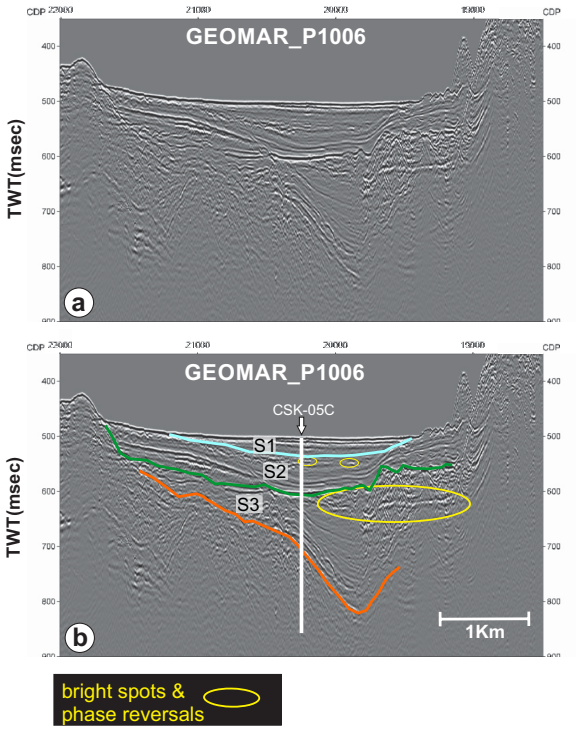

Figure AF11. Top: bathymetric map with location of proposed primary Site CSK-05C in northern basin of Santorini caldera. Bottom: (A) raw and (B) interpreted seismic section along Line GEOMAR_P1006 adjacent to intersection with Line GEOMAR_P3004.

Site CSK-06B (Santorini)

Priority:	Alternate
Position:	36.4423°N, 25.3752°E (36° 26.5380'N, 25° 22.5120' E) Northern basin Santorini caldera
Water depth (m):	383
Target drilling depth (mbsf):	360
Approved maximum penetration (mbsf):	360
Survey coverage (track map; seismic profile):	Intersection of MCS Line GEOMAR_P1006 (CDP 20648) and GEOMAR_P23003 (CDP 2159)
Objective(s):	Recover the intracaldera seismic units S1, S2, and S3 in order to characterise them, as well as to penetrate below unit S3 (probably intracaldera tuff of the LBA eruption) to elaborate, complementary with Sites in the Southern Caldera basin, on the collapse and caldera fill history of Santorini Caldera. These holes will also be used for the microbiological work of objective 7.
Coring program:	• Hole A: APC/XCB to refusal • Hole B: Drill down to 130 mbsf or to depth of refusal; RCB to 360 mbsf and wireline log
Downhole measurements program:	Hole B: Wireline log with triple combo, FMS-sonic & VSI
Nature of rock anticipated:	Coarse intracaldera sediments, breccias, landslide deposits, lavas, muds

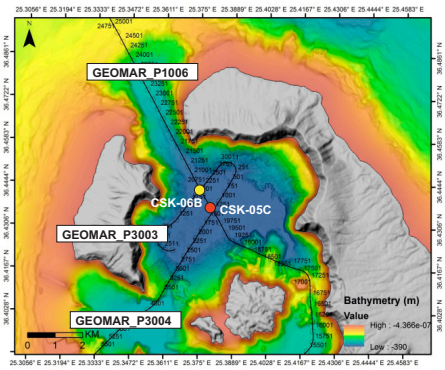

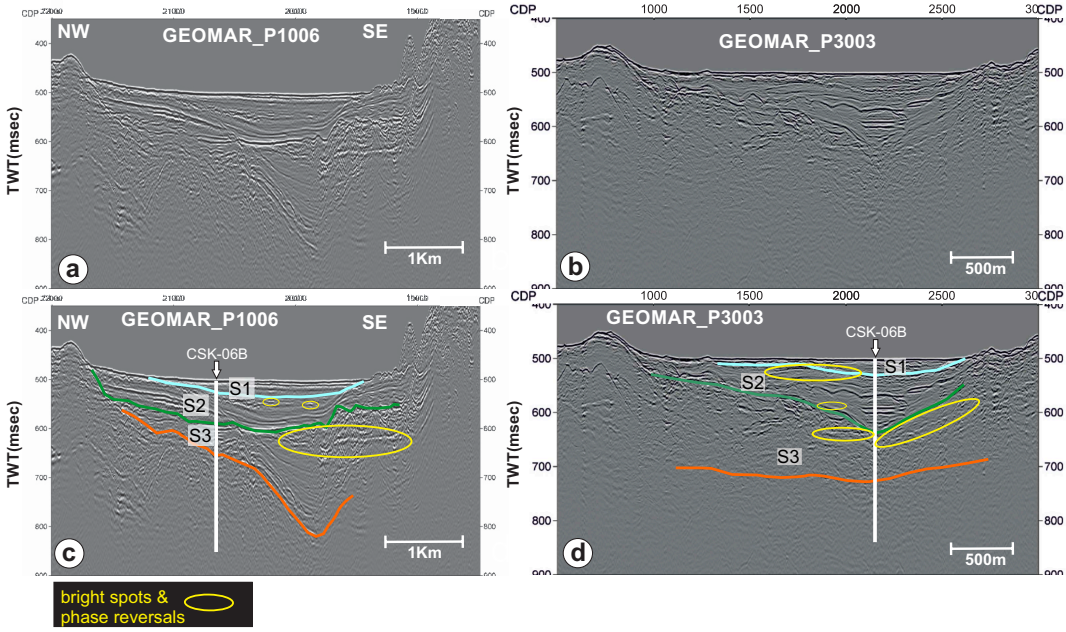

Figure AF12. Top: bathymetric map with location of proposed alternate Site CSK-06B in northern basin of Santorini caldera. Bottom: (A, B) raw and (C, D) interpreted seismic sections at intersection of Lines GEOMAR_P3003 and GEOMAR_P1006.

Site CSK-07B (Santorini)

Priority:	Primary
Position:	36.38895°N, 25.41713°E (36° 23.3370'N, 25° 25.0278' E) Southern basin Santorini caldera
Water depth (m):	292
Target drilling depth (mbsf):	360
Approved maximum penetration (mbsf):	360
Survey coverage (track map; seismic profile):	Intersection of MCS Lines GEOMAR_P1006 (CDP 15324) and 20060504_052810-REPROC (CDP 234)
Objective(s):	Recover the intracaldera seismic units S1, S2, and S3 in order to characterise them, as well as to penetrate below unit S3 (probably intracaldera tuff of the LBA eruption) to elaborate, complementary with Sites in the Northern Caldera basin, on the collapse and caldera fill history of Santorini Caldera. These holes will also be used for the microbiological work of objective 7.
Coring program:	• Hole A: APC/XCB to refusal • Hole B: Drill down to 175 mbsf or to depth of refusal; RCB to 360 mbsf and wireline log
Downhole measurements program:	Hole B: Wireline log with triple combo, FMS-sonic & VSI
Nature of rock anticipated:	Coarse intracaldera sediments, breccias, landslide deposits, lavas, muds

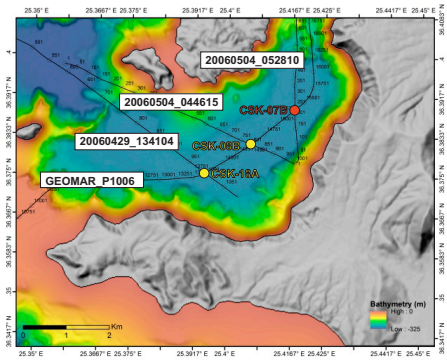

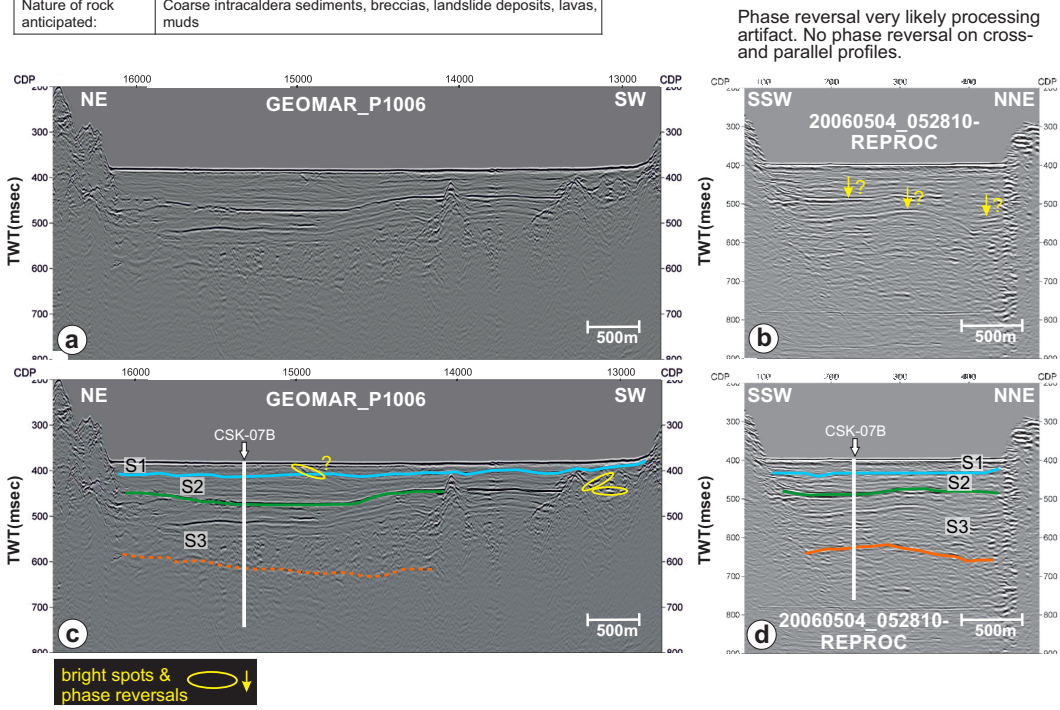

Figure AF13. Top: bathymetric map with location of proposed primary Site CSK-07B in southern basin of Santorini caldera. Bottom: (A, B) raw and (C, D) interpreted seismic sections at intersection of Lines 20060504_052810 and GEOMAR_P1006.

Site CSK-08B (Santorini)

Priority:	Alternate
Position:	36.38161°N, 25.40606°E (36° 22.8966'N, 25° 24.3636' E) Southern basin Santorini caldera
Water depth (m):	293
Target drilling depth (mbsf):	375
Approved maximum penetration (mbsf):	375
Survey coverage (track map; seismic profile):	Intersection of MCS Line GEOMAR_P1006 (CDP 14501) and 20060504_044615-REPROC (CDP 801)
Objective(s):	Recover the intracaldera seismic units S1, S2, and S3 in order to characterise them, as well as to penetrate below unit S3 (probably intracaldera tuff of the LBA eruption) to elaborate, complementary with Sites in the Northern Caldera basin, on the collapse and caldera fill history of Santorini Caldera. These holes will also be used for the microbiological work of objective 7.
Coring program:	• Hole A: APC/XCB to refusal • Hole B: Drill down to 175 mbsf or to depth of refusal; RCB to 375 mbsf and wireline log
Downhole measurements program:	Hole B: Wireline log with triple combo, FMS-sonic & VSI
Nature of rock anticipated:	Coarse intracaldera sediments, breccias, landslide deposits, lavas, muds

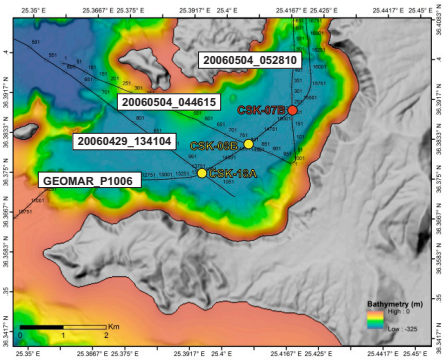

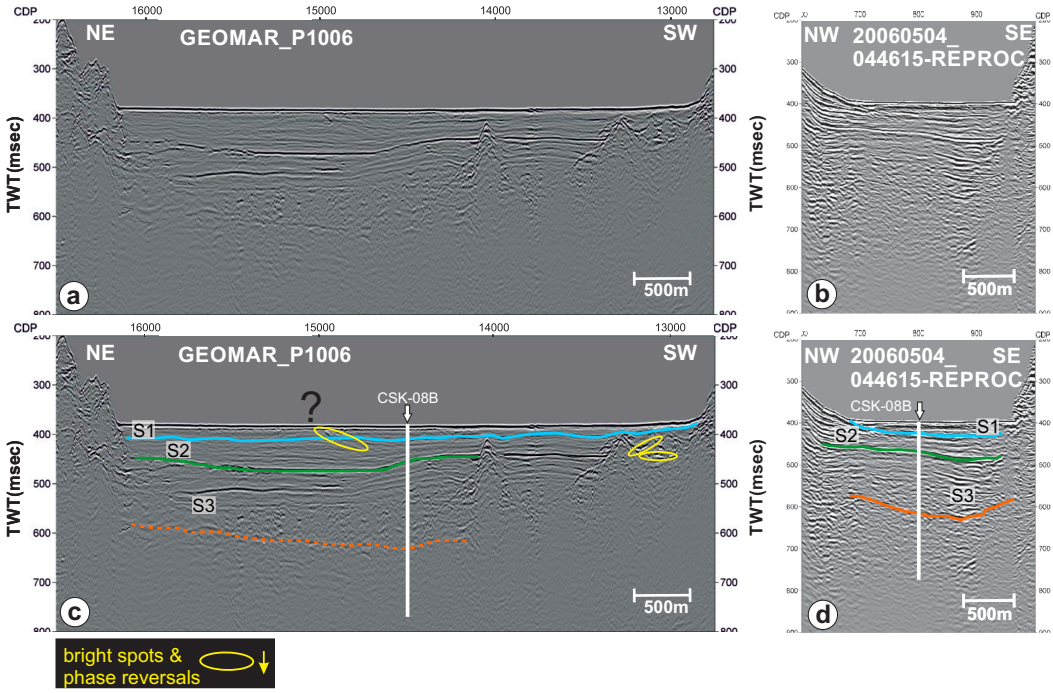

Figure AF14. Top: bathymetric map with location of proposed alternate Site CSK-08B in southern basin of Santorini caldera. Bottom: (A, B) raw and (C, D) interpreted seismic sections at intersection of Lines 20060504_044615 and GEOMAR_P1006.

Site CSK-18A (Santorini)

Priority:	Alternate
Position:	36.3755°N, 25.3942°E (36° 22.5300'N, 25° 23.6520' E) Southern basin Santorini caldera
Water depth (m):	291
Target drilling depth (mbsf):	380
Approved maximum penetration (mbsf):	380
Survey coverage (track map; seismic profile):	Intersection of MCS Lines GEOMAR_P1006 (CDP 13690) and 20060429_134104-REPROC (CDP 1845)
Objective(s):	Recover the intracaldera seismic units S1, S2, and S3 in order to characterise them, as well as to penetrate below unit S3 (probably intracaldera tuff of the LBA eruption) to elaborate, complementary with Sites in the Northern Caldera basin, on the collapse and caldera fill history of Santorini Caldera. These holes will also be used for the microbiological work of objective 7.
Coring program:	• Hole A: APC/XCB to refusal • Hole B: Drill down to 175 mbsf or to depth of refusal; RCB to 380 mbsf and wireline log
Downhole measurements program:	Hole B: Wireline log with triple combo, FMS-sonic & VSI
Nature of rock anticipated:	Coarse intracaldera sediments, breccias, landslide deposits, lavas, muds

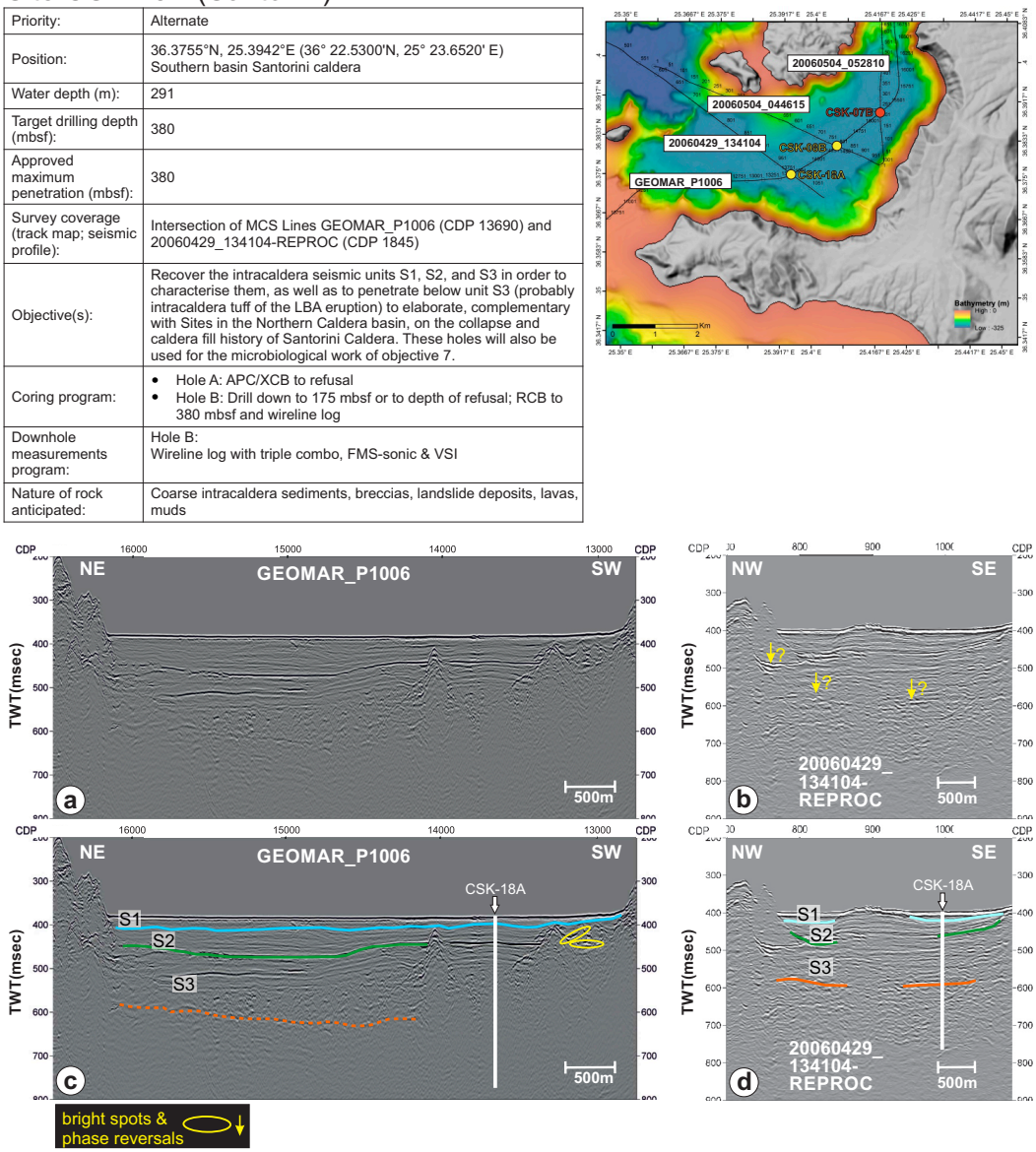

Figure AF15. Top: bathymetric map with location of proposed alternate Site CSK-18A in southern basin of Santorini caldera. Bottom: (A, B) raw and (C, D) interpreted seismic sections at intersection of Lines 20060429_134104 and GEOMAR_P1006.

Site CSK-09A (Anafi Basin)

Priority:	Primary
Position:	36.5656°N, 25.7613°E (36° 33.9360'N, 25° 45.6780' E) Anafi basin
Water depth (m):	694
Target drilling depth (mbsf):	595
Approved maximum penetration (mbsf):	to basement
Survey coverage (track map; seismic profile):	Intersection of MCS Lines HH06-15-REPROC (CDP 1067) and HH06-09-REPROC (CDP 3403)
Objective(s):	Recover the plio-quaternary volcano-sedimentary fill of the Anafi Basin, to the depth of the Alpine basement; characterize all six Pliocene to the present seismic packages (B1 to B6) of the Anhydros rift basin; Reconstruct the subsidence and sedimentary history of this basin, to compare with that of the Anhydros Basin.
Coring program:	• Hole A: APC/XCB to 595 mbsf • Hole B: APC/XCB to 595 mbsf and wireline log
Downhole measurements program:	Hole B: Wireline log with triple combo, FMS-sonic & VSI
Nature of rock anticipated:	hemipelagic muds, volcaniclastics, and turbidites

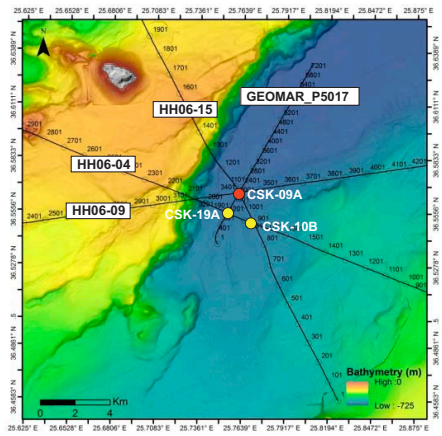

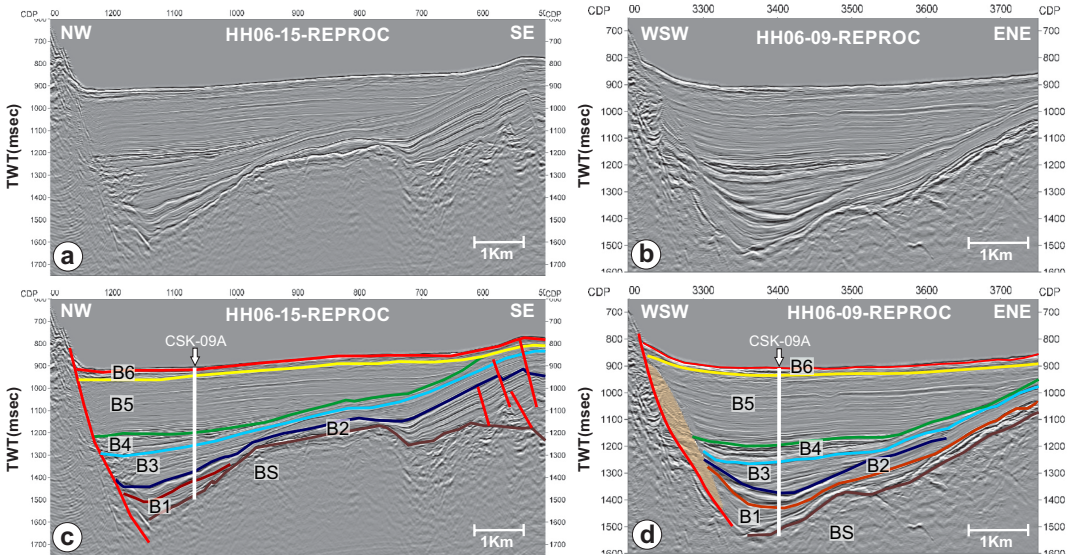

Figure AF16. Top: bathymetric map with location of proposed primary Site CSK-09A in Anafi Basin. Bottom: (A, B) raw and (C, D) interpreted seismic sections at intersection of Lines HH06-09 and HH06-15.

Site CSK-10B (Anafi Basin)

Priority:	Alternate
Position:	36.5507°N, 25.7668°E (36° 33.0420'N, 25° 46.0080' E) Anafi basin
Water depth (m):	680
Target drilling depth (mbsf):	363
Approved maximum penetration (mbsf):	to basement
Survey coverage (track map; seismic profile):	MCS Line HH06-04-REPROC (CDP 1790)
Objective(s):	Recover the plio-quaternary volcano-sedimentary fill of the Anafi Basin, to the depth of the Alpine basement; characterize four Pliocene to the present seismic packages (B3 to B6) of the Anhydros rift basin; Reconstruct the subsidence and sedimentary history of this basin, to compare with that of the Anhydros Basin.
Coring program:	• Hole A: APC/XCB to 363 mbsf • Hole B: APC/XCB to 363 mbsf • Hole C: APC/XCB to 363 mbsf and wireline log
Downhole measurements program:	Hole B: Wireline log with triple combo, FMS-sonic & VSI
Nature of rock anticipated:	hemipelagic muds, volcaniclastics, and turbidites

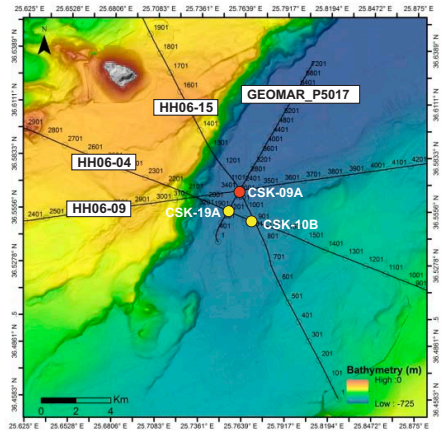

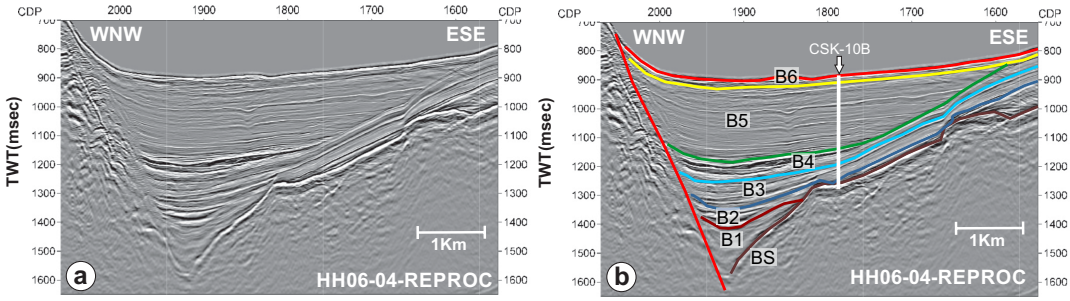

Figure AF17. Top: bathymetric map with location of proposed alternate Site CSK-10B in Anafi Basin. Bottom: (A) raw and (B) interpreted seismic section along Line HH06-04 just northwest of intersection with Line HH06-15.

Site CSK-19A (Anafi Basin)

Priority:	Alternate
Position:	36.5563°N, 25.7503°E (36° 33.3780'N, 25° 45.0180' E) Anafi basin
Water depth (m):	688
Target drilling depth (mbsf):	740
Approved maximum penetration (mbsf):	to basement
Survey coverage (track map; seismic profile):	Intersection of MCS Lines HH06-04-REPROC (CDP 1919) and 300 m N of cross line GEOMAR_P5017
Objective(s):	Recover the plio-quaternary volcano-sedimentary fill of the Anafi Basin, to the depth of the Alpine basement; characterize all six Pliocene to the present seismic packages (B1 to B6) of the Anhydros rift basin; Reconstruct the subsidence and sedimentary history of this basin, to compare with that of the Anhydros Basin.
Coring program:	• Hole A: APC/XCB to 740 mbsf • Hole B: Drilling down and APC/XCB spot coring to 740 mbsf and wireline log
Downhole measurements program:	Hole B: Wireline log with triple combo, FMS-sonic & VSI
Nature of rock anticipated:	hemipelagic muds, volcaniclastics, and turbidites

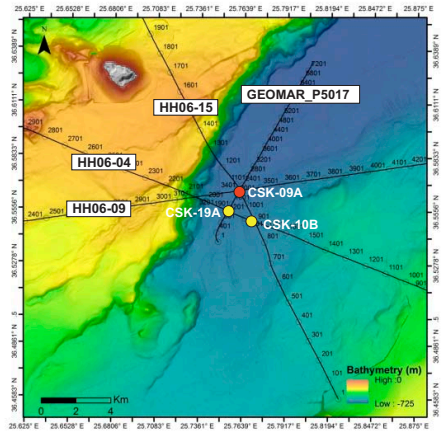

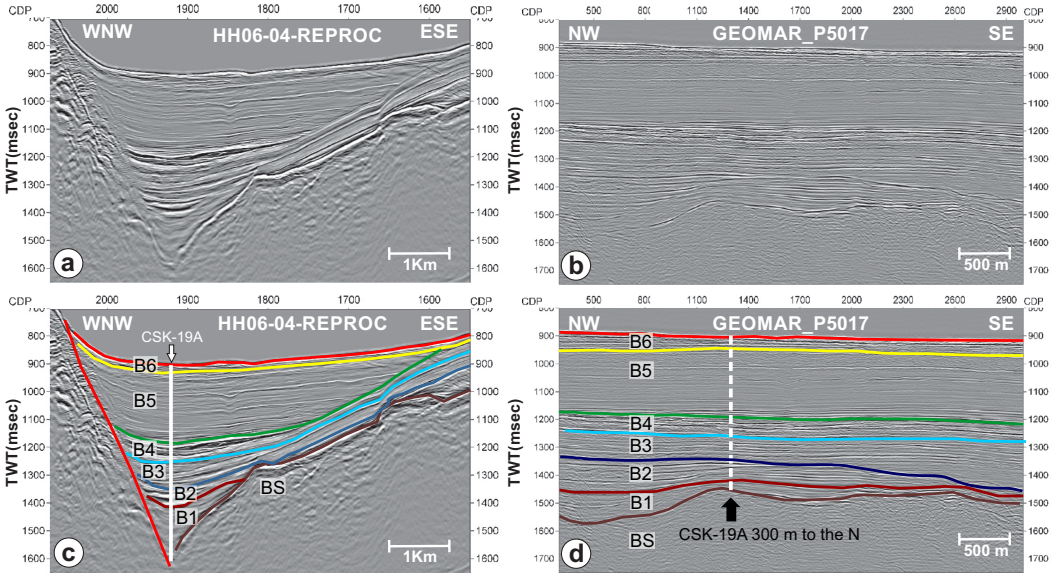

Figure AF18. Top: bathymetric map with location of proposed alternate Site CSK-19A in Anafi Basin. Bottom: (A, B) raw and (C, D) interpreted seismic sections at intersection of Lines GEOMAR_P5017 and HH06-04.